Citation: Bird, D. E., 2004, Jurassic tectonics of the Gulf of Mexico and Central Atlantic Ocean: Ph.D. Dissertation, University of Houston, 161 p.

JURASSIC TECTONICS OF THE GULF OF MEXICO AND CENTRAL ATLANTIC OCEAN

A Dissertation

Presented to

The Faculty of the Department of Geosciences

University of Houston

In Partial Fulfillment

Of the Requirements for the Degree

Doctor of Philosophy

By

Dale E. Bird

May 2002

JURASSIC TECTONICS OF THE
GULF OF MEXICO AND CENTRAL ATLANTIC OCEAN

Dale E. Bird

APPROVED:

Dr. Stuart A. Hall (Chairman)

Dr. Kevin Burke

Dr. John F. Casey

Dr. Dale S. Sawyer

Dean, College of Natural Sciences and Mathematics

ACKNOWLEDGEMENTS

About seven years ago, shortly after successfully proposing the research described in this dissertation, I told my wife, Mai Quach, that I wanted to quit my job and start a consultancy in order to pursue a doctorate degree in geophysics. At that time our four children: Zachary, Joshua, Rachel, and Ashley, were eight, five, two, and one years old. Mai did not take even a minute to think about it, but immediately agreed to support my decision. It is hard to find the words to tell her how much her support meant to me, and how much she means to me. She is the love of my life, and she is an angel.

I am grateful for the guidance, support and patience of my Research Committee: Dr. Stuart Hall, my advisor, Dr. Kevin Burke, Dr. Jack Casey, and Dr. Dale Sawyer (from Rice University). Their broad geological and geophysical knowledge of tectonics and regional geology seems to be limitless. They always have the answers and I am very fortunate to have had the opportunity to work with them. So it is with great respect that I thank them.

Over the years while working on this dissertation, I have discussed various aspects of my research with close friends. I would still like to acknowledge them and thank them for their friendship and for sharing their thoughts. Therefore, I thank Bob Lunn, Sam Mentemeier and Gary White at Anadarko Petroleum Corporation, Ed Biegert at Shell International Exploration & Production, Pat Millegan at Marathon Oil Company, and David Forel, who is completing his doctoral research at Michigan Technological University.

I would like to thank Walter Roest at the Geologic Survey of Canada for sending me a copy of the Kroonvlag project, which is a shiptrack magnetic dataset (also known as the “Collette Data”). Finally, I thank Chris Willacy at GXT Technology for allowing me to show a line-drawing interpretation of part of line 2600 from their *GulfSpan* seismic program.

PREFACE

The tectonic evolution of the Gulf of Mexico and the central Atlantic Ocean in the Jurassic includes the separation of the North America from Gondwana, the accretion of almost 1700 km of oceanic crust in the central Atlantic, and the counterclockwise rotation of the Yucatan continental block to open the Gulf of Mexico basin. Understanding the kinematic relationship between these tectonic elements provides a framework with which to interpret smaller-scaled geologic elements.

This dissertation is an interpretation of geophysical data resulting in new models for the Jurassic formation of the central Atlantic and Gulf of Mexico, including a previously unknown spreading ridge jump in the central Atlantic that possibly coincides with the opening of the Gulf of Mexico.

The shape of the Gulf of Mexico, that of a small ocean basin essentially surrounded by continental crust, indicates that the basin must have opened along at least one ocean-continent transform boundary, or shear margin. Therefore the first part of this dissertation is a review of ten shear margins around the world that was published in The Leading Edge (Bird, 2001). The second part describes a kinematic model for the formation of the Gulf of Mexico that includes the formation of hotspot tracks as the basin opened, and it has been submitted for publication. Results of the final part of this work include supporting evidence for a previously suggested spreading ridge jump at about 170 Ma, and evidence indicating the presence of a spreading ridge jump between 164 Ma and 159 Ma. The manuscript for this final section is being prepared for submission.

JURASSIC TECTONICS OF THE
GULF OF MEXICO AND CENTRAL ATLANTIC OCEAN

An Abstract of a Dissertation

Presented to

The Faculty of the Department of Geosciences

University of Houston

In Partial Fulfillment

Of the Requirements for the Degree

Doctor of Philosophy

By

Dale E. Bird

May 2002

ABSTRACT

Detailed interpretations of geophysical data have lead to the development of new models for the Jurassic evolution of the Gulf of Mexico and the central Atlantic Ocean.

The Gulf of Mexico ocean basin is essentially surrounded by continental crust, indicating that at least one ocean-continent transform boundary formed as it opened. Three distinctive gravity anomalies are interpreted to be those produced by prominent basement structures that also formed as the basin opened. Two of these structures are hotspot tracks formed during a 20° counterclockwise rotation of the Yucatan block. The third is a north-south marginal ridge along the western side of the basin that indicates the presence of a shear margin. The rotation, and hotspot track lengths considered as a function of time, account for about one-half of the total rotation and time required to form the basin (~ 10 My). Rotations prior to this involved continental extension and accompanying salt deposition. As such the basement structures appear to define the oceanic-continental crustal boundary and the approximate seaward limits of autochthonous salt deposition.

In the central Atlantic Ocean, M-Series seafloor spreading magnetic anomalies have been used to develop a kinematic reconstruction of the region. These data indicate that two seafloor spreading ridge jumps during the Jurassic were followed by a period of asymmetric seafloor spreading. The earliest ridge jump was towards the east and occurred about 170 Ma, leaving part of African lithosphere between the East Coast Magnetic Anomaly and Blake Spur Magnetic Anomaly. The second ridge jump was towards the west and occurred between 164 Ma and 159 Ma. Estimated half-spreading

rates for the North American and African flanks of the central Atlantic between 154 Ma and 120.6 Ma are 14.4 mm/a and 12.9 mm/a respectively.

TABLE OF CONTENTS

LIST OF FIGURES

LIST OF TABLES

1. SHEAR MARGINS: CONTINENT – OCEAN TRANSFORM AND FRACTURE ZONE BOUNDARIES

1.1 Summary

Shear margins are ocean-continent crustal boundaries that form along oceanic transform faults. As seafloor spreading continues, the ocean-continent boundary is defined by the fossil trace of the transform fault, or fracture zone. Shear margins typically develop after: 1) the creation of new oceanic crust on one side of the transform fault, and complex rifting on the continental side of the fault, 2) the development of an active ocean-continent transform boundary, and 3) passive margin subsidence along an inactive fracture zone (Figure 1.1), dramatic thickness variations notwithstanding.

There are at least three significant differences between shear margins and passive margins, which form by normal extension between tectonic plates. First, the transition from continental to oceanic crust is abrupt, with crustal thicknesses decreasing from over 20 km to less than 10 km over distances of 50 to 80 km. Second, since the dominant direction of crustal extension is sub-parallel to the transform boundary, complex rift basins develop along the continental sides of the transform that include a spectrum of structural trends. Third, high-standing marginal ridges, rising one to three km over the abyssal sea floor with 50 to 100 km widths, form on the continental side of the margin. Marginal ridge formation is probably due to absorbed heat from juxtaposed oceanic crust as the ridge transform intersection (RTI) moves along the plate boundary; however, the structural history of some

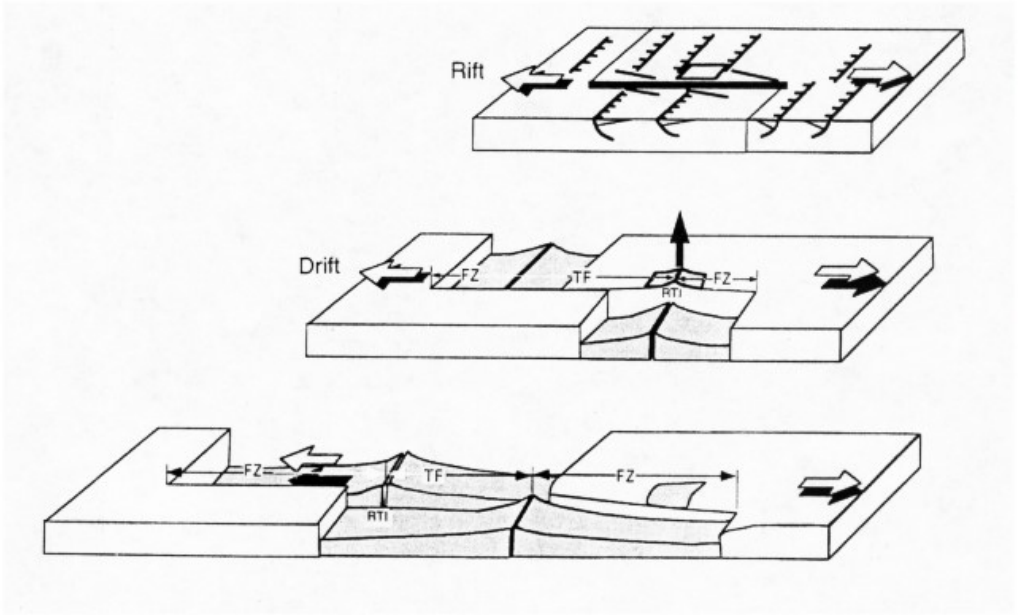

Figure 1.1

Generic three-stage model for shear margin formation (after Lorenzo, 1997, p. 2): 1) Rift: continent – continent shearing, 2) Drift: continent – ocean transform boundary (active margin), and 3) Passive margin: continent – ocean fracture zone boundary.

shear margins is complex and constructional component(s) to marginal ridge development cannot be ruled out. These marginal ridges effectively trap prograding sediments resulting in thick accumulations of rift and drift sequences.

1.2 Gulf of Guinea

The Côte d'Ivoire – Ghana transform margin formed along the Gold Coast as the South Atlantic Ocean opened. The ENE trending transform margin intersects the NNE trending cratonic Akwapim Fault Zone (Figure 1.2a), a Pan-African suture formed about 600 Ma (Edwards *et al.*, 1997). The continental crust approaching the transform margin thins, over a distance of about 20 km from 23 to 10 km (Figure 1.2b). Seismic refraction data indicate that outboard of continental crust, typical fracture zone and ocean crustal thicknesses are 3.5 to 5 km and about 7 km (Edwards *et al.*, 1997). The oceanic crust is believed to be 80 Ma old.

The Côte d'Ivoire – Ghana Marginal Ridge buttresses sediments of the deep Ivorian Basin to the north and rises 2.5 km over the abyssal plain to the south. Its overall length and width are about 130 and 25 km (Basile *et al.*, 1993). Figure 1.2c shows a N-S reflection seismic line across the Côte d'Ivoire – Ghana transform margin. Ocean Drilling Program drill sites 959 and 960 (Leg 159) reveal continuous sedimentation throughout Cretaceous time: intensely deformed deltaic – lacrustrine sequence overlain by an undeformed clastic – carbonate sequence. Figure 1.3 shows free air gravity anomalies over the Gulf of Guinea.

Figure 1.2

a) Physiography of the Gulf of Guinea and Côte d'Ivoire – Ghana shear margin (after Edwards et al., 1997, p.13). RFZ, CFZ, ChFZ, and StPFZ are Romanche, Chain, Charcot, and St. Paul Fracture Zones respectively; BT is Benue Trough.
b) Density model along transect shown in Figure 1.2a (after Edwards et a., 1997, p. 14). Density units are g/cc.
c) Reflection seismic line over the Côte d'Ivoire – Ghana transform margin (after Clift et al., 1997, p. 484).

a)

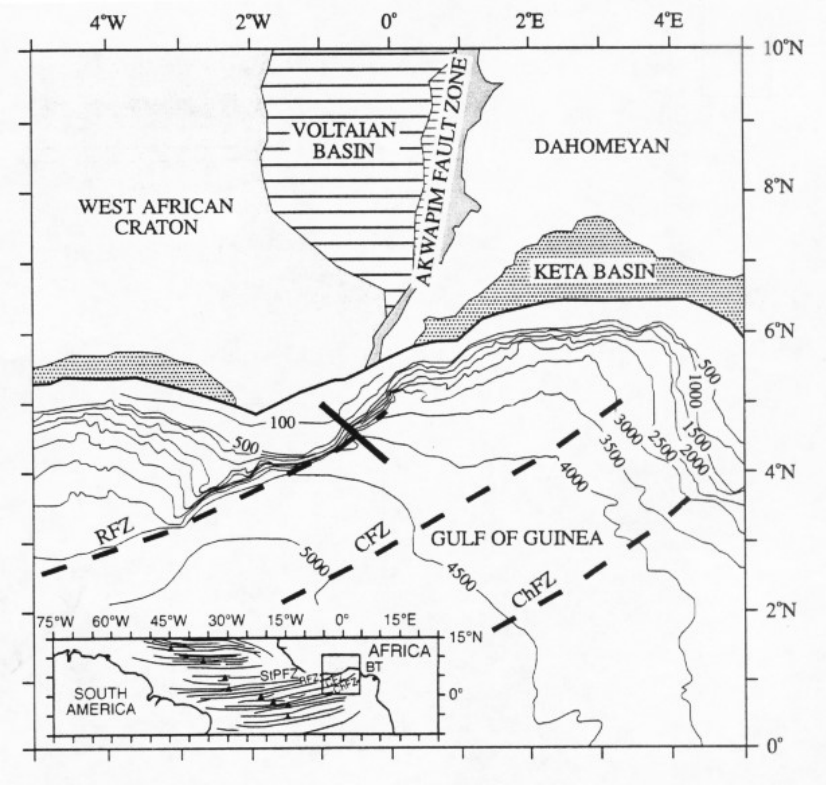
4°W
2°W
0°
2°E
4°E
10°N
8°N
6°N
4°N
2°N
0°
VOLTAIAN BASIN
AKWAPIM FAULT ZONE
DAHOMEYAN
WEST AFRICAN CRATON
KETA BASIN
100
500
1000
1500
2000
2500
3000
3500
4000
4500
5000
RFZ
CFZ
ChFZ
GULF OF GUINEA
75°W
60°W
45°W
30°W
15°W
0°
15°E
15°N
0°
AFRICA
SOUTH AMERICA
SPFZ
BT

b)

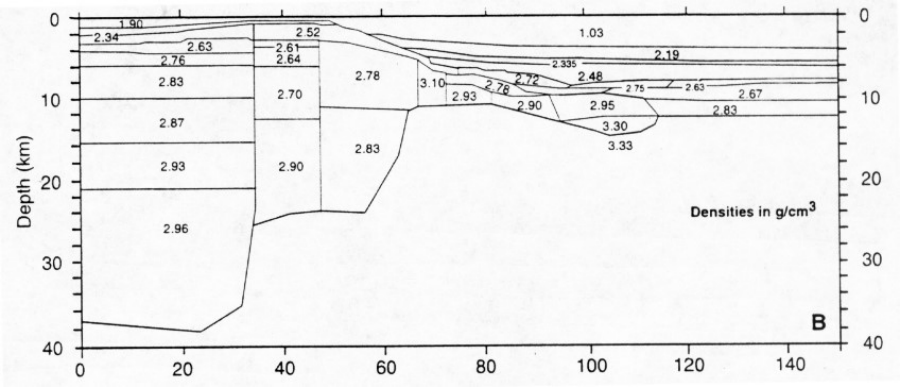
Depth (km)
0
10
20
30
40
0
20
40
60
80
100
120
140
1.90
2.34
2.63
2.76
2.83
2.87
2.93
2.96
2.52
2.61
2.64
2.70
2.90
2.78
2.83
3.10
2.93
2.72
2.76
2.90
1.03
2.335
2.19
2.48
2.75
2.63
2.67
2.95
2.83
3.30
3.33
Densities in g/cm3
B

c)

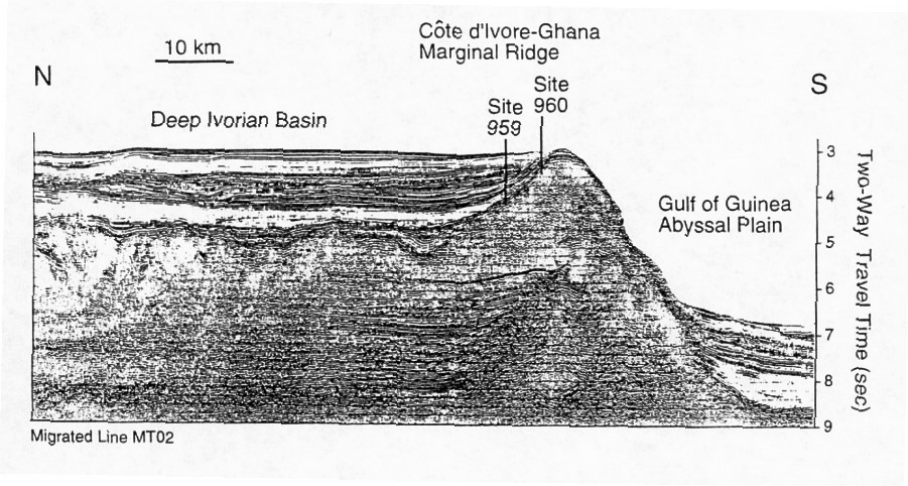
10 km
Côte d'Ivore-Ghana
Marginal Ridge
N
S
Site 959
Site 960
Deep Ivorian Basin
Gulf of Guinea
Abyssal Plain
Two-Way Travel Time (sec)
3
4
5
6
7
8
9
Migrated Line MT02

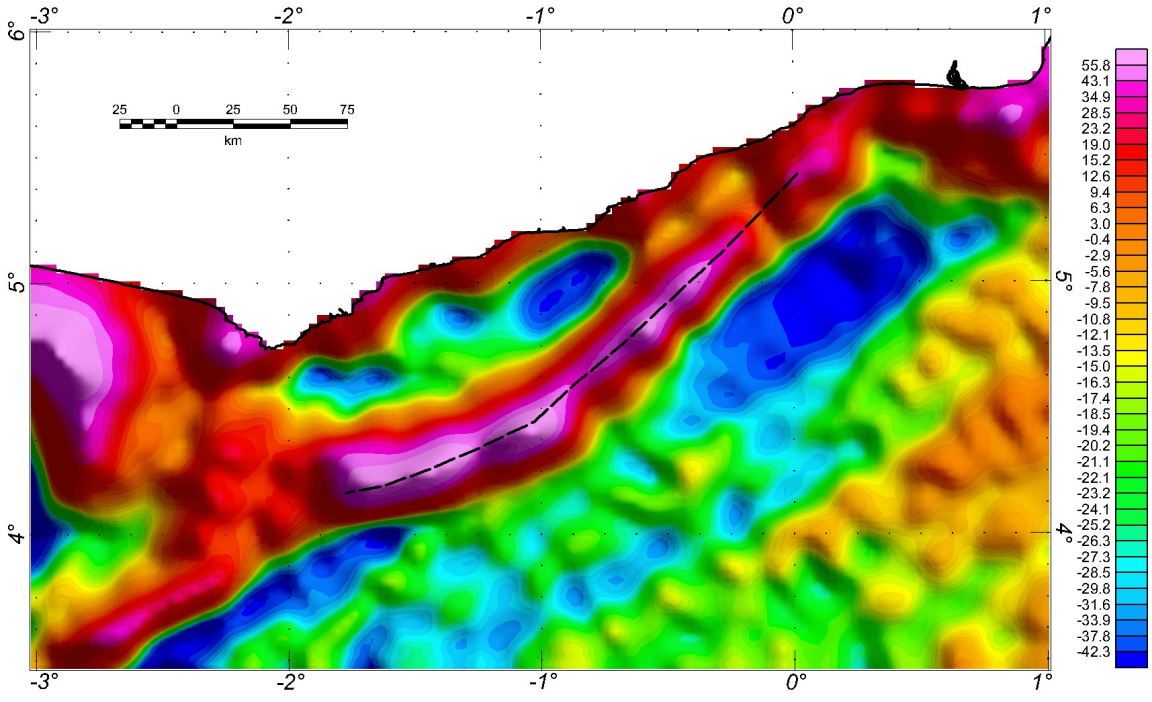

Figure 1.3

Offshore satellite-derived free air gravity anomalies over the Côte d'Ivoire – Ghana fracture zone margin.. The dashed line traces the marginal ridge.

1.3 Davie Fracture Zone

The N-S trending Davie Fracture Zone in the Mozambique Channel (Figure 1.4) is a fossil transform fault that formed during the Late Jurassic to Early Cretaceous southward drift of Madagascar-Antarctica-India ("Greater Antarctica"), and the opening of the West Somali Basin (Droz and Mougenot, 1987). The ridge longitudinally bisects the channel from the northern coast of Mozambique to the southwestern coast of Madagascar.

Based on morphology, Mascle *et al.* (1987) divided the channel into three regions: 1) 9º to 13º S, 2) 13º to 17º S, and 3) 17º to 20º S. They report that gravity data in the north indicate a strong crustal change and interpreted an anomaly that coincides with the transition from continental to oceanic crust. East dipping horst blocks in the central part of the ridge may be related to Late Cretaceous rifting and the northward drift of India. To the south in the Mozambique Upper Fan, reflection seismic data reveal disconnected, NW-SE trending anticlines. The offshore Zambezi Valley serves as a conduit for sediment deposition SE of Mozambique, but deposition is restricted farther east by the Davie Ridge (Droz and Mougenot, 1987).

1.4 Owen Fracture Zone

The NNE oriented Owen Fracture Zone extends from the Northern Somali Basin through the Carlsberg Ridge to the Makran Subduction Zone (Figure 1.5). It records the Late Cretaceous to Paleogene northward motion of India. The Owen Basin, which formed in Late Jurassic to Early Cretaceous, is coincident with the breakup of Gondwanaland and the formation of the Somali Basins (Minshull *et al.*, 1992). The Owen Fracture Zone is

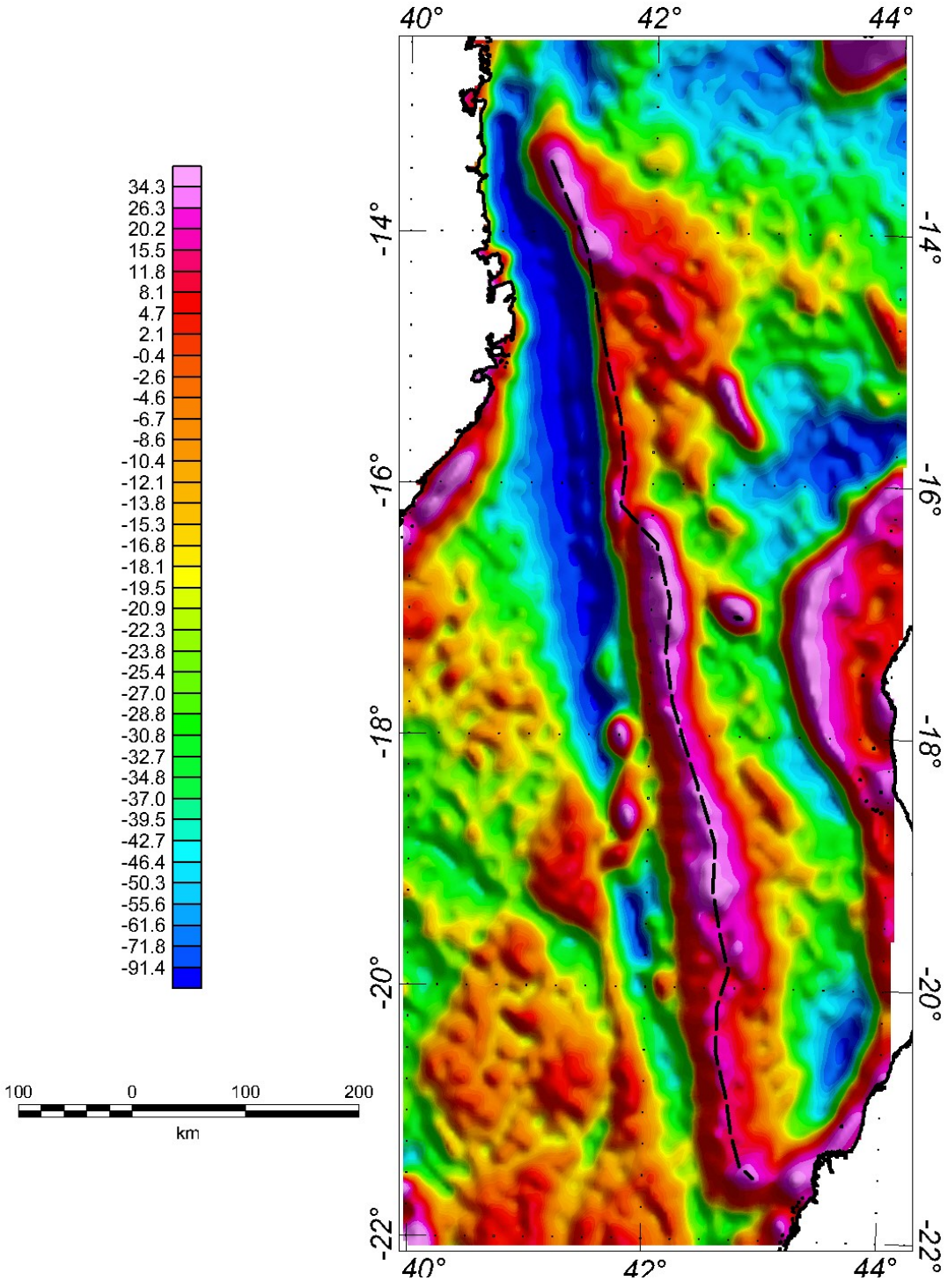

Figure 1.4

Offshore satellite-derived free air gravity anomalies over the Davie fracture zone margin. The dashed line traces the marginal ridge.

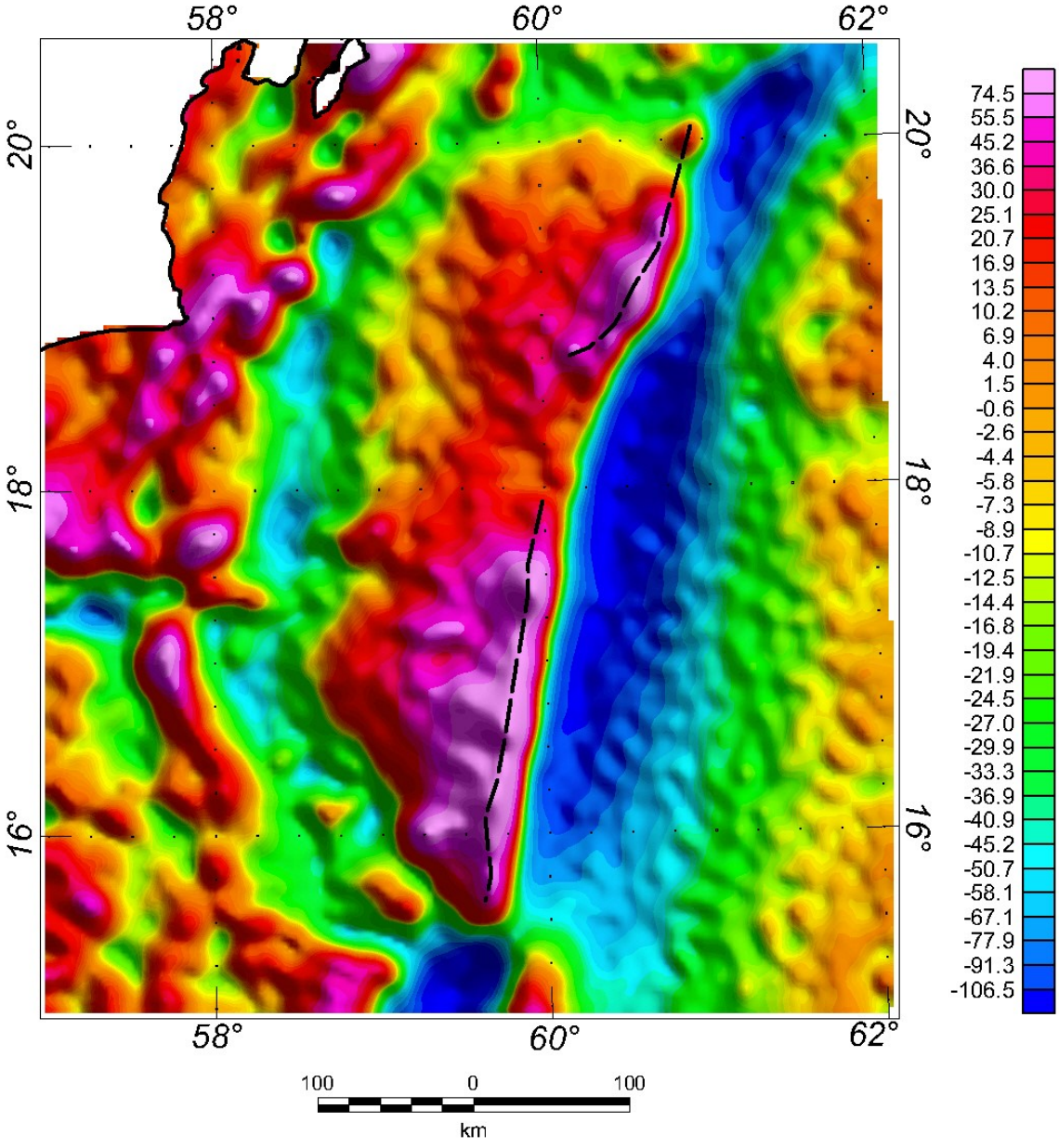

Figure 1.5

Offshore satellite-derived free air gravity anomalies over the Owen fracture zone margin. The dashed line traces the marginal ridge.

probably a transform fault, although slip along the boundary is by far the slowest in the world: 2 mm/a right lateral motion (Gordon and DeMets, 1989). The Owen Ridge, NW of the Owen Fracture Zone, limits and traps sediment deposition from the Saudi Arabian Peninsula.

1.5 Southern Exmouth Plateau

Lorenzo *et al.* (1991) proposed a two-stage model for the continent – ocean transform boundary formation south of the Exmouth Plateau, northwestern Australia (Figure 1.6). The Exmouth Plateau is a continental block that was deformed during Jurassic rifting prior to Early Cretaceous sea-floor spreading in the Indian Ocean. During the rift stage, detachment surfaces formed by right lateral strike-slip motion and fault block rotation. During the drift stage, thermal conditions and seafloor spreading resulted in magmatic underplating beneath the continental side of the margin. Lorenzo *et al.* (1991) have mapped a prominent basement ridge (marginal) and suggest that it is a zone of igneous intrusion. Lorenzo and Vera (1992) estimate marginal ridge uplift lead to erosion of up to 3.5 km of sediments such that 1000 km^3 of sediments are eroded for every 10 km of transform length.

1.6 Agulhas – Falkland Fracture Zone

The Agulhas – Falkland Fracture Zone is one of the Earth's most spectacular transform / fracture zone systems. Its Early Cretaceous 1200 km offset, coinciding with the

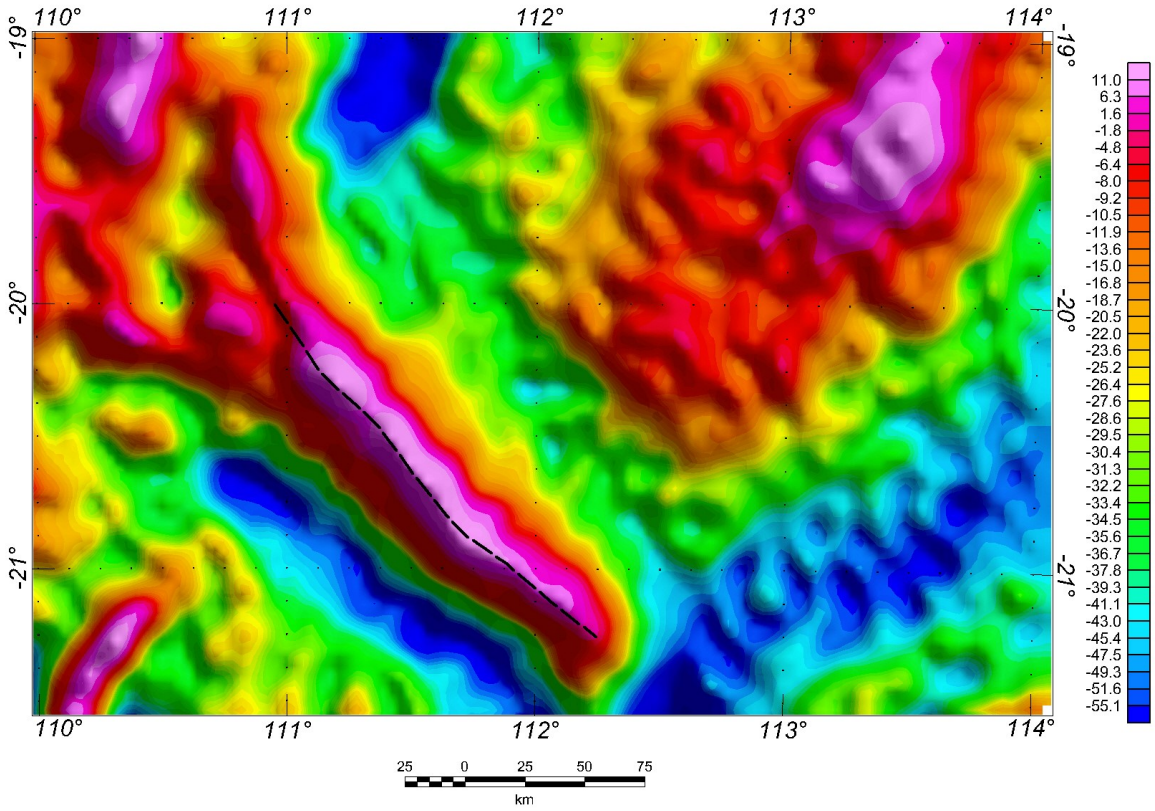

Figure 1.6

Offshore satellite-derived free air gravity anomalies over the fracture zone margin along the southwest margin of the Exmouth Plateau. The dashed line traces the marginal ridge.

breakup of Western Gondwana, made it a giant class transform fault, similar to the San Andreas and Dead Sea transforms (Ben-Avraham *et al.*, 1997). Ben-Avraham *et al.* (1997) also report that this offset endured for about 65 Myr (from 130 to 65 Ma) until a major ridge jump reduced its size to about 180 km.

The Falkland Plateau and Basin is a foundered complex of oceanic and continental blocks that traveled along the Algulhas – Falkland Fracture Zone after Middle Jurassic separation of Antarctica from Africa and South America (Lorenzo and Wessel, 1997). Along the northern edge of the Plateau a prominent marginal ridge forms the Falkland Escarpment and rises as much as 2 km over the South Atlantic Ocean (Figure 1.7). Lorenzo and Wessel (1997) report that the transition from oceanic to continental crust is less than 50 km wide. They suggested that mechanical coupling and thermal subsidence of oceanic and continental crust after the ridge segment passed caused the continental and oceanic sides of the margin flex towards each other.

SE of the Agulhas Bank and Mallory Trough, offshore South Africa, the Agulhas Marginal Fracture Ridge and the Diaz Ridge (Figure 1.8) form an overlapping, en-echelon trap for sediment deposition to the NW (Ben-Avraham *et al.*, 1997). Lower units in the Mallory Trough and Southern Outeniqua Basin (NW of the Diaz Ridge) consist of rotated blocks related to transverse rifting and formation of the continent – ocean shear margin. (Ben-Avraham *et al.*, 1997).

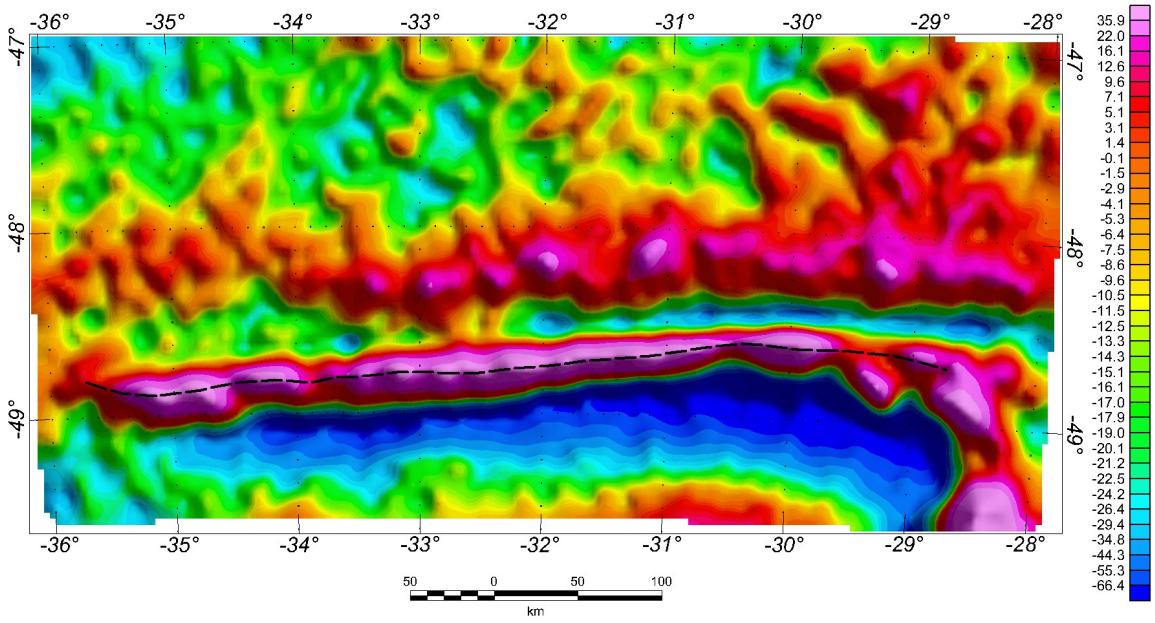

Figure 1.7

Offshore satellite-derived free air gravity anomalies over the fracture zone margin along the northern Falkland Plateau and Maurice Ewing Bank. The dashed line traces the marginal ridge.

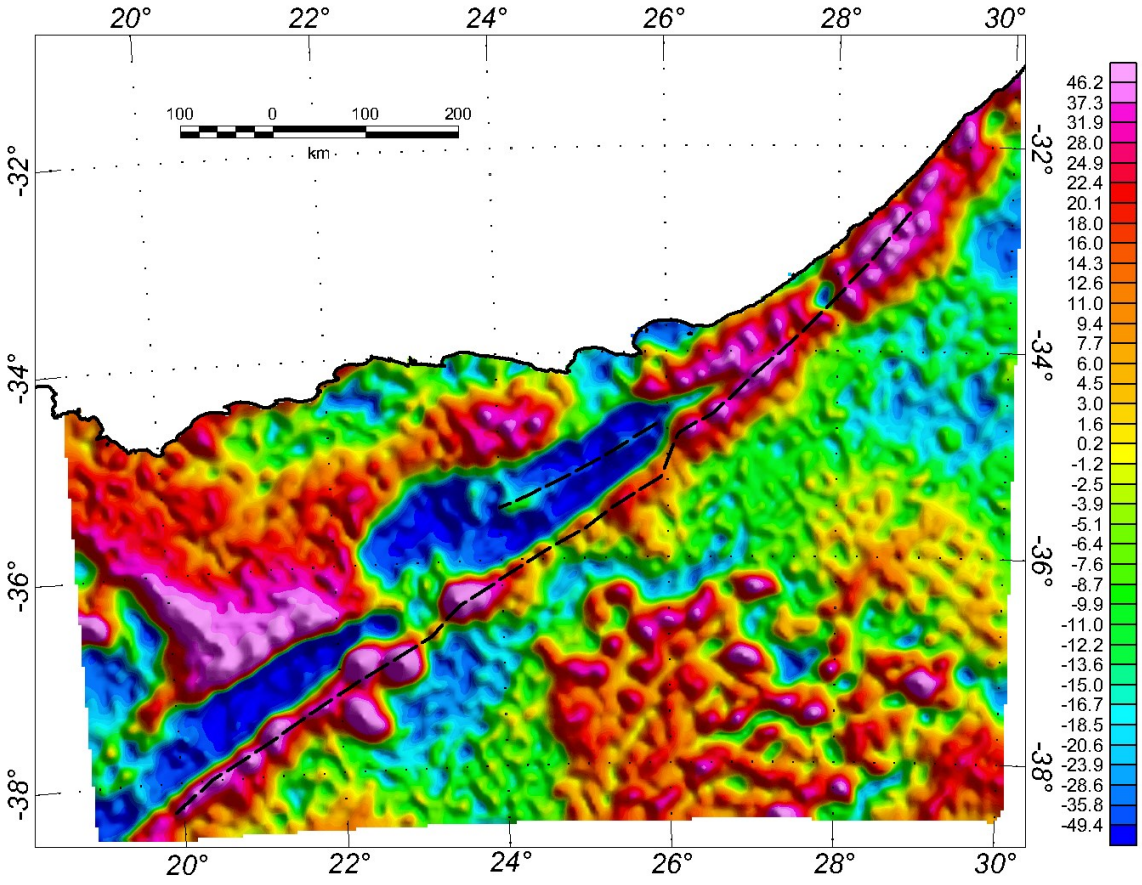

Figure 1.8

Offshore satellite-derived free air gravity anomalies over the Agulhas – Falkland fracture zone off South Africa. The dashed line traces the marginal ridge.

1.7 Queen Charlotte Transform Margin

The Queen Charlotte Transform Margin (Figure 1.9) extends from the Queen Charlotte triple junction (Pacific, Juan de Fuca and North American Plates) to the south Alaskan subduction zone and has been stable for 40 Ma (Prims *et al.,* 1997). Relative motion along the boundary is 50 mm/a right-lateral. Discrepancies in the relative directions of plate motions imply a component of convergence along the boundary. Hence, Prims *et al.* (1997) suggested that the Queen Charlotte Trough formed by transpressional flexure, related to10 to 15 km of Pacific Plate underthrusting, over the past 5 Ma. The marginal ridge along the boundary is the Queen Charlotte Islands and Terrace.

Mackie *et al.* (1989) proposed two evolutionary models including possible oblique Pacific Plate subduction. One model assumed oblique subduction while the other assumed only dextral slip along the boundary. They preferred oblique subduction, but noted crustal thickening and lateral distortion are also possible. Refraction experiments indicate: anomalous crustal velocities to the west of the Queen Charlotte Terrace and above the mantle; 21 to 27 km thick crust beneath Queen Charlotte Islands; and gentle crustal thinning to the mainland (Mackie *et al.,* 1989). Finally, they report that an obliquely subducting slab would extend no further than the 30 km thick crust of the mainland.

1.8 Northeastern Canada

The Southwest Newfoundland Transform Margin (Figures 1.10 and 1.11, between 40°N and 45°N) developed in response to Early Jurassic separation of North American and

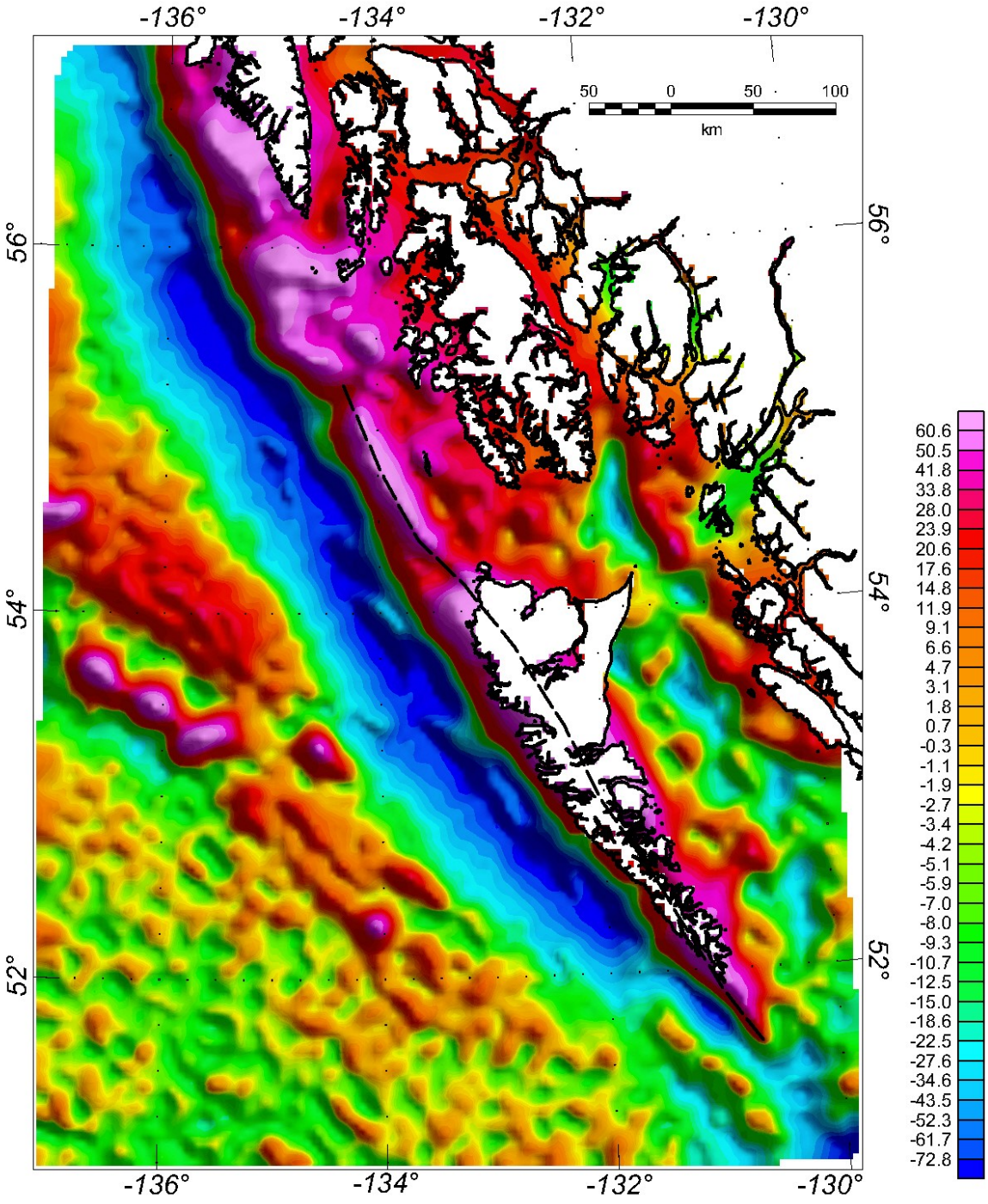

Figure 1.9

Offshore satellite-derived free air gravity anomalies over the Queen Charlotte Islands transform margin. The dashed line traces the marginal ridge.

Figure 1.10

Offshore satellite-derived free air gravity anomalies over the fracture zone margins of southern Grand Banks (the Newfoundland transform margin), southern Baffin Island (the Ungava transform margin), and northern Baffin Bay. The dashed line traces the marginal ridge.

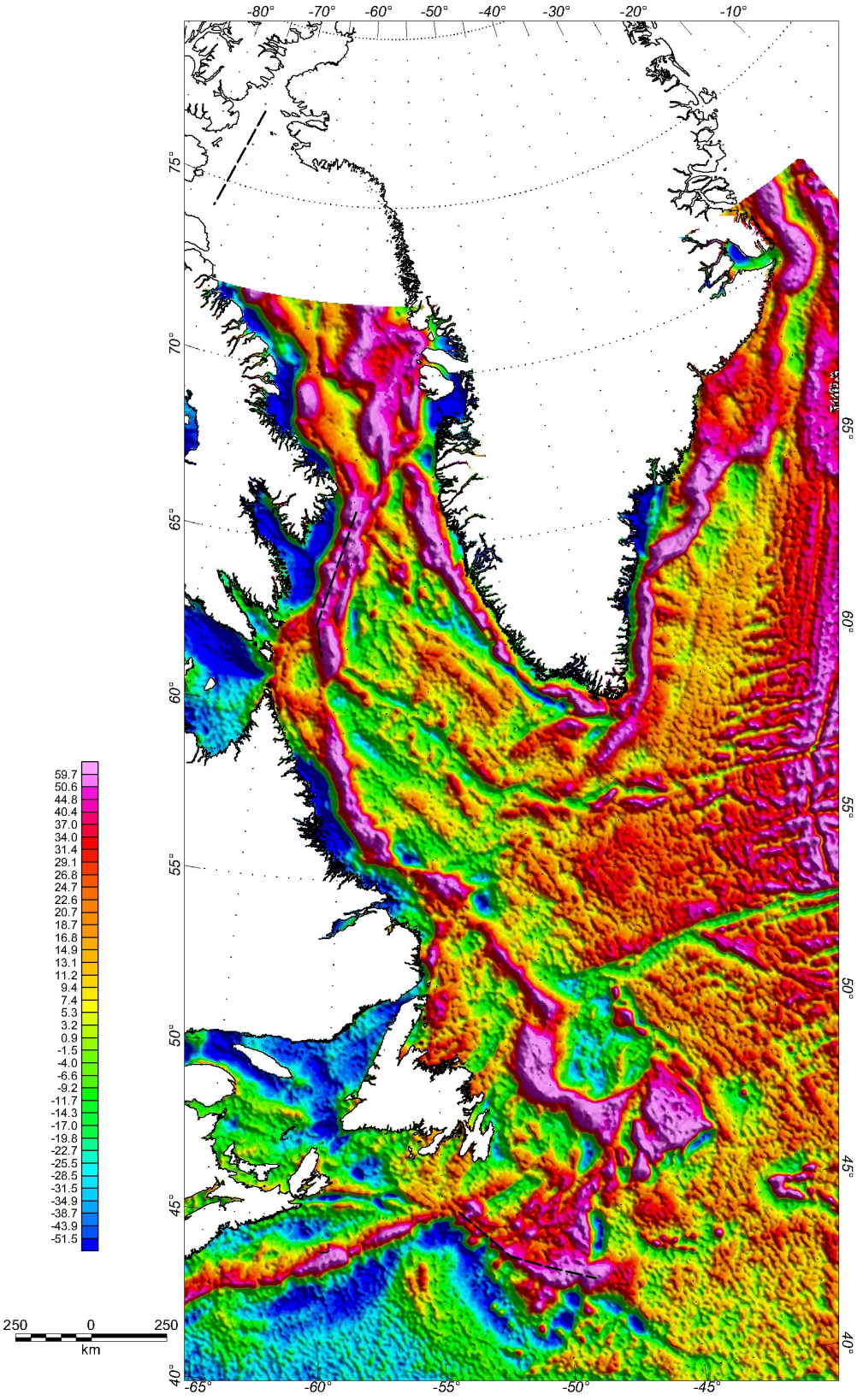
-80°
-70°
-60°
-50°
-40°
-30°
-20°
-10°
75°
70°
65°
60°
55°
50°
45°
40°
-65°
-60°
-55°
-50°
-45°
59.7
50.6
44.8
40.4
37.0
34.0
31.4
29.1
26.8
24.7
22.6
20.7
18.7
16.8
14.9
13.1
11.2
9.4
7.4
5.3
3.2
0.9
-1.5
-4.0
-6.6
-9.2
-11.7
-14.3
-17.0
-19.8
-22.7
-25.5
-28.5
-31.5
-34.9
-38.7
-43.9
-51.5
250
0
250
km

Figure 1.11

Total intensity magnetic anomaly anomalies over the fracture zone margins of southern Grand Banks (the Newfoundland transform margin), southern Baffin Island (the Ungava transform margin), and northern Baffin Bay. The dashed line traces the marginal ridge.

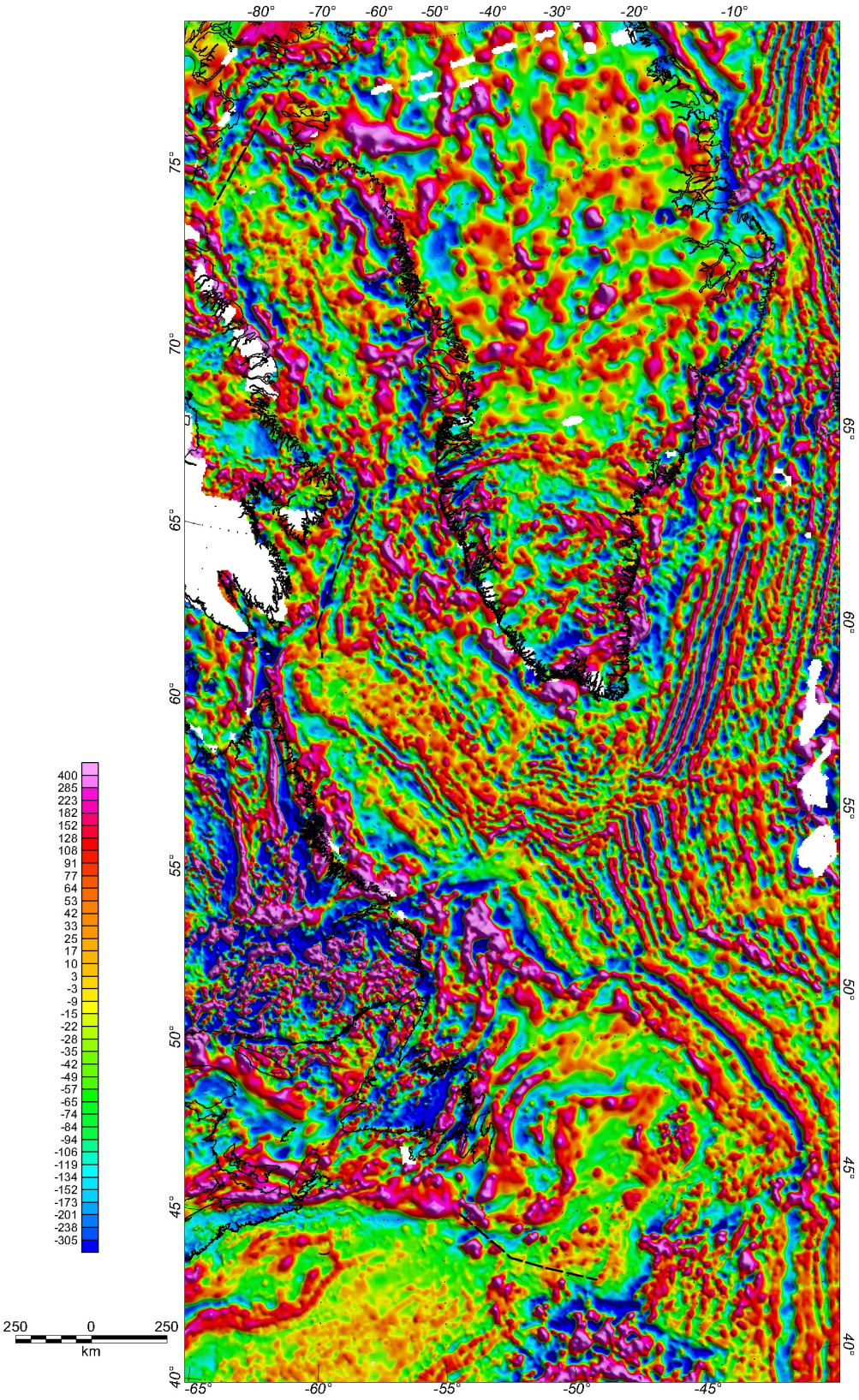
-80°
-70°
-60°
-50°
-40°
-30°
-20°
-10°
75°
70°
65°
60°
55°
50°
45°
40°
65°
60°
55°
50°
45°
40°
-65°
-60°
-55°
-50°
-45°
400
285
223
182
152
128
108
91
77
64
53
42
33
25
17
10
3
-3
-9
-15
-22
-28
-35
-42
-49
-57
-65
-74
-84
-94
-106
-119
-134
-152
-173
-201
-238
-305
250
0
250
km

African Plates. The crust thins from just over 20 km to about 6 km beneath an apparent slice of obducted oceanic crust along the transform margin (Reid and Jackson, 1997). A marginal ridge does not exist along this margin, probably due to tectonic processes different from other shear margins since obducted oceanic crust exists onto the island.

Since deep seismic data do not exist across the Ungava Transform Margin (Figures 1.10 and 1.11, between 60°N and 65°N), regional crustal thicknesses were estimated by inversion of gravity data (Reid and Jackson, 1997). Crustal thinning of continental to oceanic crust (35 km to 12 km) spans 50 km. The inversion model revealed only a slight expression of a marginal ridge, but Reid and Jackson (1997) noted that the margin is slightly oblique to the spreading direction.

The northern Baffin Bay margin (Figures 1.10 and 1.11, north of 75°N) is complex and affected by transcurrent, extension and compressional forces related to interaction between Greenland and North American Plate motions. Offshore basement structures reveal basin forming normal faults, flower structures and folding (Reid and Jackson, 1997). Continent – ocean crustal thinning occurs over 60 km, from 28 to 10 km. The existence of a marginal ridge cannot be confirmed.

1.9 Senja Fracture Zone

The Senja Fracture Zone (Figures 1.12 and 1.13) formed in response to the formation of the Norwegian Greenland Sea (Vågnes, 1997) at about 57 Ma (Paleocene – Eocene boundary). Sea floor extension was nearly parallel to the coast, but shifted to nearly east-west at 35 Ma (Eocene – Oligocene boundary). Then, due to oblique rifting, the active

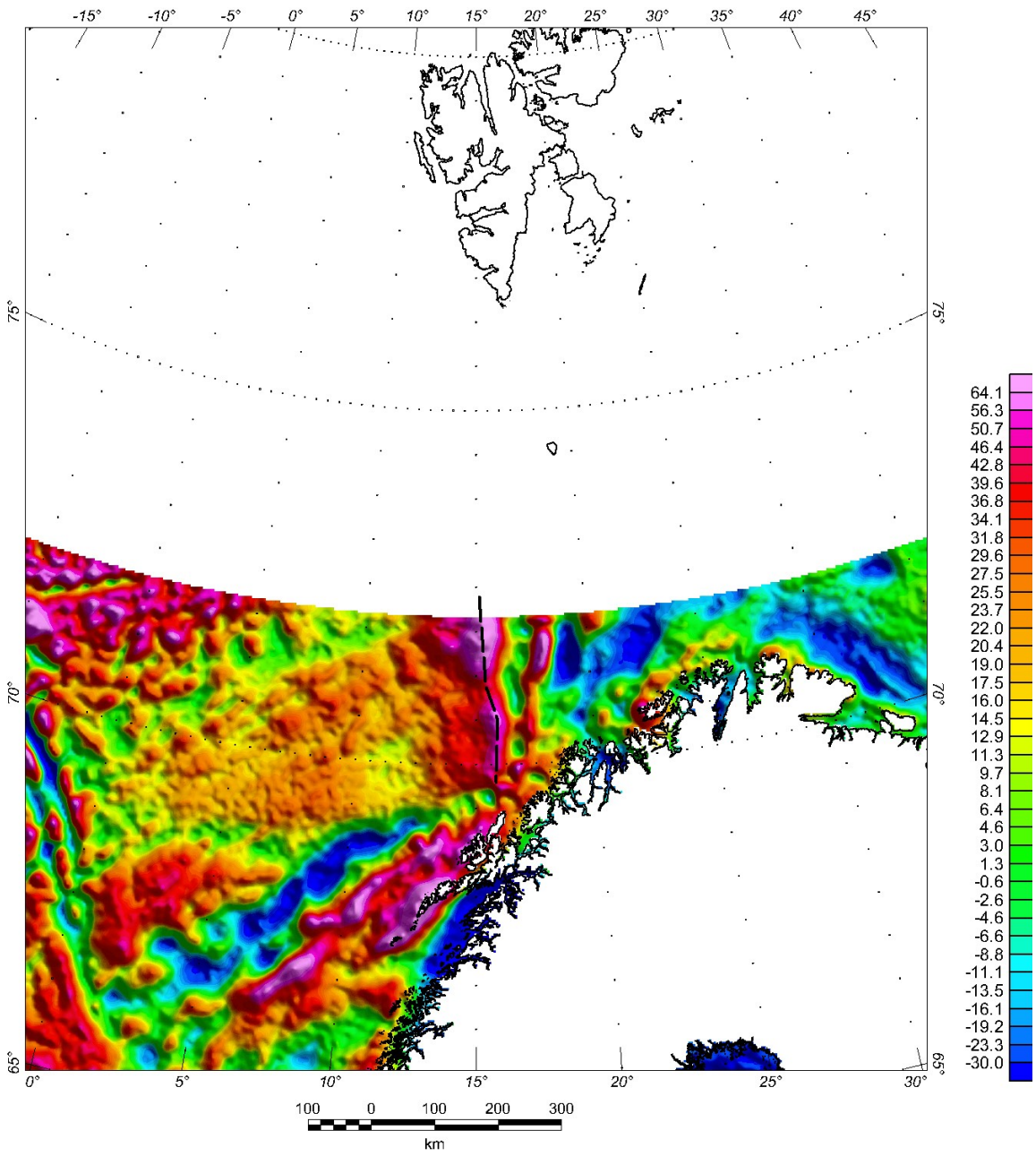

Figure 1.12

Offshore satellite-derived free air gravity anomalies over the Senja fracture zone. The dashed line traces the marginal ridge.

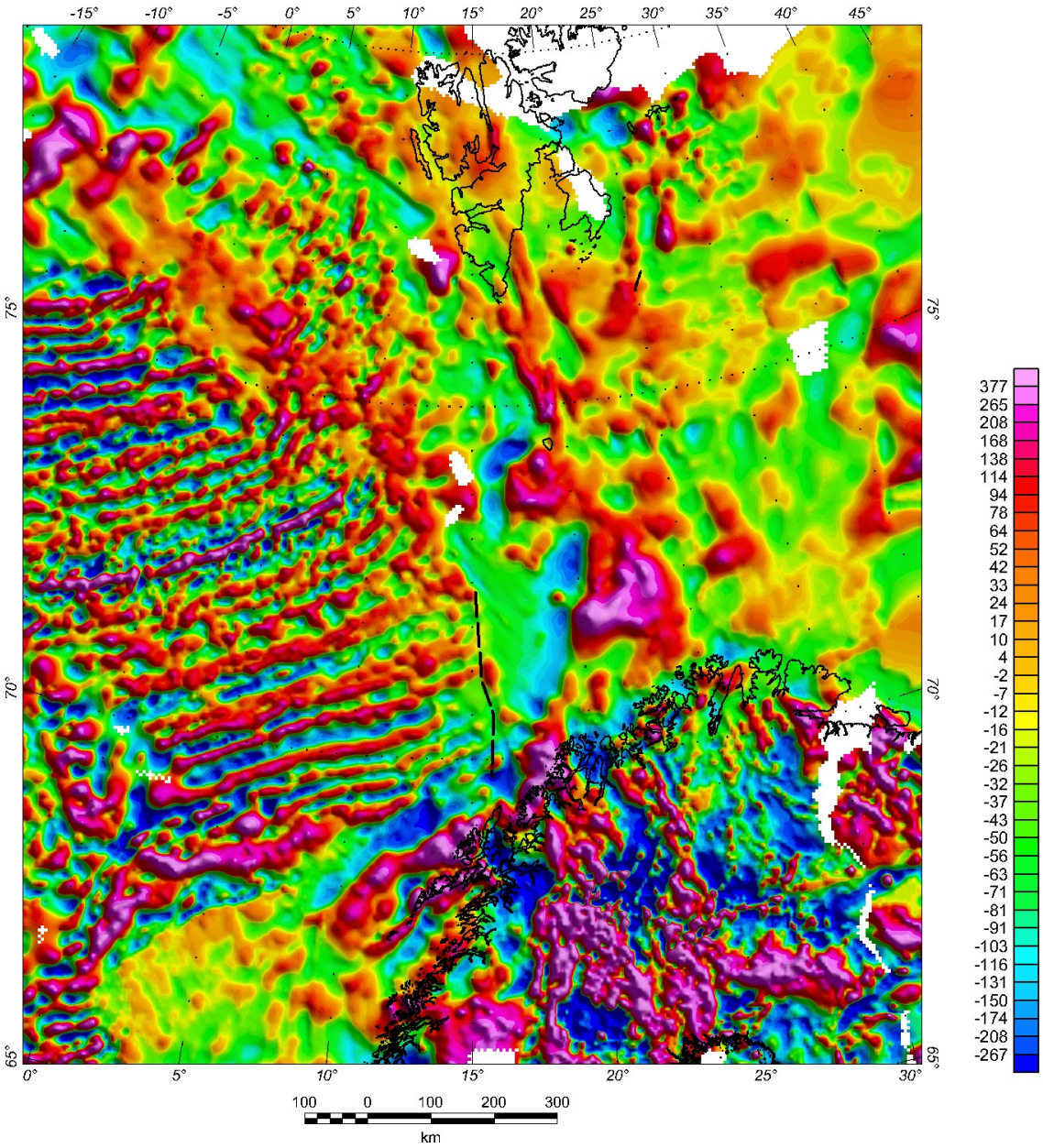

Figure 1.13

Total intensity magnetic anomalies over the Senja fracture zone. The dashed line traces the marginal ridge.

transform became part of the present Knipovich spreading axis (Vågnes, 1997), so the margin was active for ~21 Ma. This timing, and preservation of predrift sediments along the margin, provide good constraints for estimating the amount of erosion. Vågnes (1997) reported that uplift began after the initial formation of the Senja Fracture Zone and lasted until Middle or Late Eocene and further estimated the maximum amount of erosion near the transform to be 1.5 km.

1.10 Marginal Ridge Formation

Vågnes (1997) compared thermal models based on conduction only with models based on combined conduction and advection related to viscous coupling of lower, ductile lithosphere. Results of these experiments show that more heat is predicted from the combined model, but uplift is only half that predicted by the conductive only model. Vågnes (1997) compared model results with erosion estimates from the Senja Transform margin and found that predicted uplift from the combined model corresponds best to erosion estimates.

Gadd and Scrutton (1997) calculate 1300 to 1400 m of uplift from thermal effects for a 900 km long transform segment, but note that it is reduced to 335 to 470 m when considering regional isostatic effects. They also report that the amount of uplift depends on the degree of ocean – continent coupling. Frictional heating is negligible, contributing only 5% of that from conduction (Gadd and Scrutton, 1997). Todd and Keen (1989) modeled thermal effects of a 500 km long transform segment with spreading half-rates of 10 and 40

mm/a and report that over 2 km of crustal uplift may occur at the margin and decreases over a distance of 60 to 80 km away from the margin.

Dewey (1975) demonstrated that the deformation of rock masses at plate boundaries, in a system where more than three plates are in relative motion, can be complicated with the formation of transpressional and transtentional structures. Therefore the constructional formation of shear margins cannot be ruled out.

1.11 Conclusion

The evolution of shear margins typically involves continental rifting and intensly deformed rift sequences over rotated basement blocks. As the sea-floor spreading axis moves along the margin thermal processes produce a marginal ridge that traps sediments allowing thick sedimentary sequences to accumulate. After the ridge axis passes the margin is characterized by typical thermal subsidence.

2. GULF OF MEXICO TECTONIC HISTORY: HOTSPOT TRACKS, CRUSTAL BOUNDARIES, AND EARLY SALT DISTRIBUTION

2.1 Abstract

A Late Jurassic mantle plume may have generated hotspot tracks on the North American plate and Yucatan block as the Gulf of Mexico opened (ca. 150 Ma). The tracks are identified from deep basement structural highs that have been mapped by integrating seismic refraction and gravity data. They are associated with high-amplitude, distinctive gravity anomalies that provide the basis for a kinematic reconstruction that restores the western ends of the hotspot tracks with a 20° clockwise rotation of the Yucatan block, or almost one-half the total rotation required to open the Gulf of Mexico basin. The duration of track generation is estimated to have been about 8 to 10 My, or almost one-half the total time required to open the Gulf of Mexico basin. Prior to this rotation, extension of continental crust over a 10 to 12 My interval was the result of approximately 22° of counterclockwise rotation and crustal thinning. Autochthonous salt appears to be confined to the continental flanks of the hotspot tracks confirming that salt deposition occurred primarily during continental extension and ended shortly after ocean floor had begun to form. A prominent gravity anomaly along the western boundary of the basin is interpreted to be produced by a marginal ridge, which was created along the ocean-continent transform boundary as the basin opened. The eastern flank of this marginal ridge, and the northernmost, easternmost, and southernmost terminations of the hotspot tracks, are interpreted to coincide with the oceanic-continental crustal boundary in the basin.

2.2 Introduction

The shape of the Gulf of Mexico requires that at least one ocean-continent transform boundary was active while the basin was opening. Evolutionary models differ between those that require the basin to open by rotation along a single ocean-continent transform boundary, and those that require the basin to open by rotation along a pair of parallel ocean-continent transform boundaries. Although many models have been proposed most workers now agree that counterclockwise rotation of the Yucatan Peninsula block away from the North American Plate, involving a single ocean-continent transform boundary, led to the formation of the basin; and many of these workers suggest that this rotation occurred between 160 Ma (Callovian) and 140 Ma (Valanginian) about a pole located within 5° of Miami, Florida (Buffler and Thomas, 1994; Burke, 1988; Christenson, 1990; Dunbar and Sawyer, 1987; Hall and Najmuddin, 1994; Humphris, 1979; Marton and Buffler, 1994; Pindell, 1985, 1994; Ross and Scotese, 1988; Salvador, 1987, 1991; Shepherd, 1983). Evidence cited for this model of basin evolution includes paleomagnetic data from the Chiapas massif of the Yucatan Peninsula (Gose *et al.*, 1982; Molina-Garza *et al.*, 1992), fracture zone trends interpreted from magnetic data (Hall and Najmuddin, 1994; Shepherd, 1983), non-rigid tectonic reconstruction (Dunbar and Sawyer, 1987; Marton and Buffler, 1994), and kinematic reconstructions making use of geological constraints, well data, and geophysical data such as seismic refraction, gravity and magnetics (Christenson, 1990; Marton and Buffler, 1994; Pindell, 1985, 1994).

Determining the tectonic events that contributed to the formation and evolution of the Gulf of Mexico depends on an ability to define the size, shape and extent of major structures within the basin and at its margins. Integrating gravity and seismic refraction data to interpret the Gulf of Mexico basin has been used since the mid-1960s (Dehlinger and Jones, 1965; Ebeniro *et al.*, 1986; Hales *et al.*, 1970a; Martin and Case, 1975; Mooney *et al.*, 1983; Moore and del Castillo, 1974). Qualitatively, these data have been combined to interpret the extent of basin structures and regions of varying crustal thickness (Ebeniro *et al.*, 1986; Martin and Case, 1975). Quantitatively, 2D forward modeled cross sections have been constructed to test the gravitational response of basin structures and density distributions. Models can be constrained by depths interpreted from refraction and well data, and densities obtained from wells or converted from refraction velocities (Dehlinger and Jones, 1965; Grant and West, 1965; Hales *et al.*, 1970b; Mooney *et al.*, 1983; Moore and del Castillo, 1974). Integrating gravity and seismic refraction data is useful because the depth to anomaly source ambiguity associated with gravity data can be reduced by refraction depths, and the localized nature of refraction data can be extrapolated away from, or interpolated between, acquisition locations using the areal coverage provided by gravity data.

Gravity data over the Gulf of Mexico includes onshore Bouguer gravity anomalies compiled by the Society of Exploration Geologists (SEG) and the U.S. Geological Survey and offshore satellite-derived free air gravity anomalies (Figure 2.1). Global satellite-derived gravity data have been calculated from satellite altimetry data acquired during the Geosat Geodetic Mission and the ERS 1 Geodetic Phase along closely spaced satellite tracks (Sandwell and Smith, 1997). The reported data resolution is

Figure 2.1

Gulf of Mexico region gravity anomalies. Offshore satellite-derived free air, and onshore Bouguer, gravity anomalies. Open circles around Florida are proposed Euler pole locations given in Table 1 and yellow circles connected by lines along the Keathley Canyon (KC) and Yucatan Parallel (YP) hotspot tracks (outlined anomalies) are calculated at 5° increments to a total of 20° counterclockwise rotation of the Yucatan Block about an Euler Pole interpreted by Hall and Nadjmuddin (1994). A generalized spreading center (white line) separates conjugate plume tracks between the North American Plate and the Yucatan Block. After approximately 10° of rotation the spreading center is interpreted to have passed over the plume (dashed line connecting open circles between KC and YP anomalies), leaving another approximate 10° of rotation of the Yucatan Block over the plume. Gravity anomaly signatures: SN = Sisgbee Nappe; MF = Mississippi Fan; TC = Thin Crust; CB = Carbonate Buildups; SCS = South Campeche Salt Nappe; RGD = Rio Grande Delta; TGLC = Tamaulipas – Golden Lane – Chiapas marginal ridge; YP = Yucatan Parallel anomaly; KC = Keathley Canyon anomaly. The NW-SE dotted line over the KC and YP anomalies is the profile location of the marine and satellite-derived free air gravity data comparison shown in Figure 2. Satellite gravity data is available as a 2 arc-minute grid and can be downloaded from the internet at http://topex.ucsd.edu/marine_grav/mar_grav.html; the SEG gravity data is available as a 4 kilometers grid from the U.S. Department of Commerce, National Oceanic and Atmospheric Administration (NOAA), National Geophysical Data Center (NGDC).

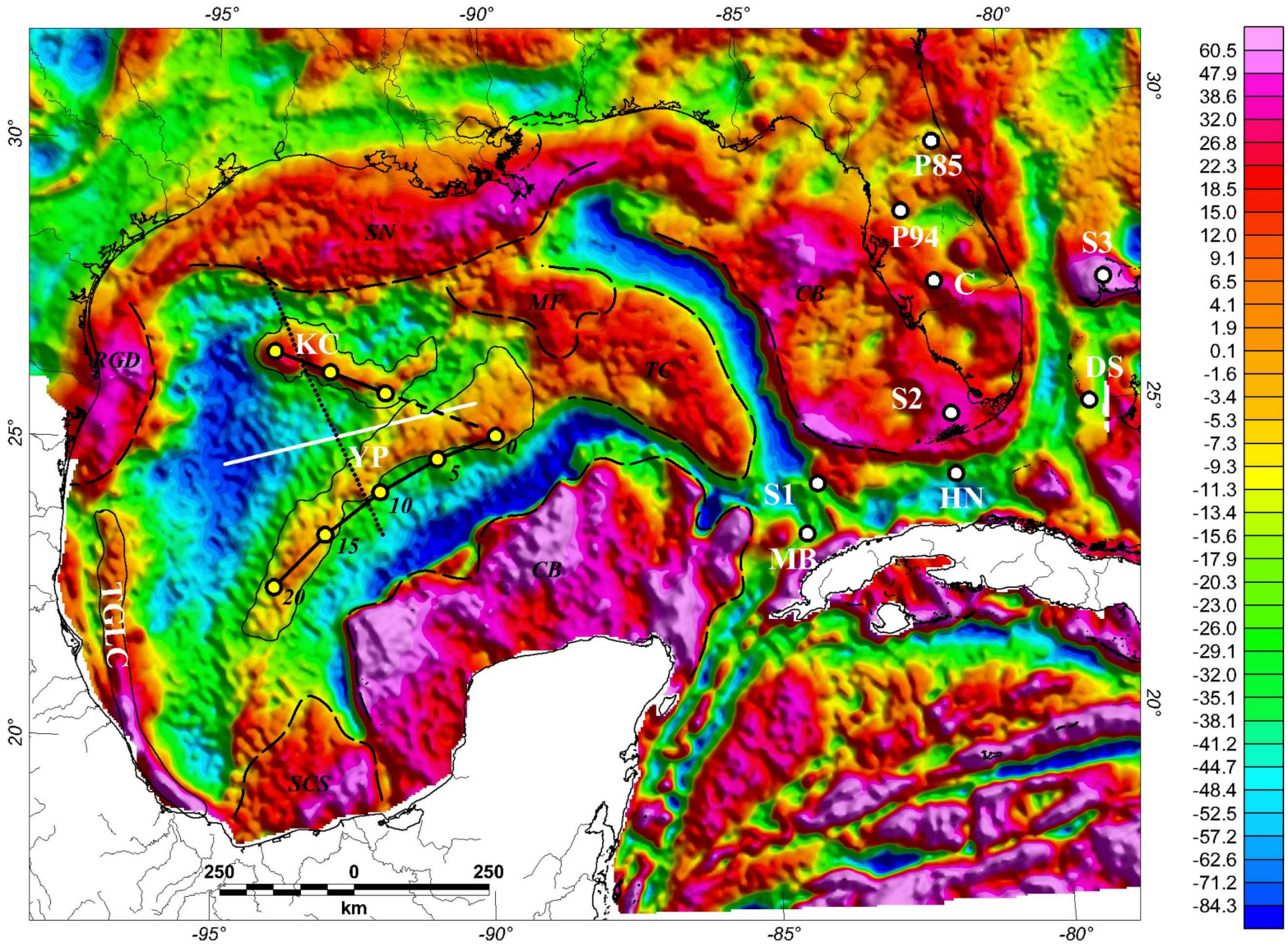
-95°
-90°
-85°
-80°
30°
25°
20°
SN
MF
CB
TC
RGD
TGLC
SCS
KC
YP
0
5
10
15
20
P85
P94
C
S3
DS
S2
S1
HN
MB
250
0
250
km
60.5
47.9
38.6
32.0
26.8
22.3
18.5
15.0
12.0
9.1
6.5
4.1
1.9
0.1
-1.6
-3.4
-5.3
-7.3
-9.3
-11.3
-13.4
-15.6
-17.9
-20.3
-23.0
-26.0
-29.1
-32.0
-35.1
-38.1
-41.2
-44.7
-48.4
-52.5
-57.2
-62.6
-71.2
-84.3

about 5 mGal in amplitude over 20 km wavelengths. The resolution is locally better than these reported values for much of the Gulf of Mexico (Figure 2.2).

Seismic refraction data coverage in the Gulf of Mexico region is extensive (Figures 2.3 and 2.4) (Antoine and Harding, 1963, 1965; Antoine and Ewing, 1963; Buffler *et al.*, 1980; Cram, 1961; Del Castillo, 1974; Ebeniro *et al.*, 1986, 1988; Ewing *et al.*, 1960, 1962; Hales, 1973; Hales *et al.*, 1970a, 1970b; Ibrahim *et al.*, 1981; Ibrahim and Uchupi, 1982; Keller and Shurbert, 1975; Kim *et al.*, 2000; Moore and Del Castillo, 1974; Nakamura *et al.*, 1988; Warren *et al.*, 1966). In the central parts of the basin, refraction depths and velocities indicate oceanic basement and upper mantle. Crustal thicknesses range from about 5 to 8 km in these deeper parts of the basin, where water depths are generally greater than 3 km, and clearly indicate the presence of oceanic crust. The data also indicate prominent basement structures, with relief of several kilometers, in the deep parts of the basin.

Three prominent positive gravity anomalies over the western part of the Gulf of Mexico are the focus of this work. One is centered over the Keathley Canyon (KC) concession area and extends 200 km from 26.4°N, 93.9°W along a roughly WNW-ESE trend to 25.9°N, 91.7°W. This gravity anomaly is here called the KC anomaly. The second gravity anomaly curves for about 630 km north and east from 22°N, 94°W to 24.8°N, 89.8°W concentric with the Yucatan coast. This gravity anomaly is here called the Yucatan Parallel (YP) anomaly. The third gravity anomaly is a north-south linear anomaly, concentric with the east coast of central Mexico, and extends from the Rio Grande Delta in the north to just offshore Veracruz in the south. It is related to the

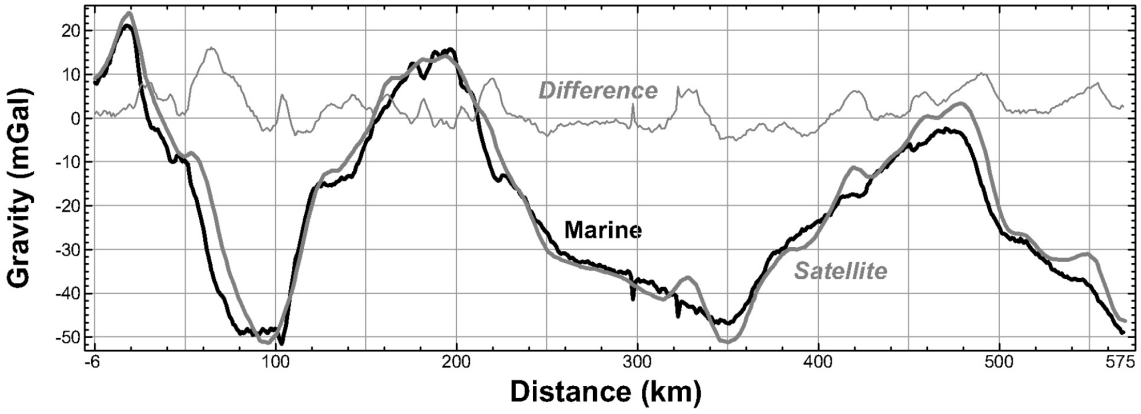

Figure 2.2

Marine versus satellite-derived free air gravity data. Heavy black, heavy gray, and thin gray are marine gravity, satellite gravity (italics), and the difference (italics) between them respectively. The displayed profile, acquired by Oregon State University in 1985 (YUCAT-TR, NGDC number 07270001) is located in Figure 1. The overall correlation between the two data sets is good although the difference between the marine and the satellite-derived data is greater than the estimated 5 milligals limit in some places.

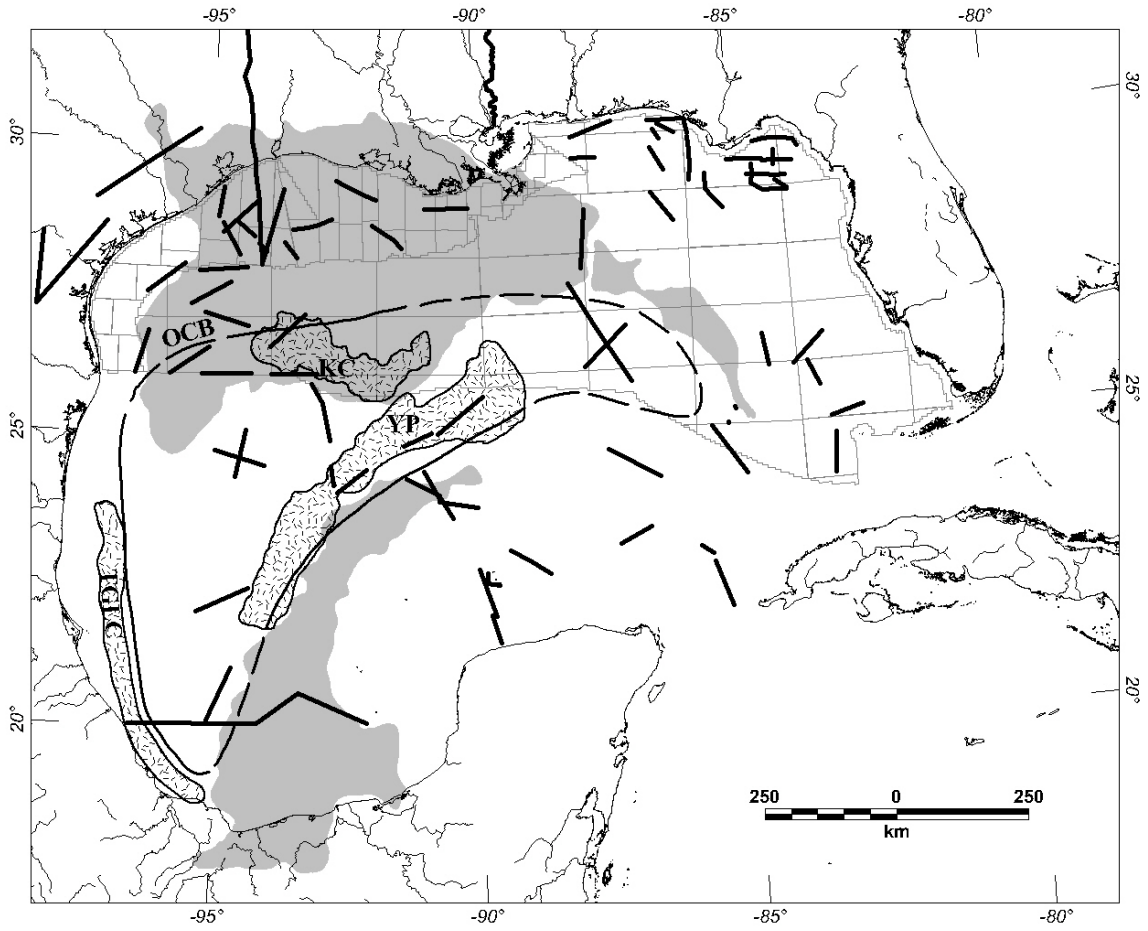

Figure 2.3

Gulf of Mexico salt distribution and seismic refraction data locations. Salt is primarily divided into the northern Gulf of Mexico salt province and the Campeche salt province to the south (gray). Refraction control = short heavy black lines; OCB = Ocean-Continent Boundary (black line); TGLC = Tamaulipas – Golden Lane – Chiapas marginal ridge; YP = Yucatan Parallel structure; KC = Keathley Canyon structure.

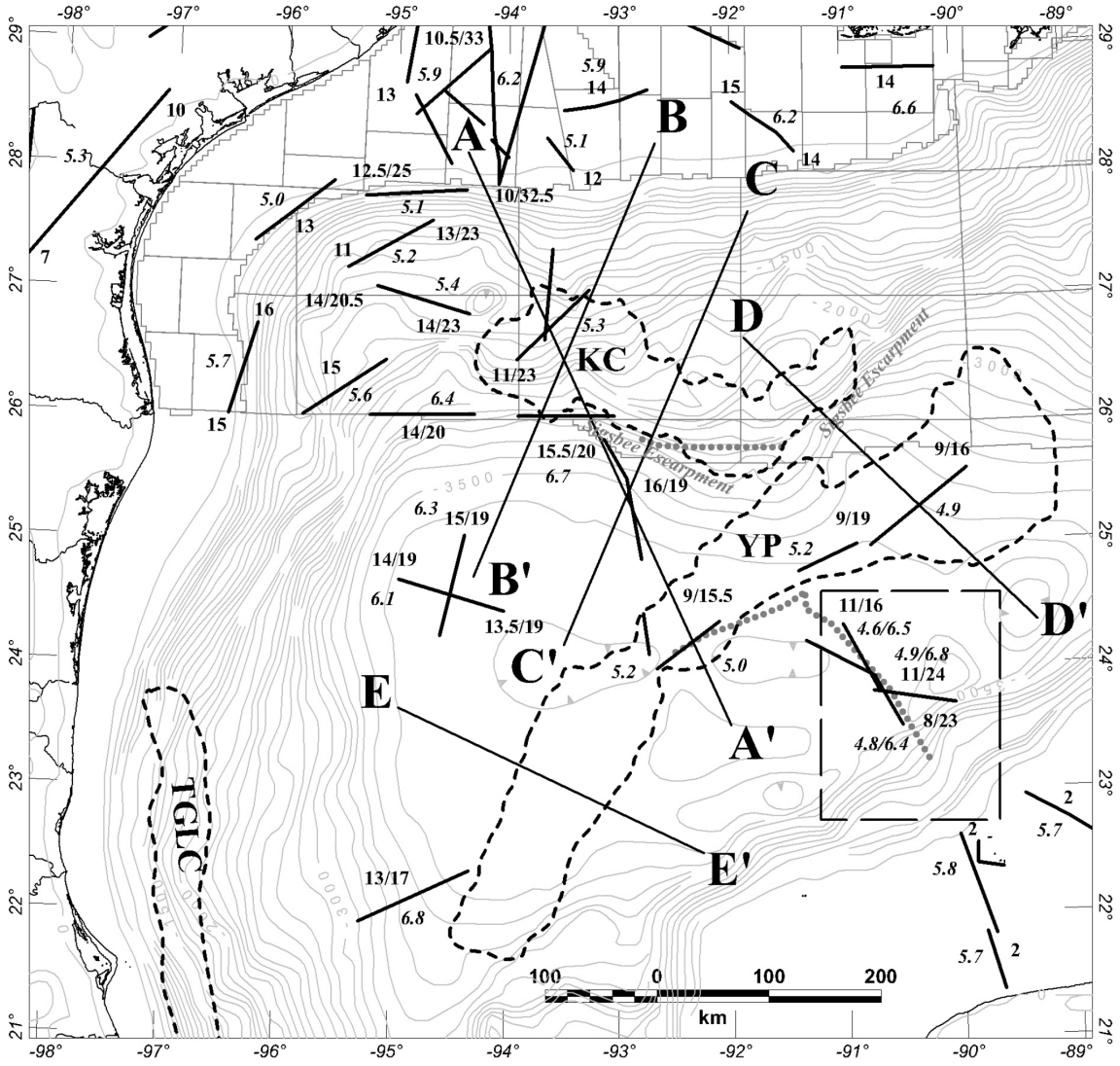

Figure 2.4

Seismic control and modeled gravity cross section locations in the western Gulf of Mexico. Bathymetry contour interval = 200 meters, KC, YP and TGLC gravity anomaly outlines (dashed lines), 2.5D model locations (A-A', B-B', C-C', D-D' and E-E'), and seismic refraction information. Short solid line segments coincide with seismic refraction profiles. Non-italic numbers expressed as fractions are generalized from literature sources and indicate depths in kilometers to the top and base of the crust, single numbers indicate depths to the top of crust only. Italics numbers are upper crustal P-wave velocities generalized from literature sources in kilometers/second. Thick gray dotted lines are the locations of seismic reflection interpretations shown in Figure 5. Velocities inside the dashed box were reinterpreted (see text).

Tamaulipas – Golden Lane – Chiapas (TGLC) fracture zone defined by Pindell (1985, 1994) and it is referred to here as the TGLC anomaly.

We interpret existing open-file gravity and seismic refraction data to identify these three deep basin structures that may be related to the tectonic evolution of the Gulf of Mexico basin (the KC structure, YP structure and TGLC structure). These results provide additional constraints for models involving counterclockwise rotation of the Yucatan block. The basement structures:

1. Are interpreted to include two extinct hotspot tracks, named Keathley Canyon track (or KC track) and Yucatan Parallel track (or YP track), which are used as a basis for a 20° clockwise rotation of the Yucatan block to close the oceanic part of the basin,
2. Include a north-south oriented marginal ridge just offshore central Mexico, which formed along the TGLC transform as the basin opened,
3. Define northern, southern, and eastern estimates of the ocean – continent boundary (OCB) at the hotspot track terminations and the western OCB just outboard of the marginal ridge at the TGLC fracture zone, and
4. Define the limits of autochthonous salt deposition prior to sea floor spreading (Figure 2.3) inboard of the hotspot tracks.

2.3 Two-dimensional Gravity Modeling

Modeling is an effective way to integrate various types of data. Basement and Moho depths from refraction data can be combined with gravity, magnetic, well and seismic reflection data into a single cross section. Modeled cross sections, constrained by seismic refraction and gravity data, have been constructed to interpret the KC and YP structures (Figures 2.4 and 2.5). Modeled sedimentary rocks, except salt, are divided into layers of constant thickness, concentric with the sea bottom, and assigned densities that approximate a continuous density-depth function (Cordell, 1973; Sykes, 1996). For consistency, density values were held constant for each of the modeled layers for all models. Modeled salt body geometries are largely schematic and if we assume that salt bodies might include small amounts of clastic sediments, then the density of these salt bodies would be slightly higher than the density of pure halite (2.16 g/cc). The modeled crust is divided into three layers representing upper, middle, and lower crust (Mooney *et al.*, 1998).

Crustal thicknesses from refraction data, roughly north of the Texas - Louisiana shelf edge (near 28°N, 94°W) and south near the Yucatan escarpment (near 23.5°N, 90.5° W), vary from 12.5 to 22.5 km, indicating thinned continental crust (Figure 2.4). Except for the KC and YP structures, the crustal thickness decreases to about 4 to 6 kilometers (2.5 to 3.7 miles) in the center of the basin. South of the YP structure the crust thickens from 5 to 15 km indicating an oceanic to continental crust transition. The crust of the YP structure is 6.5 to 10 km thick and is well-defined by seismic reflection and refraction data along its crest and to the north and south of the structure (Antoine and Ewing, 1963; Buffler *et al.*, 1980; Ewing *et al.*, 1960; Ibrahim *et al.*, 1981).

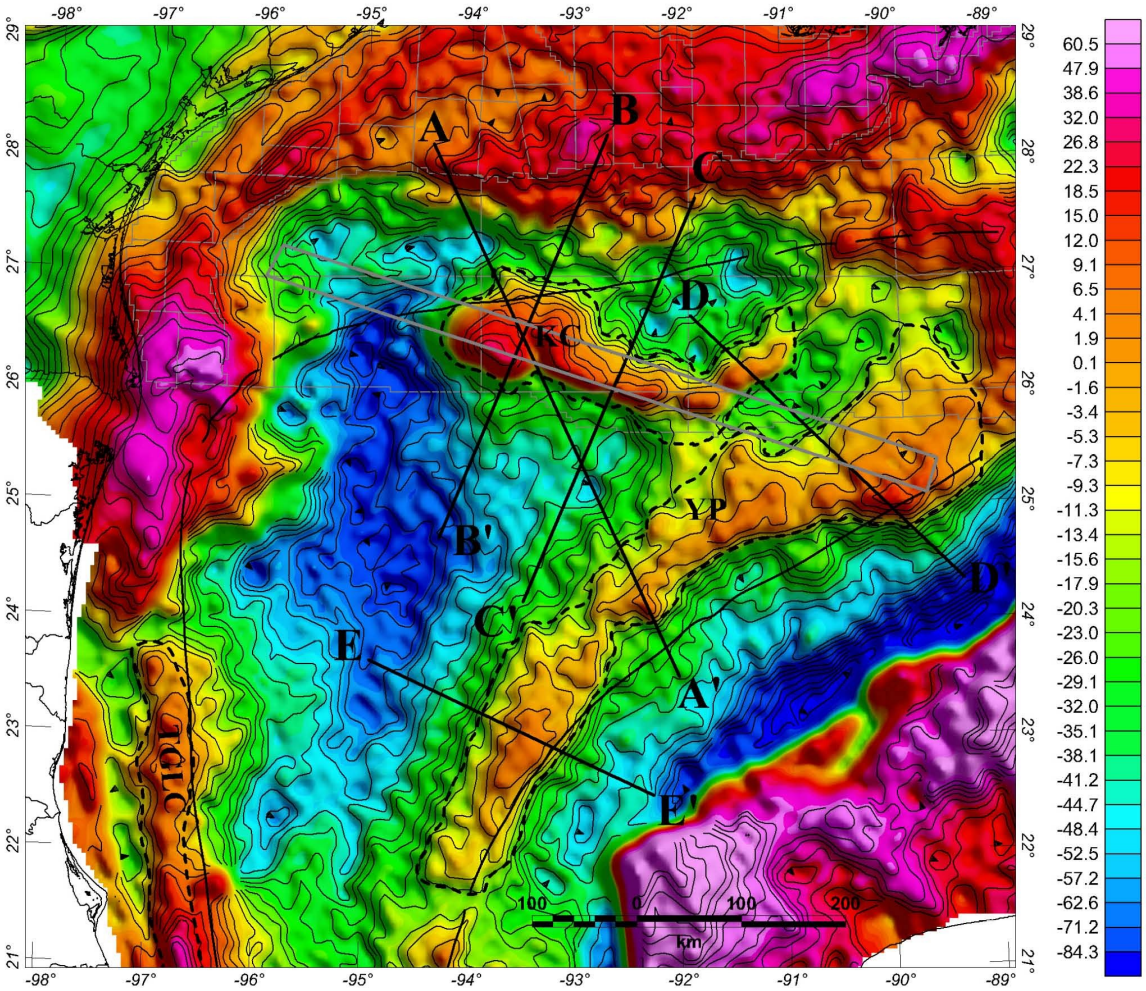

Figure 2.5

Free air gravity anomalies, contoured at 5 mGal. Lines indicate the locations of 2D gravity models (A-A', B-B', C-C', D-D' and E-E') and the interpreted ocean-continent boundary (OCB). Hotspot-referenced trajectories for 160, 150 and 140 Ma (Morgan, 1983) fit within the rectangular gray box. Dashed lines outline the Keathley Canyon (KC), Yucatan Parallel (YP) and Tamaulipas – Golden Lane – Chiapas fracture zone (TGLC) gravity anomalies and interpreted basement structures.

Thick and complex allochthonous salt over the KC structure masks its shape from seismic reflection data; however, the existence of this large basement structure is supported by observations from seismic refraction data over and near the structure (Ebeniro *et al.*, 1988; Ewing *et al.*, 1960; Ibrahim *et al.*, 1981). Ewing *et al.* (1960) noted that a large ridge, composed of 5 km/s material, separates the Sigsbee deep from the Gulf geosyncline. Ebeniro *et al.* (1988) estimate the thickness of the KC structure to be 12 km and reported that the high velocity layer, associated with the top of the structure, beneath the Mid-Cretaceous Unconformity (MCU) may be shallow basement. Autochthonous salt north of the Keathley Canyon is modeled as overlapping onto oceanic crust indicating that, although the major salt provinces were split by the formation of seafloor, deposition may have continued on the ocean floor.

We reference two examples of seismic reflection data that show deep basement structures coinciding with our interpretation of the gravity and seismic refraction data (Figures 2.4 and 2.6). Buffler *et al.* (1980, p. 4) interpreted a basement structure, or "outer basement high", from many seismic sections northwest of the Campeche Escarpment. They noted that this high is located just north and west of the major salt features. The second example is a newly acquired long-offset (9 km), long-record (18 s), large source array line over the southernmost flank of the KC structure (Figure 2.4), which confirms prominent basement structuring with well-defined onlapping horizontal reflectors at about 12.5 km depth (Figure 2.6). This line is part of the regional *GulfSpan* survey that was specifically designed to improve imaging of the deep basin structural architecture in the northern Gulf of Mexico.

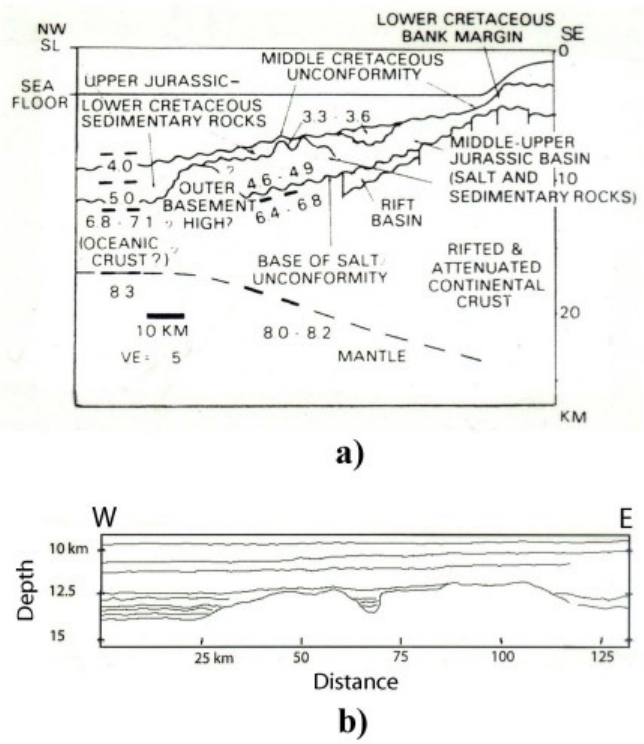

Figure 2.6

Seismic reflection interpretations, see Figure 2.4 for line locations.

a) The YP structure identified from seismic reflection data (after Buffler et al., 1980). Schematic cross section of central Gulf of Mexico. Upper velocities correspond those generalized in Figure 2.4 and the "Outer Basement High?" corresponds with the Yucatan Parallel structure.
b) Line drawing of recently acquired data over the southernmost flank of the KC structure shows deep sediment onlapping deep basement structures.

A primary objective of our modeling is to estimate the shape of the crust beneath the KC and YP anomalies and we interpret this crust to be modified oceanic crust, similar to seamounts and island chains of other hotspot tracks around the world (Caress *et al.*, 1995; Furumoto *et al.*, 1965; Furumoto and Woollard, 1965; Grevemeyer *et al.*, 2001; Watts and Brink, 1989). Elsewhere in the models, based on thickness and location, the crust was interpreted to be either continental, oceanic, or transitional between continental and oceanic (Christensen and Mooney, 1995; White *et al.*, 1992).

2.3.1 Model A – A'

This cross section is approximately 560 km long, passes through both KC and YP structures, and is well constrained by refraction data (Figure 2.7a). Except for the KC structure and the southeasternmost end, the entire model is controlled by basement and Moho depths. Basement depths define only the top of the KC structure. Along strike extrapolation of basement and Moho depths southeast of the YP anomaly are assumed for the southeastern end of the model. From northwest to southeast the total crustal thickness decreases from 16.7 to 9.5 km at the OCB, then increases to 17 km at crest of the KC structure, then decreases to 4 km in the center of the basin, increases again to 12.5 km at the crest of the YP structure, and finally decreases to 7.5 km. We interpret oceanic crust between KC and YP structures, and transitional to oceanic crust to lie just northwest of the KC structure and just southeast of the YP structure.

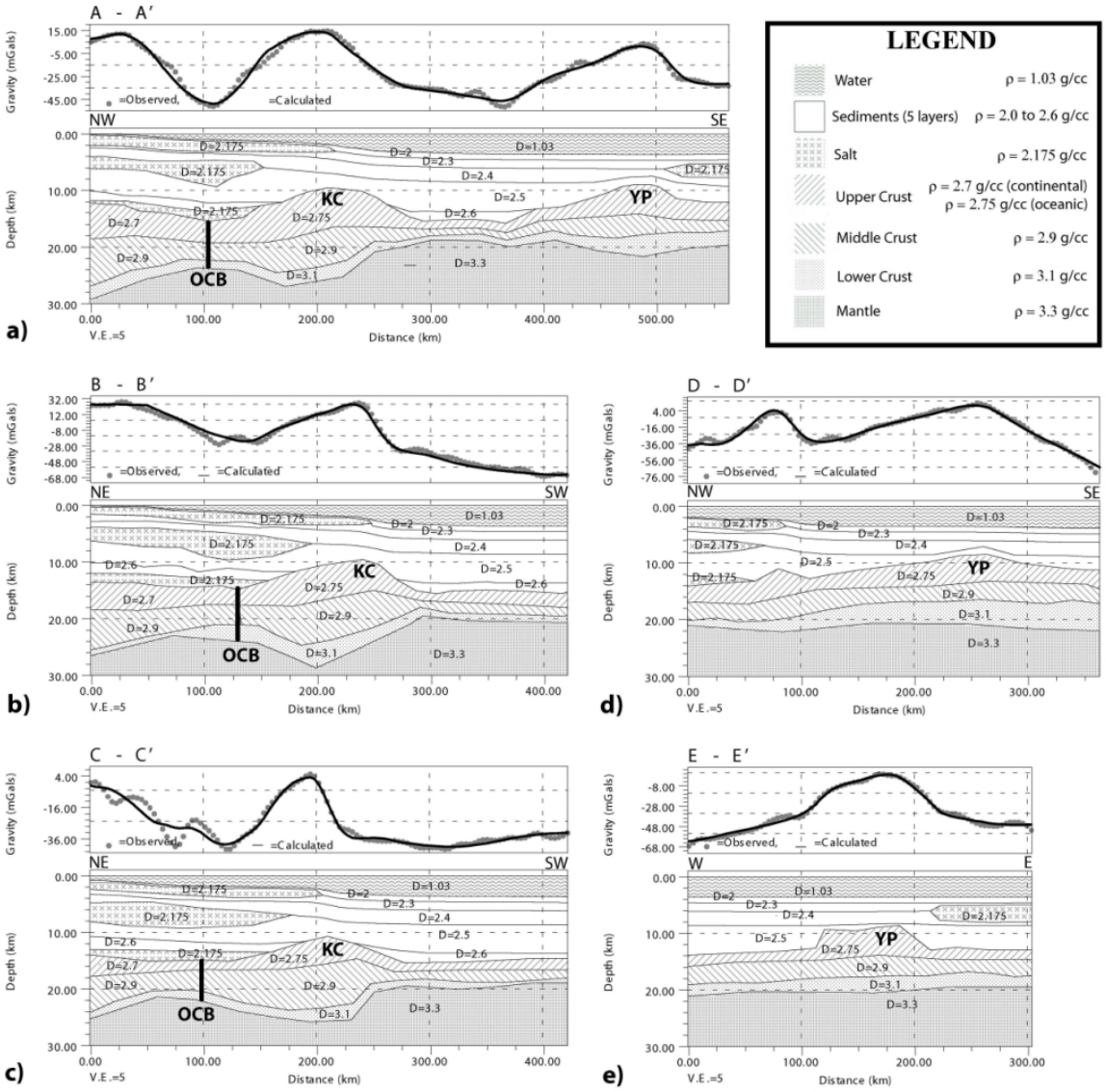

Figure 2.7

2D modeled cross sections. All models have the same scale: vertical exaggeration is 5, observed and calculated free air gravity anomalies are dotted and solid lines respectively. Densities used in modeling are displayed in the legend. OCB is thick vertical lines through upper and lower crusts. Models are located in Figures 4, 6 and 11: g/cc = grams/cubic centimeter.

2.3.2 Model B – B'

Model B – B' is about 420 km long and passes through the KC structure (Figure 2.7b). Basement and Moho depths from refraction data control the southwestern half of the model. Basement control for the northeastern end of the model consists of refraction profiles located about 50 km to the west, northwest and northeast. From northeast to southwest the total crustal thickness decreases from 12 to 9 km at the OCB, then increases to 19 km at the crest of the KC structure, and decreases again to 5.5 km in oceanic crust. We interpret transitional to oceanic crust to lie immediately northeast of the KC structure along this cross section.

2.3.3 Model C – C'

Model C – C' is also about 420 km long and also passes through the KC structure (Figure 2.7c). Refraction control for this model consists of basement and Moho depths from about 50 km west of the southwestern end, basement and Moho depths just south of the KC structure, and basement depths about 50 km beyond the northeastern end of the model. From northeast to southwest the total crustal thickness decreases from 11 to 6.5 km at the OCB, then increases to 15 km at the crest of the KC structure, and decreases again to 5 km. Except for the northeasternmost part of this model, which we interpret to be continental crust, we interpret the thin crust northeast and southwest of the KC structure along this profile to be oceanic.

2.3.4 Model D – D'

This model is about 360 km long and passes through the relatively smaller northeast trending dogleg of the eastern part of the KC anomaly, and then through the YP structure (Figure 2.7d). The only refraction control for this model are basement and Moho depths of the YP structure. Along strike extrapolation of basement and Moho depths southeast of the YP anomaly is assumed for the southeastern end of the model. From northwest to southeast the total crustal thickness increases from 7 to 11 km beneath the KC anomaly dogleg, then decreases to 8.5 km, then increases again to 12 km at the crest of the YP structure, and finally decreases to 9 km. The crustal structure modeled beneath the KC anomaly dogleg is different from those of the larger part of the KC structure and the YP structure. That is, it has less relief and width and it is not rooted. We therefore interpret this part of the KC anomaly to be an anomalous crustal element such as an extinct spreading ridge segment. We interpret all the crust along this profile, except that of the YP structure, to be oceanic.

2.3.5 Model E – E'

Model E – E' is about 300 km long and passes through the southern part of the YP structure (Figure 2.7e). Refraction control for this model consists of basement and Moho depths from over 100 km to the north and south of the western end of the model, and along strike extrapolation (over 200 km) from the southeast of the YP structure to the northeast of the eastern end of the model. This modeled cross section is not as well constrained as the other models, however its construction is consistent with the other models in this study. From west to east the total crustal thickness increases from 7 to 11.5

km at the crest of the YP structure, and then decreases to 6.5 km. We interpret all the crust along this profile, except for the YP structure, to be oceanic.

2.4 Interpretation

2.4.1 Basement structures

Prominent, long wavelength free air gravity anomaly highs over the Gulf of Mexico basin include: 1) those over deltas and regions of recent deposition, 2) carbonate buildups, 3) thin oceanic crust, and 4) major basement structures (Figure 2.1). Anomaly catagories 1) and 2) describe anomalies that are produced by relatively shallow density contrasts. In the case of deltas and areas of relatively recent sedimentation long wavelengths are related to isostatic effects. Anomaly catagories 3) and 4) represent anomalies that are produced by crustal variations and deep structures.

The large triangular shaped gravity high centered around 26.5°N, 87.5°W is related to thin oceanic crust bounded to the east and south by the thick continental carbonate laden crusts of Yucatan and Florida. Shorter wavelength anomalies superimposed on the northwestern corner of this triangular high are produced by the southern limit of the Mississippi fan. The crust of the west-central area of the Gulf, between the KC and YP structures, is also oceanic but it is characterized by relatively low gravity values because the basement in this part of the basin is over 14 km deep, or much deeper than the basement beneath the eastern triangular shaped gravity high (about 9 km).

As the Yucatan block rotated, a shear margin was created along the east coast of central Mexico (Marton and Buffler, 1994; Pindell, 1985, 1994). Shear margins are

continent-ocean transform or fracture zone boundaries and typically form after: 1) rupture of continental crust and rifting and the formation of a continental transform boundary such as the San Andreas Fault, 2) the development of an active oceanic transform boundary between ridge axes, and off-axes fracture zone boundaries, as the continental blocks separate transtensionally, and 3) passive margin formation via thermal subsidence along the fracture zones that also separate oceanic and continental crust (Lorenzo, 1997). Several examples of shear margins reveal that high-standing marginal ridges, rising one to three kilometers over the abyssal sea floor and ranging from 50 to 100 km wide, form along the continental sides of these margins (Bird, 2001). The formation of the marginal ridges has been attributed to the absorption of heat from juxtaposed very thin (essentially zero at the spreading center) oceanic lithosphere as the ridge transform intersection moves past the relatively very thick (over 30 km) continental lithosphere (Lorenzo, 1997; Todd and Keen, 1989).

Marginal ridges can be topographic features such as the Côte d'Ivoire – Ghana marginal ridge, the Davie Ridge, and the Queen Charlotte Islands; or, depending on sedimentation rates, they can be completely buried by sediments such as in the southern Exmouth Plateau and the Agulhas / Diaz Ridges (Ben-Avraham *et al.*, 1997; Edwards *et al.*, 1997; Lorenzo *et al.*, 1991; Lorenzo *et al.*, 1997; Mackie *et al.*, 1989; Mascle *et al.*, 1987). Similarly, the TGLC anomaly in the Gulf of Mexico is not correlated with bathymetric relief and therefore must be attributed to a density contrast at depth. In both cases marginal ridges produce prominent free air gravity anomaly highs that are similar in amplitude, wavelength, and orientation to the TGLC anomaly (global satellite-derived free air gravity data, Sandwell and Smith, 1997). The anomalies are approximately 30 to 80

mGal in amplitude, 20 to 70 km in wavelength, and oriented parallel to bounding oceanic transforms or fracture zones.

Gravity anomaly amplitudes and wavelengths over hotspot tracks can vary widely: 20 to 160 mGal and 20 to 140 km respectively over Galapagos Islands, New England Seamounts, Walvis Ridge, Rio Grande Rise, Ninetyeast Ridge, Hollister Ridge, Emperor Seamounts, and the Hawaiian Islands (global satellite-derived free air gravity data, Sandwell and Smith, 1997). These relatively long and narrow curvilinear volcanic chains of islands and seamounts, often displaying an increase in age with distance relationship, are distinctive features common to ocean basins. KC and YP gravity anomaly amplitudes and wavelengths range from 30 to 80 mGal and 30 to 100 km respectively.

The crustal structure of hotspot tracks is similar to that of oceanic crust but with greater variability in thickness and velocity (Caress *et al.*, 1995; Furumoto *et al.*, 1965; Furumoto and Woollard, 1965; Grevemeyer *et al.*, 2001; Watts and Brink, 1989). Upper crustal velocities range from about 4.2 to 6.0 km/s, and lower crustal velocities range from about 6.0 to 7.5 km/s. Sometimes an additional deeper high velocity layer is present, often thought to represent magmatic underplating, with velocities that range from about 7.4 to 7.9 km/s. Refraction data from several seamounts along hotspot tracks indicate that they typically rise 2 to 5 km above the ocean floor, are deeply rooted, and range in total thickness from 14 to 24 km (Caress *et al.*, 1995; Furumoto *et al.*, 1965; Furumoto and Woollard, 1965; Grevemeyer *et al.*, 2001; Watts and Brink, 1989).

A comparison of gravity anomalies over other hotspot tracks with the KC and YP anomalies, and crustal structures of other hotspot tracks with 2D modeling results, indicates

that the KC and YP anomalies are produced by deep basement structures that are similar to seamounts created by mantle plumes. We suggest that these structures are Late Jurassic hotspot tracks that were created by a single mantle plume during the formation of the Gulf of Mexico basin (Bird *et al.*, 2001), and that the TGLC structure is a marginal ridge located just inboard of the TGLC transform, which also formed during the opening of the basin (Figures 2.1 and 2.6). The length of the marginal ridge is therefore coincides with the minimum north-south extent of oceanic crust along the westernmost part of the basin.

2.4.2 Formation Kinematics

Winker and Buffler (1988) summarized Gulf of Mexico evolutionary models and divided them into six categories. All but one of these categories fall into one of two groups: either those that require rotation of the Yucatan block along two subparallel ocean-continent transform boundaries, or those that require rotation of the Yucatan block along a single ocean-continent transform boundary. The Yucatan block is not included in the remaining model. The prevailing consensus favors rotation with a single ocean-continent transform boundary, or shear margin, located just offshore and subparallel to the eastern coast of central Mexico (Burke, 1988; Hall and Najmuddin, 1994; Marton and Buffler, 1994; Pindell, 1994). Proposed rotation poles for these models, and additional published poles, are shown in Figure 2.1 and listed in Table 2.1 (Christenson, 1990; Dunbar and Sawyer, 1987; Pindell, 1985; Shepherd, 1983).

Counterclockwise rotation of the Yucatan is further indicated by paleomagnetic data (Gose *et al.*, 1982; Molina-Garza *et al.*, 1992), but the amount of rotation has been difficult to interpret with 75° and 130° counterclockwise rotation, relative to the paleopole, reported

	Longitude	Latitude	Symbol, Fig. 2.1
Marton and Buffler, 1994	-84.24	23.18	MB
Hall and Najmuddin, 1994	-81.50	24.00	HN
Pindell, 1985	-81.40	29.50	P85
Pindell, 1994	-82.10	28.40	P94
Dunbar and Sawyer, 1987	-79.00	25.00	DS
Shepard et al., 1983	-84.00	24.00	S1
Shepard et al., 1983	-81.50	25.00	S2
Shepard et al., 1983	-78.50	27.00	S3
Christenson, 1990	-81.60	27.20	C

Table 2.1

Poles for counterclockwise rotation of the Yucatan block, located in Figure 2.1.

by Molina-Garza *et al.* (1992) and Gose *et al.* (1982) respectively. Most workers consider total counterclockwise rotation of the Yucatan to be between 42° and 60° (Dunbar and Sawyer, 1987; Hall and Najmuddin, 1994; Marton and Buffler, 1994 and 1999; Ross and Scotese, 1988; Schouten and Klitgord, 1994). We use Marton and Buffler's (1994) estimate of 42° for our reconstruction. In a contrasting study, Steiner (in press) reports 105° ± 11° of clockwise rotation about a Triassic paleopole.

Hall and Najmuddin (1994) interpreted discontinuities in linear magnetic anomaly patterns over the eastern Gulf of Mexico to be fracture zones, which they used to calculate a pole of rotation for the Yucatan block. They also observed, as have other workers, that the anomaly patterns are dominated by east-west trends (Buffler and Sawyer, 1985; Dunbar and Sawyer, 1987; Hall *et al.*, 1982; Pindell and Dewey, 1982; Pindell, 1985, 1994; Shepherd, 1983), which again is consistent with counterclockwise rotation of the Yucatan block.

A gap between the current edges of the northern Yucatan shelf and the western Florida shelf exists after reconstruction by the single ocean-continent transform boundary model. Pindell (1985, 1994) and Marton and Buffler (1994) suggested a modification to the model whereby southern Florida is displaced to the southeast along a hypothesized Bahama fracture zone (Klitgord and Popenoe, 1984) prior to the rotation of the Yucatan block. Burke (1988) suggested that the Yucatan was originally longer, thus filling the gap, and that it was later shortened to its present length. This explanation is supported by the Mesozoic Guaniguanico terrane of western Cuba that was sheared from the Yucatan as the Caribbean Plate was inserted between North and South America (Pszczolkowski, 1999).

A narrow rectangular box in Figure 2.6 encloses trajectories for hotspot-referenced motion of North America for 140, 150 and 160 Ma (Morgan, 1983). The trend of these trajectories and the overall trend of the KC anomaly are the same, indicating that the KC structure could be a hotspot track on the North American Plate. Furthermore, the easternmost termination of the YP structure also falls along the hotspot referenced trajectories.

Two end members exist for the relative motions of the North American Plate and Yucatan block with respect to a mantle plume as the Gulf opened. The two velocities to consider are the spreading rate between the North American Plate and the Yucatan block, and the velocity at which these two plates passed over the proposed mantle plume. In considering these end members, it is best to reference the spreading center and KC hotspot track with respect to a fixed North America, because in this frame of reference the direction of motion for both the spreading center and the KC hotspot track growth is to the southeast. The spreading center velocity is called SC, and hotspot track growth due to the velocity of the plume location relative to North America is called PL. If SC is greater than PL, then the hotspot track will always exist only on the North American Plate (Figures 2.8b and 2.8c). But if the PL is greater than SC, then the hotspot track will always exist only on the Yucatan block. We interpret the distinctive shapes of KC and YP anomalies to indicate that initially SC and PL were similar, such that conjugate hotspot tracks formed on both the North American Plate and on the Yucatan block (Figures 2.8d and 2.8e). Later, PL increased relative to SC and the hotspot track continued to grow only on the Yucatan block. Therefore, although the KC track shows the relative motion between North America and the mantle plume, it only records part of the total opening history. It is the YP track that

Figure 2.8

Hotspot referenced opening of the Gulf of Mexico with a mantle plume. From an initial position where the spreading center and hot spot coincide (a), two cases are considered over a 10 My seafloor spreading interval: Case 1) the opening of the basin was faster than the velocity of both the North American plate and the Yucatan Block over the plume forming the Keathley Canyon hotspot track (KC) only, and Case 2) the opening of the basin was overall slower than both the velocity of the North American plate and the Yucatan Block over the plume. b) and c) show the expected geometry for Case 1 with rotation in two 5° steps; d) through g) show the expected geometry for Case 2 with four 2.5° steps. In case 2 the seafloor spreading rate was roughly equal to North American plate motion over the mantle plume such that the plume remained beneath the spreading center for part of the opening, producing conjugate hotspot tracks (the Keathley Canyon (KC) and Yucatan Parallel (YP) tracks) on both the North American plate and the Yucatan block (about 5 My). Later the seafloor spreading rate was less and the mantle plume ended up beneath the Yucatan Block (another 5 My). Rotations were calculated using an Euler pole described by Hall and Nadjmuddin (1994, “HN”).

a)

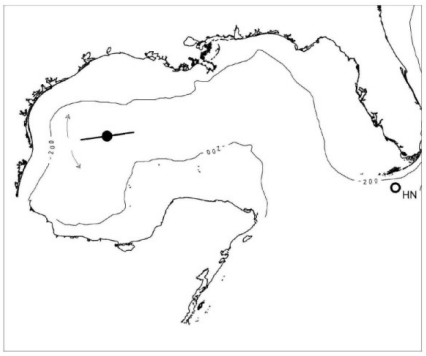

b)

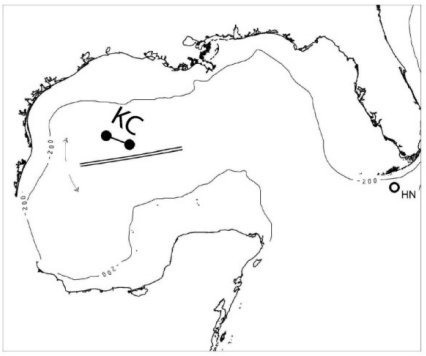

c)

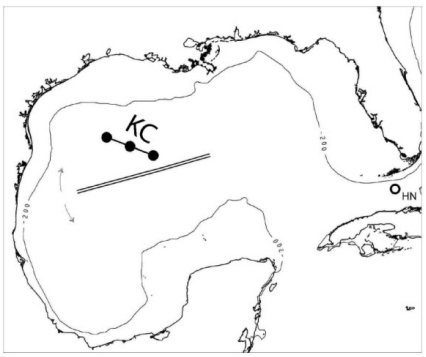

d)

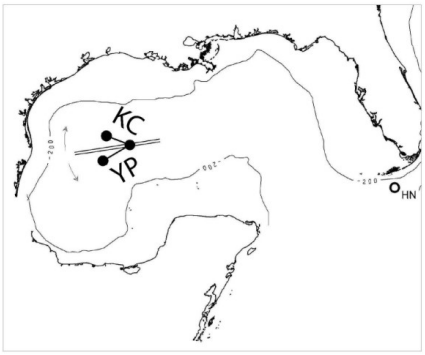

e)

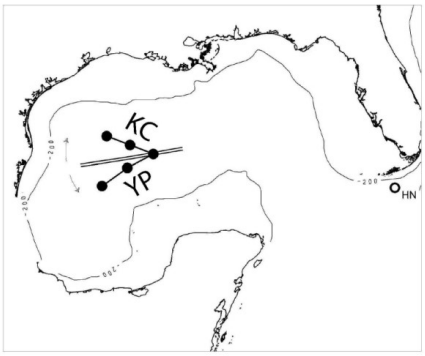

f)

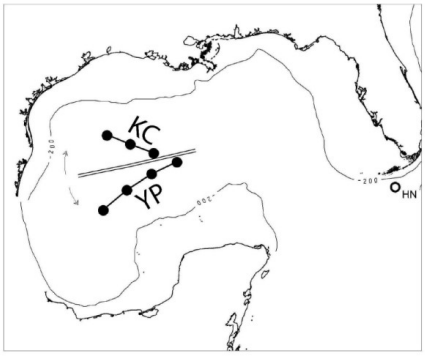

g)

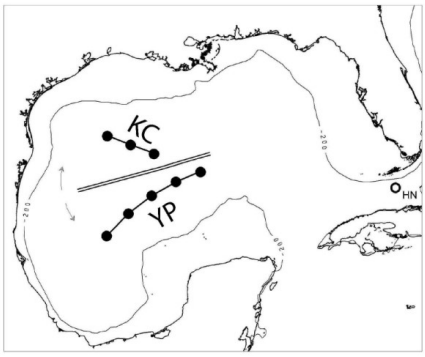

records the total rotation history during the seafloor spreading phase of the evolution of the Gulf of Mexico (Figures 2.8f and 2.8g).

The two interpreted hotspot tracks are on parts of the basin that are underlain by oceanic crust and their formation was from the west to the east over time. A line drawn from the northwestern end of the Keathley Canyon anomaly to the eastern end of the Yucatan Parallel anomaly is the full length of the hotspot track. Reconstruction diagrams (Figure 2.8) illustrate our version of the two end member scenarios: tracks were calculated in 2.5° and 5° increments, totaling 20° of seafloor spreading, using an Euler pole from Hall and Nadjmuddin (1994) located about 100 kilometers south of Key West at 24°N 81.5°W. Reconstruction tracks from our preferred opening scenario (Figure 2.8g) are superimposed on free air gravity anomalies in Figure 2.1.

If the plume was active only during sea floor spreading, then oceanic crust can be defined with confidence in four areas of the Gulf of Mexico. The southern and the eastern ends of the YP structure, and the northwestern end of the KC structure, are the southern, eastern and northern limits of oceanic crust. However, if the plume ceased to be active before seafloor spreading ceased, then oceanic crust could exist between the eastern end of the YP structure and the continental crust of the Yucatan block. Therefore this end of the YP structure marks the farthest seaward limit of the OCB. The eastern flank of the TGLC structure (marginal ridge) along the east coast of central Mexico defines the western limit of oceanic crust. Using these areas as control (solid lines) the oceanic-continental boundary (OCB) has been completed using dashed lines in Figures 2.3, 2.5, 2.9, 2.10 and 2.11. Our 20° seafloor spreading phase of basin formation agrees well with Hall and Najmuddin's (1994) calculation of 25°. The 5° discrepancy between our

estimate and that of Hall and Najmuddin (1994) may be attributed to differences in method and study area; that is, they mapped fracture zones using aeromagnetic data over the eastern Gulf of Mexico.

2.4.3 Formation Chronology

Mesozoic tectonic and geologic events that occurred in the history of the Gulf of Mexico are summarized in Table 2.2 (Marton and Buffler, 1994; Pindell, 1985, 1994; Salvador, 1987, 1991; Winker and Buffler, 1988). Intracontinental rifting between the Yucatan and North America began with the collapse of the Appalachians and Ouachitas in Middle to Late Triassic time (230 Ma) (Olsen *et al.*, 1982), and is thought to have continued until about 160 Ma with salt being deposited in the rift basins shortly before sea floor spreading began. Marton and Buffler (1994) and Salvador (1987, 1991) suggested that Yucatan block rotation and extensive salt deposition were initiated in late Middle Jurassic time, or about 160 Ma (Callovian). The cessation of sea floor spreading in the basin coincided with geomagnetic chron M16 (Pindell, 1994; Winker and Buffler, 1988), corresponding to about 138 Ma (Channell *et al.*, 1995).

The time required to span the distance from the northwesternmost end of the KC anomaly to the eastern end of the YP anomaly in the hotspot reference frame is 8 to 10 My (Morgan, 1983), or nearly one-half the time interval required for Yucatan block rotation and extensive evaporite deposition in the late Middle Jurassic (Marton and Buffler, 1994; Salvador, 1987, 1991). Since 20° counterclockwise rotation is needed to restore the western ends of the KC and YP tracks, and it occurred over 8 to 10 My, then this 20° of rotation should be roughly one-half the total Yucatan block rotation, which makes the total rotation

Rifting begins	Salt Deposition	Yucatan Rotation begins	Seafloor Spreading begins	Seafloor Spreading ends	Source
Late Triassic to Early Jurassic	completed by Oxfordian, 160 Ma	Late Middle Jurassic (Callovian)	Callovian, 166 Ma	Berriasian, 140 Ma	Marton and Buffler, 1994
Late Triassic, 200 Ma	Callovian (or earlier) to middle Oxfordian, by 160 Ma		Early Oxfordian, 160 Ma	Berriasian, 137.85 Ma (M16)	Pindell, 1994
Late Triassic, 210 Ma	Late Callovian, by 160 Ma		Late Callovian, 160 Ma	Berriasian, 140 Ma	Pindell, 1985
Late Triassic to Early Jurassic	late Middle Jurassic to early Late Jurassic		latest Callovian or early Oxfordian	early Late Jurassic but not later than mid-Oxfordian	Salvador, 1991
Late Triassic to end of Middle Jurassic	Late Middle Jurassic		Late Jurassic	early part of Late Jurassic	Salvador, 1987
Late Triassic	Callovian, ~168 to 163 Ma		Early Oxfordian, 160 Ma	Berriasian, 140 Ma	Winker and Buffler, 1988
Middle to Late Triassic, 230 Ma	Late Callovian / Early Oxfordian to Kimmeridgian, 160 to 150 Ma	Late Callovian to Early Oxfordian, 160 Ma	Kimmeridgian, 150 Ma	Berriasian, 140 Ma	This paper

Table 2.2

Summary of Gulf of Mexico formation events.

and total time of approximately 42° and 20 My consistent with evolutionary data presented by other workers (Figure 2.9). Exactly when this 20 My period occurred is difficult to determine, but stratigraphic relationships indicate that the basin must have been completely formed by ca. 140 Ma. Therefore we choose the 160 to 140 Ma time period for the basin to open emphasizing that this time interval is not well constrained.

Our conclusion that seafloor spreading occurred between 160 Ma and 140 Ma implies that the Gulf of Mexico opened about 20 My after sea floor spreading began in the central Atlantic Ocean (Withjack *et al.*, 1998), and probably includes seafloor spreading between North and South America. This allows us to distinguish several tectonic events, including early salt deposition, of North America beginning with the break-up of Gondwana (Table 2.2): onset of rifting, salt deposition, onset of Yucatan rotation and continental extension, onset of seafloor spreading, and the end of seafloor spreading.

2.4.4 Salt Distribution

The original distribution of salt deposition in the Gulf of Mexico is important for petroleum exploration and this distribution is probably closely related to basement structuring over the extent of continental crust. Exhaustive studies of salt structures in the Gulf of Mexico have lead workers to categorize northern Gulf of Mexico and Campeche salt provinces into smaller provinces based on size, shape, occurrence, timing, and stratigraphic relationship of salt structures and surrounding clastic rocks (Diegel *et al.*, 1995; Hall, 2001; Martin, 1980; Peel *et al.*, 1995). The salt itself has been categorized into various individual structures such as rooted stocks, massifs, domes, anticlines, walls, ridges, tongues, sheets, and pillows (Martin, 1980). Cenozoic deformation in the Gulf of

Figure 2.9

Reconstruction of Gulf of Mexico, 20 My evolution of Yucatan motion.

Pole used by Hall and Najmuddin (1994) = HN

a) Initial position – about 160 Ma (exact age unknown). Yucatan occupies what is the Gulf of Mexico basin now. The Yucatan was probably extended, to fill the gap between it and western Florida, at this point (Burke, 1988).
b) 10 to 12 My and 22° of rotation and continental crust extension (about 150 to 152 Ma), with the sea floor spreading commencing at the end of this time period when the plume became active.
c) 20 My and 42° total rotation (adding 20° of rotation of seafloor spreading), present position achieved (about 140 Ma).

a)

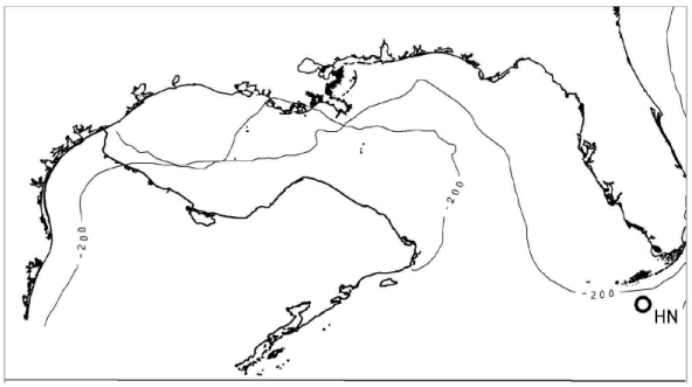
-200
-200
-200
HN

b)

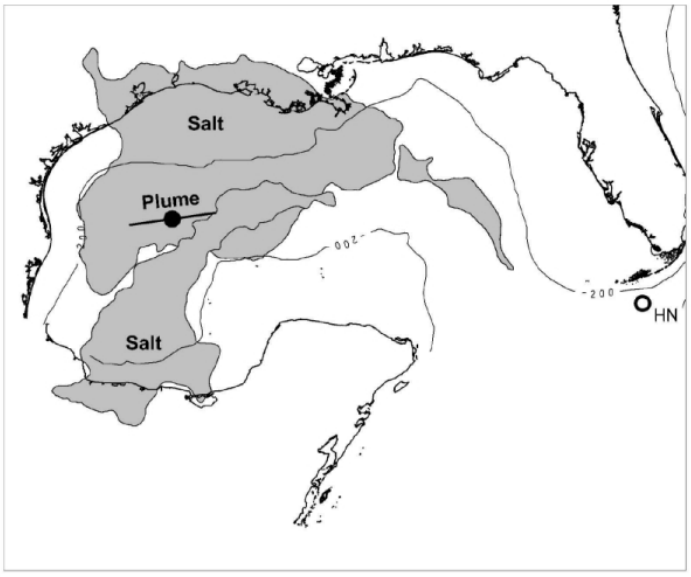
Salt
Plume
Salt
-200
-200
-200
HN

c)

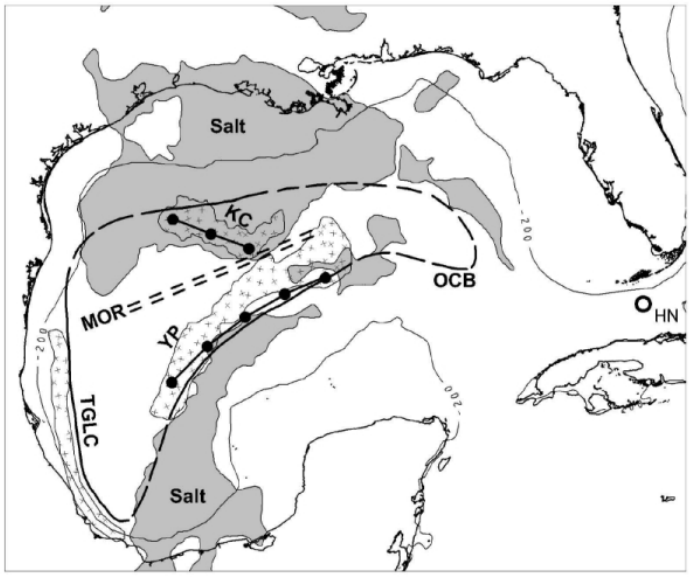
Salt
KC
OCB
MOR
YP
TGLC
Salt
-200
-200
-200
HN

Mexico has been driven by gravity as the shelf margin has prograded several hundred kilometers basinward and complex, linked systems of salt canopies are produced by variations in timing and amount of updip sedimentation (Peel *et al.*, 1995). Diegel *et al.* (1995) reported that Cenozoic structural styles are due to the original distribution of earlier salt structures, varying slope depositional environments, and varying amounts of salt withdrawal from allochthnonous sheets. Salvador (1991) suggested that salt was deposited coeval with rift sediments, however Peel *et al.* (1995) suggested that salt deposition was controlled by post-rift geometries. The Campeche salt was deposited in Callovian time and ranges in thickness from 3000 m in the southwest to 160 m in the northeast, and mobilized during Oligocene with deformation continuing to earliest Miocene time (Angeles-Aquino, 1994).

Salt in the Gulf of Mexico can be generally divided into two large regions, the northern Gulf of Mexico salt basin and the Campeche salt basin (Figure 2.2), which are interpreted to have formed contemporaneously (Marton and Buffler, 1994; Pindell, 1994; Salvador, 1991; Winker and Buffler, 1988; Angeles-Aquino, 1994). Using the distribution of Jurassic evaporite deposits as a geometrical constraint, White (1980) and White and Burke (1980) showed that the Yucatan block can be restored by counterclockwise rotation. They reasoned that the landward morphology of the southern Campeche salt margin, and the northern Gulf salt basin, represent rift valley walls that formed as the continental blocks separated.

Hall (2001) interprets the lack of salt related sedimentary structures in the Keathley Canyon concession area as evidence that little or no authochthonous salt was deposited. Furthermore he reports that thick allochthonous salt sheets in Keathley Canyon

concession area were probably sourced from the north. Peel *et al.* (1995) also suggest that the seaward extent of autochthonous salt in the northern salt basin did not extend over the KC area.

Prior to sea floor spreading, continental crustal extension of the Yucatan, as it rotated about 22° counterclockwise between 160 Ma and 150 Ma, allowed intermittent sea water influx producing massive salt deposition. The lack of evidence for autochthonous salt in the Keathley Canyon (Hall, 2001; Peel *et al.*, 1995) supports our interpretation for the formation of Late Jurassic hotspots and probably means that the KC and YP structures formed seaward boundaries for autochthonous Louann and Campeche salt as seafloor spreading continued until about 140 Ma. The KC structure is now hidden beneath the Plio-Pleistocene allochthonous salt nappe, however the YP structure is clearly a boundary that separates the Campeche salt from the center of the basin.

2.5 Discussion

2.5.1 Oceanic and continental crust

White *et al.* (1992) reported the results of three world-wide compilations of oceanic crustal thickness and layer velocities. Mean velocities for Layer 2, Layer 3, and upper mantle are 5.09 ± 0.74 km/s, 6.69 ± 0.26 km/, and 8.15 ± 0.31 km/s respectively. The mean thickness of oceanic crust is 6.33 ± 1.85 km. Christensen and Mooney (1995) report that the average thickness of extended continental crust is 30.5 km. They subdivide continental crustal velocities into three groups: upper (5.7 to 6.4 km/s), middle (6.4 to 6.8 km/s), and lower (6.8 to 7.8 km/s). Tanimoto (1995) reports the average continental

crustal thickness is 39 km. Transitional crust is generally thought of as extended and thinned continental crust, or crust that is characterized by an intermediate composition between oceanic and continental material.

Continental crustal velocities in the northern and southeastern parts of the Gulf of Mexico region shown in Figure 2.4 range from 5.7 to 6.2 km/s. Velocities of 6.6 and 6.7 km/s between 90° and 92° W in the north can be interpreted as either lower continental crust or lower oceanic crust. Between 26° and 28° N and west of 94°W, crustal velocities ranging from 5.0 to 5.6 km/s are upper oceanic crust. Velocities reported south of the Sigsbee Escarpment in the central part of the basin, ranging from 6.1 to 6.8 km/s are lower oceanic because the crust is thin (5 to 8 km). Upper crustal velocities in the KC and YP structures range from 4.9 to 5.3 km/s and are typical upper oceanic crustal values.

There are difficulties associated with interpreting seismic refraction data in deep basins. Ibrahim *et al.* (1981) suggested that the upper oceanic crustal layer may be too thin to be detected. Ewing *et al.* (1962) noted that the ~4.9 km/s layer of the deep Gulf of Mexico is too thick (over 3 km) to be Layer 2. They also noted that Layer 2 velocities are similar to velocities of evaporites and carbonates, therefore at great depths Layer 2 might not be easily distinguished from these rocks.

Pairs of velocities inside the area of the dashed box (Figure 2.4) have been reported by Ewing *et al.* (1960) for upper and lower crust. Later workers have indicated that the upper crustal layer interpreted by Ewing *et al.* (1960) is actually deeply buried sediment and that upper crustal velocities cannot be reliably interpreted (Ebinero *et al.*, 1988; Hales *et al.*, 1970a; Ibrahim *et al.*, 1981; Ibrahim and Uchupi, 1982; Nakmura *et al.*, 1988). Therefore, we have interpreted these velocities in the same way as later

workers, and posted depths corresponding with these interpreted velocities. This approach is also reflected in Figure 2.5a where the “outer basement high” corresponds with the YP structure (Buffler *et al.*, 1980, p. 4).

The shape and velocity structure of the KC and YP structures differ greatly from those of continental fragments such as the Rockall Bank, Seychelles Bank, Broken Ridge and Lord Howe Rise. Table 2.3 summarizes the crustal structure of these fragments (Bunch, 1979; Davies and Francis, 1964; Francis and Raitt, 1967; Matthews and Davies, 1966; Scrutton, 1970; Sundaralingam and Denham, 1987). Total crustal thickness from seismic refraction data is not available for the numerous continental fragments surrounding the South China Sea: the Hainan Qiongzhong and Yaxian terranes, Paracel Islands, Macclesfield Bank, Reed Bank, Spratley Islands – Dangerous Ground, and Luconia (Hayes *et al.*, 1978; Metcalfe, 1996; Taylor and Hayes, 1980); however, all of these continental blocks are nearly circular in shape. The dimensions of KC and YP structures are less than 100 km wide, 100’s kilometers in length, and 10 to 12 km thick. Upper and lower crustal velocities range from 4.9 to 5.5 km/s and 6.2 to 7.4 km/s respectively (Ebinero *et al.*, 1988; Ewing *et al.*, 1960).

2.5.2 Oceanic – Continental Boundary (OCB)

The boundary between oceanic and continental crust in the Gulf of Mexico has been interpreted in several ways (Figure 2.10) using seismic reflection, seismic refraction, gravity and magnetic data as well as kinematic reconstructions (Buffler, 1989; Buffler and Sawyer, 1985; Buffler and Thomas, 1994; Dunbar and Sawyer, 1987; Hall

Continental Fragment	Total Crust Thickness	Velocity Upper Crust	Velocity Lower Crust	Velocity Deep Crust	Dimensions	Source
	(km)	(km/s)	(km/s)	(km/s)	(km)	
Rockall Bank	30 to 32	4.8	6.36	7.02	200 x 400	Bunch, 1979; Scrutton, 1970
Seychelles	32	5.7 to 5.72	6.26 to 6.3	6.78 to 6.8	200 x 300	Davis and Francis, 1964; Francis et al., 1966; Matthews and Davies, 1966
Madagascar Ridge	18	4.5 to 6.2	7.0 to 7.2	7.9 to 8.2	400 x 1000	Sinha et al., 1981
Broken Ridge	22	5.81 to 6.43	7.25		200 x 1400	Francis and Raitt, 1967
Lord Howe Rise	27	5.95	6.82		500 x 2000	Sundaralingam and Denham, 1987

Table 2.3

Continental fragment size, thickness and velocity structure.

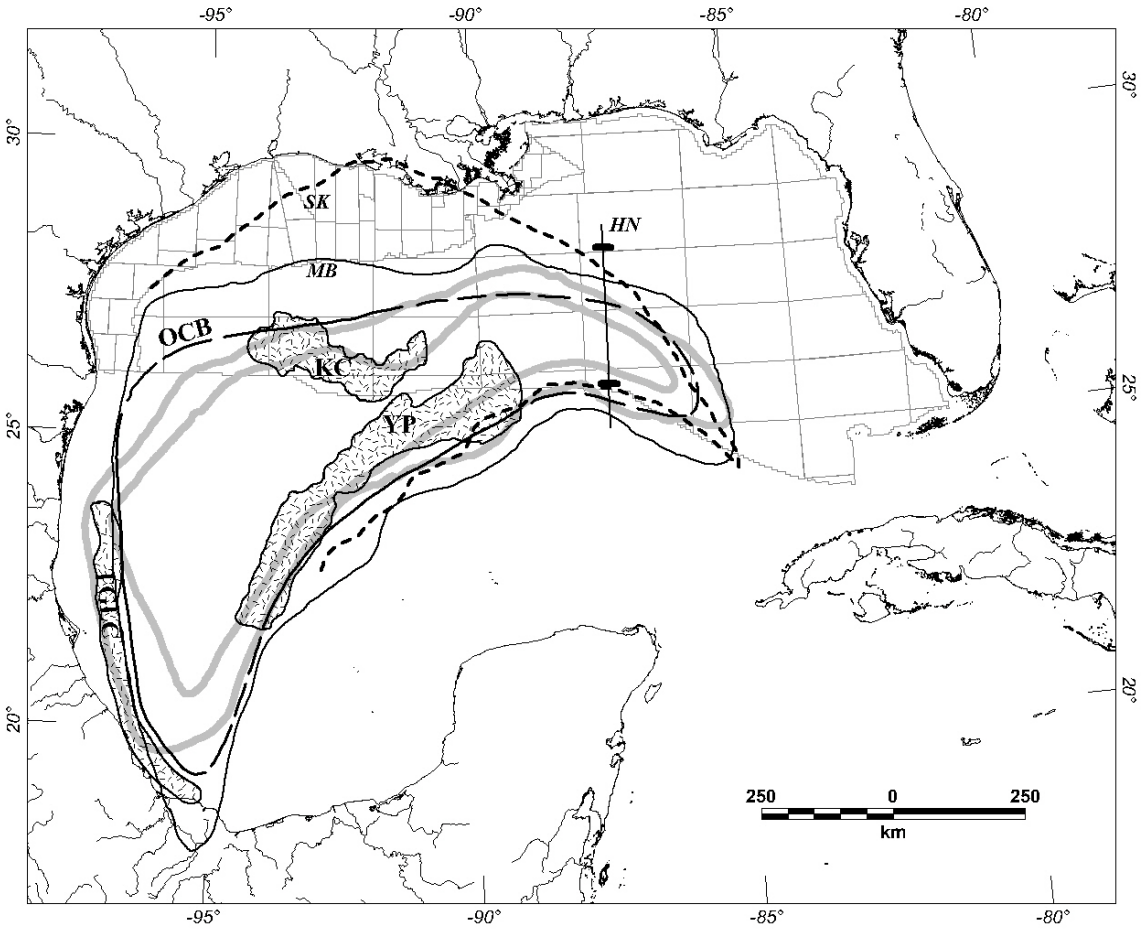

Figure 2.10

Gulf of Mexico ocean basin proposed Ocean-Continent Boundaries (OCB) From this work = OCB; SK = interpreted from DNAG magnetic anomaly grid (Schouten and Klitgord, 1994); HN = ticks are interpreted OCB from a 2D magnetic model (Hall and Najmuddin, 1994); MB = interpreted from seismic refraction data (Marton and Buffler, 1994); Heavy gray lines = envelope of several OCBs (Buffler and Sawyer, 1985; Buffler and Thomas, 1994; Pindell, 1994; Ross and Scotese, 1988; Salvador, 1991; Winker and Buffler, 1988). TGLC = Tamaulipas – Golden Lane – Chiapas marginal ridge; YP = Yucatan Parallel structure; KC = Keathley Canyon structure.

and Najmuddin, 1994; Marton and Buffler, 1994; Pindell, 1994, 1985; Ross and Scotese, 1988; Salvador, 1991; Schouten and Klitgord, 1994; Winker and Buffler, 1988). The ocean – continent crustal boundary (OCB) is interpreted to coincide roughly with the 3000 m isobath except where it passes beneath the Plio-Pleistocene Sigsbee salt nappe (Dunbar and Sawyer, 1987; Pindell, 1994, 1985; Ross and Scotese, 1988; Salvador, 1991; Winker and Buffler, 1988). Schouten and Klitgord (1994) identified magnetic edge anomalies that border the OCB. They proposed that high amplitude, short wavelength anomalies over continental crust surround relatively low amplitude, long wavelength anomalies over oceanic crust in the center of the basin. Hall and Najmuddin (1994) constructed a 2D forward magnetic model to interpret the OCB along an aeromagnetic profile and their results are similar to Schouten and Klitgord's (1994) regarding the position of the OCB on the profile.

The occurrence of extended transitional crust, or attenuated continental crust in the Gulf of Mexico, was suggested by Buffler (1989), Buffler and Sawyer (1985), and Buffler and Thomas (1994). This transitional crust was further subdivided into thick and thin transitional crust based on horizontal crustal extension and tectonic subsidence calculations. Thick transitional crust was defined as being moderately attenuated, including broad sags and flexures with amplitudes ranging from 3 to 4 km and thin transitional crust was defined by extreme stretching and thinning. McKenzie (1978) was one of the first to suggest a method for basin formation by thinning continental crust: extensional plate tectonic forces stretched the lithosphere causing initial subsidence and mantle upwelling, as the upwelled mantle cooled, secondary thermal subsidence occurred in order to maintain isostatic equilibrium. Dunbar and Sawyer (1987) quantified this idea

by relating total tectonic subsidence to crustal extension or β, such that β = 2 when surface area is doubled and crustal thickness is halved. They concluded that β ≅ 4.5 at the OCB.

A thorough analysis of seismic refraction data by Marton and Buffler (1994) extended the OCB 200 kilometers (124.3 miles) north of the Sigsbee Escarpment (Figure 2.10). The area of oceanic crust derived from this analysis was then defined such that northern and southern edges of the OCB would close exactly upon reconstruction. The wealth of data included in their work (same as this study, Figure 2.3) makes this interpretation of oceanic and continental crust in the Gulf of Mexico superior to previous interpretations. We have also analyzed and interpreted these refraction data, but we modify the OCB according to our kinematic model.

2.5.3 Density, topography, and Bouguer gravity anomalies

The YP structure underlies flat ocean floor and the lack of correlation with topography indicates that the gravity anomaly is produced by density contrasts beneath the water bottom. In contrast the southern flank of the Keathley Canyon anomaly corresponds with the Sigsbee Escarpment (Figure 2.4). The offshore Bouguer correction essentially replaces the water with a slab, equal to the depth to the sea floor, of an assumed density (Blakely, 1995, p. 143). Typically, a density is selected such that when added to water density (1.03 for sea water) the total is equal to the density of shallow sediments. In other words, Bouguer gravity anomalies are calculated to minimize the effect of the large density contrast at the sea bottom (Figure 2.11). This contrast is estimated to be 0.87 grams/cubic

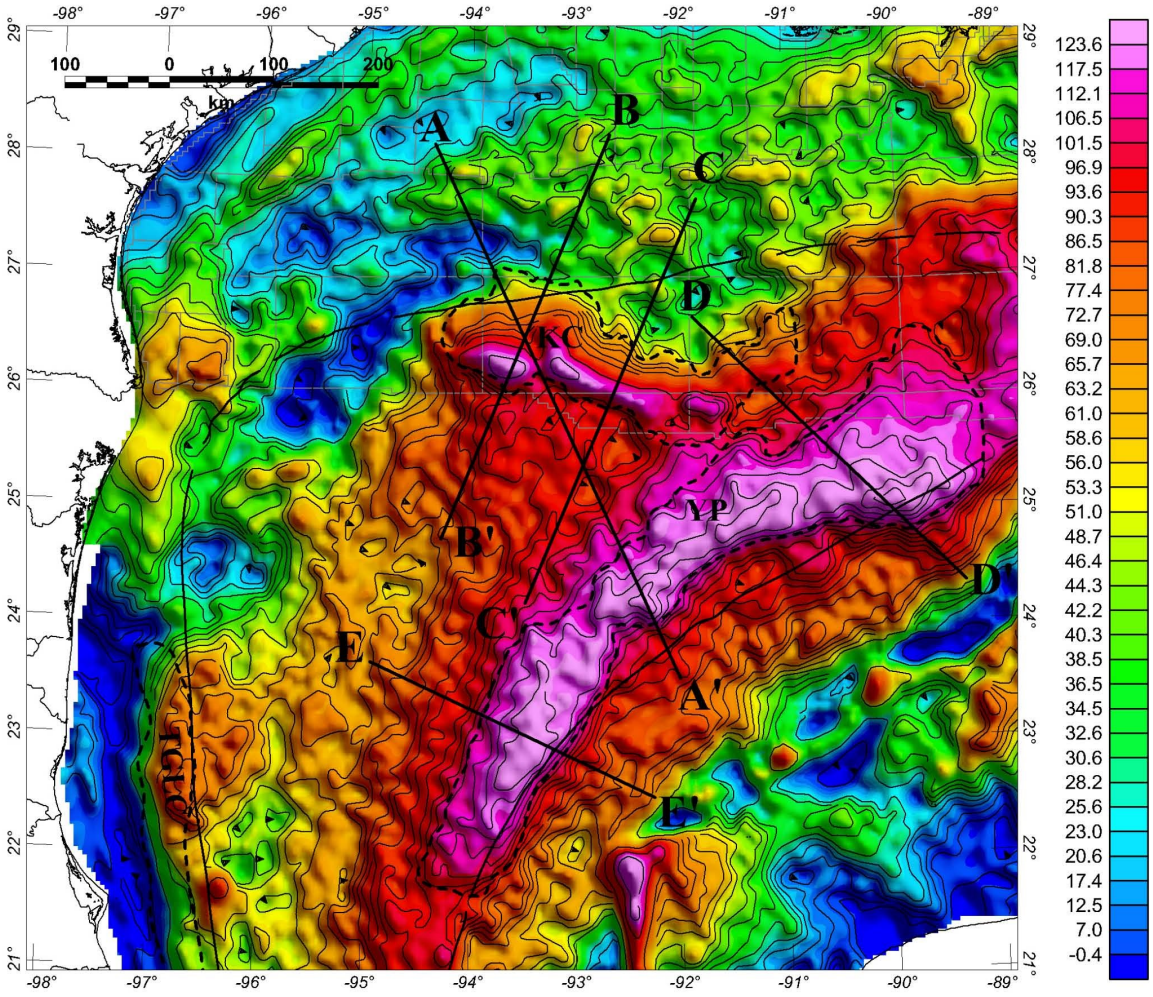

Figure 2.11

Bouguer gravity anomalies, contoured at 5 mGal. Lines indicate the locations of 2D gravity models (A-A', B-B', C-C', D-D' and E-E') and the interpreted ocean-continent boundary (OCB). Dashed lines outline the Keathley Canyon (KC), Yucatan Parallel (YP) and Tamaulipas – Golden Lane – Chiapas fracture zone (TGLC) gravity anomalies.

centimeter, which is the difference between sea water and shallow sediments (1.03 g/cc and 2.0 g/cc). Although the amplitude of the KC anomaly is decreased after the Bouguer correction is applied, the anomaly remains prominent when compared with other anomalies over the basin. The broad region of higher gravitational intensity over the center of the basin is produced by thin oceanic crust. The Tamaulipas – Golden Lane – Chiapas fracture zone (TGLC) anomaly (Figure 2.1 and Figure 2.4) is somewhat masked by this increased gravitational intensity to the east.

2.6 Conclusion

The economic importance of the Gulf of Mexico has led to the acquisition of vast amounts of geophysical data in the basin. These data have in turn led to extensive geologic studies. However, complexly structured salt has masked important details of the great thickness of sediments in the basin. It is ironic that this richness of data cannot fully explain first-order parameters such as the depth to the crystalline basement, distribution of source rocks, details of deep structures related to salt withdrawal basins and carbonate platform development, or even the tectonic evolution of the basin. A full understanding of these parameters would provide the bases for superior integrated basin analyses and petroleum system modeling.

The first-order knowledge required for mapping and interpreting deep geologic elements in the Gulf of Mexico, as well as its tectonic evolution, is an understanding of the nature of major basement structures. This is especially true for areas in the Gulf of Mexico that are hidden beneath near-opaque, complex and extensive allochthonous salt

bodies. Once the shape of the basement is known, then an evolutionary model can be developed followed by mapping and interpretation of smaller geologic elements and processes. Using this approach we have integrated and interpreted gravity and seismic refraction data, and:

1. Established that the size, shape and orientation of major basement structures are consistent with the size, shape and orientation of similar structures around the world. Detailed 2D cross sectional models, constrained by seismic refraction and gravity data, indicate that two deep basement structures in the Gulf of Mexico (the Keathley Canyon and Yucatan Parallel hotspot tracks) are similar to hotspot tracks around the world, including crustal structure (velocity and thickness) and areal gravity signatures. These structures are not continental fragments as indicated by their size, shape and crustal structure. Another deep basement structure (the Tamaulipas – Golden Lane – Chipas marignal ridge) is consistent in size and shape with other marginal ridges around the world. The eastern flank of this ridge, and the northern and southern terminations of the hotspot tracks coincide with the oceanic – continental crustal boundary. The eastern termination of the YP track coincides with the farthest seaward limit of the OCB.

2. Proposed a plate kinematic model that is consistent with established parameters including rotation pole, fracture zone and boundary, and crustal types. Basin formation began with about 22° of counterclockwise rotation and

continental extension, which coincided with early salt deposition. Then another 20° of counterclockwise rotation and seafloor spreading coincided with the formation of hotspot tracks.

3. Demonstrated that the interpreted basement structures and kinematic reconstruction are consistent with established tectonic and depositional events including the onset of rifting, early salt deposition, and deep water marine sedimentation. Continental extension related to the rotation of the Yucatan block occurred roughly between 160 Ma and 150 Ma and seafloor spreading occurred between 150 Ma and 140 Ma.

3. RIDGE JUMPS AND ASYMMETRIC SPREADING IN THE CENTRAL ATLANTIC OCEAN

3.1 Abstract

An integrated interpretation of extensive magnetic and gravity data sets over the central Atlantic Ocean has resulted in the detailed mapping of magnetic anomalies associated with 18 Chrons from M0 to M25 between the Atlantis and Fifteen-Twenty fracture zones on the North American plate, and between Atlantis and Kane fracture zones on the African plate. Five Chrons from M28 to M40, in the Jurassic Magnetic Quiet Zone (JQMZ), have been mapped between the same fracture zones. Three periods of asymmetric seafloor spreading between North America and Africa appear to have occurred between: 1) the present and 84 Ma, with faster accretion to the west; 2) 84 Ma and 120.6 Ma, with faster accretion to the east, and 3) 120.6 Ma and 154 Ma, with faster accretion to the west.

Two ridge jumps, identified during the early evolution of the central Atlantic, could be related to plate interactions as North America separated from Gondwana. Chron 40 (167.5 Ma) has been mapped about 65 km outboard of the Blake Spur Magnetic Anomaly (BSMA) on North American flank, and its conjugate S1 anomaly on the African flank. About 180 km inboard of the BSMA is the East Coast Magnetic Anomaly (ECMA) which coincides with seaward-dipping reflectors. The interpreted conjugate to ECMA is the S3 anomaly, which is about 30 km inboard of S1. Therefore the long-hypothesized ridge jump to the east between BSMA and ECMA anomalies at about 170 Ma is supported by this study. The width of the JMQZ on the African flank is about 70 km greater than that on the

North American flank yielding an asymmetry of about 22%. Inspection of magnetic anomalies over this range reveals that additional, correlatable anomalies exist over Africa, suggesting that a second ridge jump, to the west, occurred. Modeling results indicate that this jump occurred between 164 Ma and 159 Ma.

3.2 Introduction

The overall kinematic history of the central Atlantic Ocean, between 10° and 40° N (Figure 3.1), is generally well understood (Klitgord and Schouten, 1986; Muller and Roest, 1992; Muller and Smith, 1993; Vogt, 1986; Withjack *et al.*, 1998). Following Middle to Late Triassic rifting between North America and Africa, seafloor spreading began about 185 Ma (Withjack *et al.*, 1998). Fracture zones identified from Geosat and Seasat altimetry data have been combined with magnetic isochrons to estimate the age and relative rotation history between the North American and African Plates (Klitgord and Schouten, 1986; Muller and Roest, 1992).

Flow lines calculated from poles that describe the history of rotation between North America and Africa, and South America and Africa, were used by Muller and Smith (1993) to interpret the location of the plate boundary between North and South America in the central Atlantic as well as the triple junction it forms with Africa. They report that the boundary and triple junction migrated from the Guinea-Demarrara shear margin northward to the Mercurius Fracture Zones (about 12°N) between Chrons 34 and 13, or between 84 and 33 Ma. Therefore our study area, which extends from the coasts of

Figure 3.1

Topography and bathymetry of the central Atlantic Ocean. The offshore grid is part of the global TerrainBase 5 arc-minute grid, and the onshore grid is part of the global GTOPO30 30 arc-second grid.

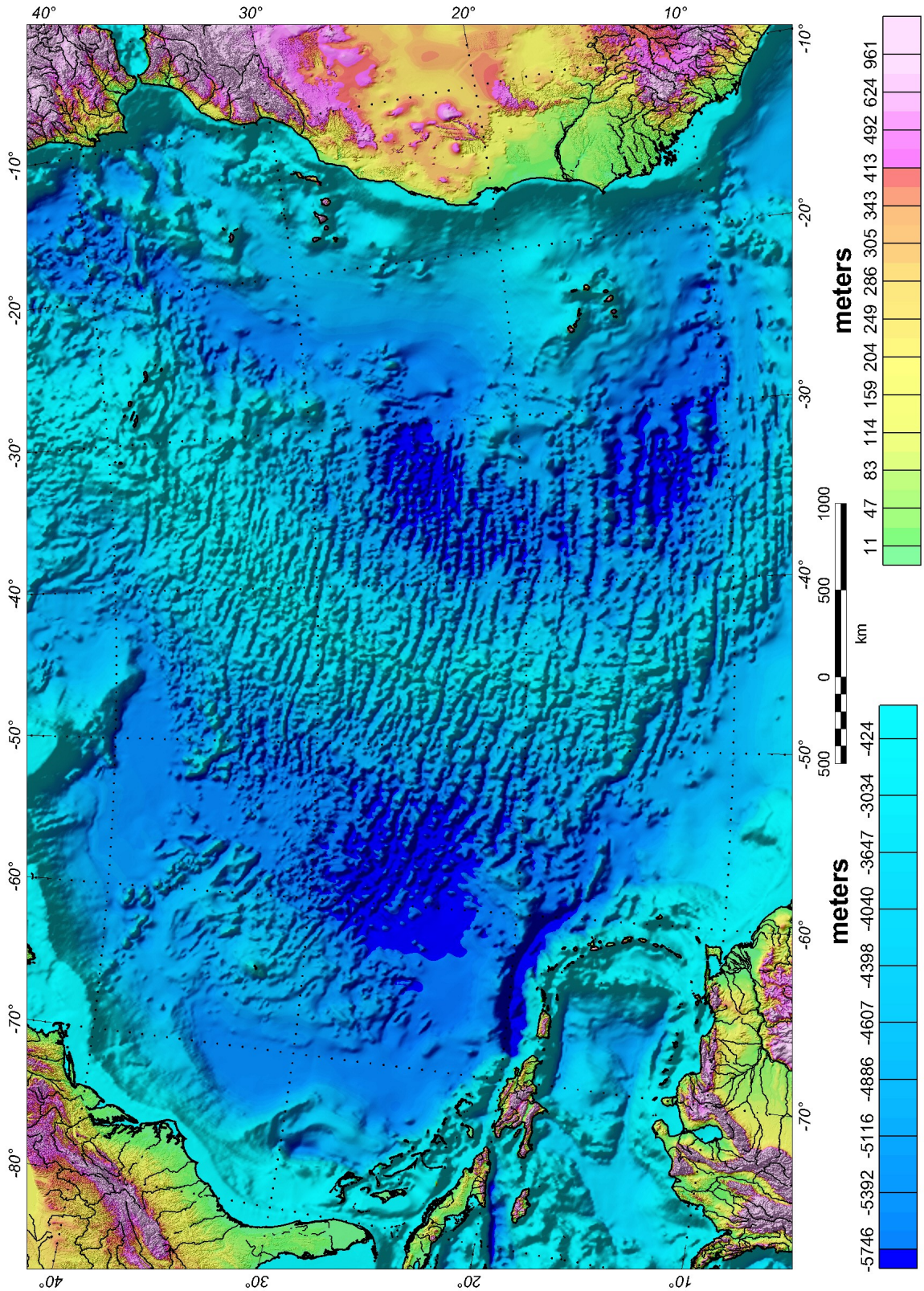
40°
30°
20°
10°
-10°
-20°
-30°
-40°
-50°
-60°
-70°
-80°
meters
961
624
492
413
343
305
286
249
204
159
114
83
47
11
meters
-424
-3034
-3647
-4040
-4398
-4607
-4886
-5116
-5392
-5746
500
0
500
1000
km

North America and Africa and between the Atlantis and Fifteen-Twenty fracture zones, is entirely located on the North American and African Plates.

Magnetic anomalies, west and east from the Mid-Atlantic ridge (MAR) towards the continental shelves of North America and Africa, have been interpreted as geomagnetic isochrons produced by geomagnetic polarity reversals during seafloor spreading (Klitgord and Schouten, 1986). Five major magnetic anomaly provinces have been identified in the central Atlantic: 1) MAR to Chron C34; 2) the Cretaceous Magnetic Quiet (CMQZ or long normal); 3) Mesozoic isochrons, or M-Series Chrons M0 to M25; 4) Jurassic Magnetic Quiet Zone (JMQZ or smooth zone, which are M-Series Chrons M26 to M41); and 5) another zone of low amplitude anomalies between the East Coast Magnetic Anomaly (ECMA) and Blake Spur Magnetic Anomaly (BSMA) over the North American plate (IMQZ). Seafloor spreading anomalies have been well documented for Chrons C1 to C34 and M0 to M25 provinces (Klitgord and Schouten, 1986; Muller and Roest, 1992). Sixteen Chrons, including six M-Series Chrons used in this study, have been globally mapped by Muller *et al.* (1997). These six M-series Chrons are M0 (120.6 Ma), M4 (126.6 Ma), M10N (130.5 Ma), M16 (137.9 Ma), M21 (146.6 Ma), and M25 (154.0 Ma).

We have integrated gridded magnetic data with a recently compiled, extensive profile-based magnetic data set to:

1. correlate 17 additional M-series Chrons in the central Atlantic,
2. locate the Chron-fracture zone intersections between Chrons C34, M0, and M25, and the Fifteen-Twenty, Kane, and Atlantis fracture zones in order to

calculate finite difference poles needed to reconstruct the relative plate motion between North America and Africa between 84 and 154 Ma,

3. identify three periods of asymmetric spreading: 1) the present to 84 Ma when seafloor accretion on the North American flank was about 10.0% faster than accretion on the African flank, 2) from 84 Ma to 120.6 Ma when African accretion was about 3.5% faster, and 3) from 120.6 Ma to 154 Ma when North American accretion was about 10.5% faster,
4. confirm a ridge jump to the west on the North American plate that occurred at approximately 170 Ma (Vogt, 1973, 1986), and propose the existence of another ridge jump to the east that occurred on the African plate between 159 Ma and 164 Ma.

3.3 Geophysical Data

3.3.1 Magnetic Data

Two magnetic anomaly grids partially cover the central Atlantic Ocean (Figures 3.2 and 3.3). The first, the Magnetic Anomaly Map of North America was compiled and processed as part of the Geological Society of America's Decade of North American Geology (DNAG) project (Committee for the Magnetic Anomaly Map of North America, 1985). The second, the Magnetic Anomalies of the Arctic and North Atlantic Oceans and Adjacent Land Areas grid was compiled and processed between 1988 and 1995 by the Geological Survey of Canada (GSC) (Verhoef *et al.*, 1996). The grid cell intervals of

Figure 3.2

Total intensity magnetic anomalies – DNAG. Part of the Magnetic Anomaly Map of North America, which was compiled and processed as part of the Geological Society of America's Decade of North American Geology (DNAG) project (Committee, 1985). The grid cell interval is 2 km.

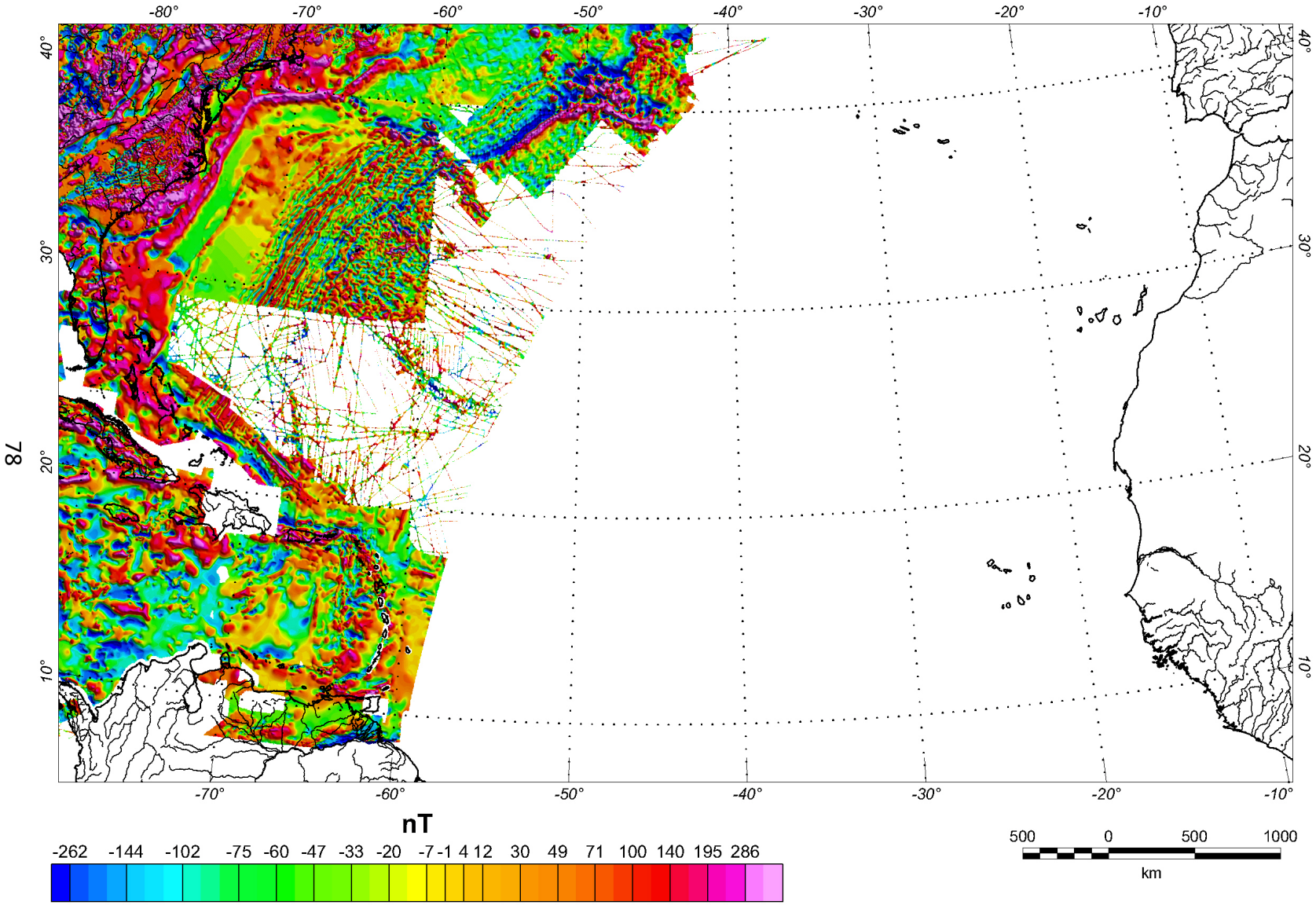
-80°
-70°
-60°
-50°
-40°
-30°
-20°
-10°
40°
30°
20°
10°
78
nT
-262 -144 -102 -75 -60 -47 -33 -20 -7 -1 4 12 30 49 71 100 140 195 286
500 0 500 1000
km

Figure 3.3

Total intensity magnetic anomalies – GSC. Part of the Magnetic Anomalies of the Arctic and North Atlantic Oceans and Adjacent Land Areas grid was compiled and processed between 1988 and 1995 by the Geological Survey of Canada (GSC) (Verhoef et al., 1996). The grid cell interval is 5 km.

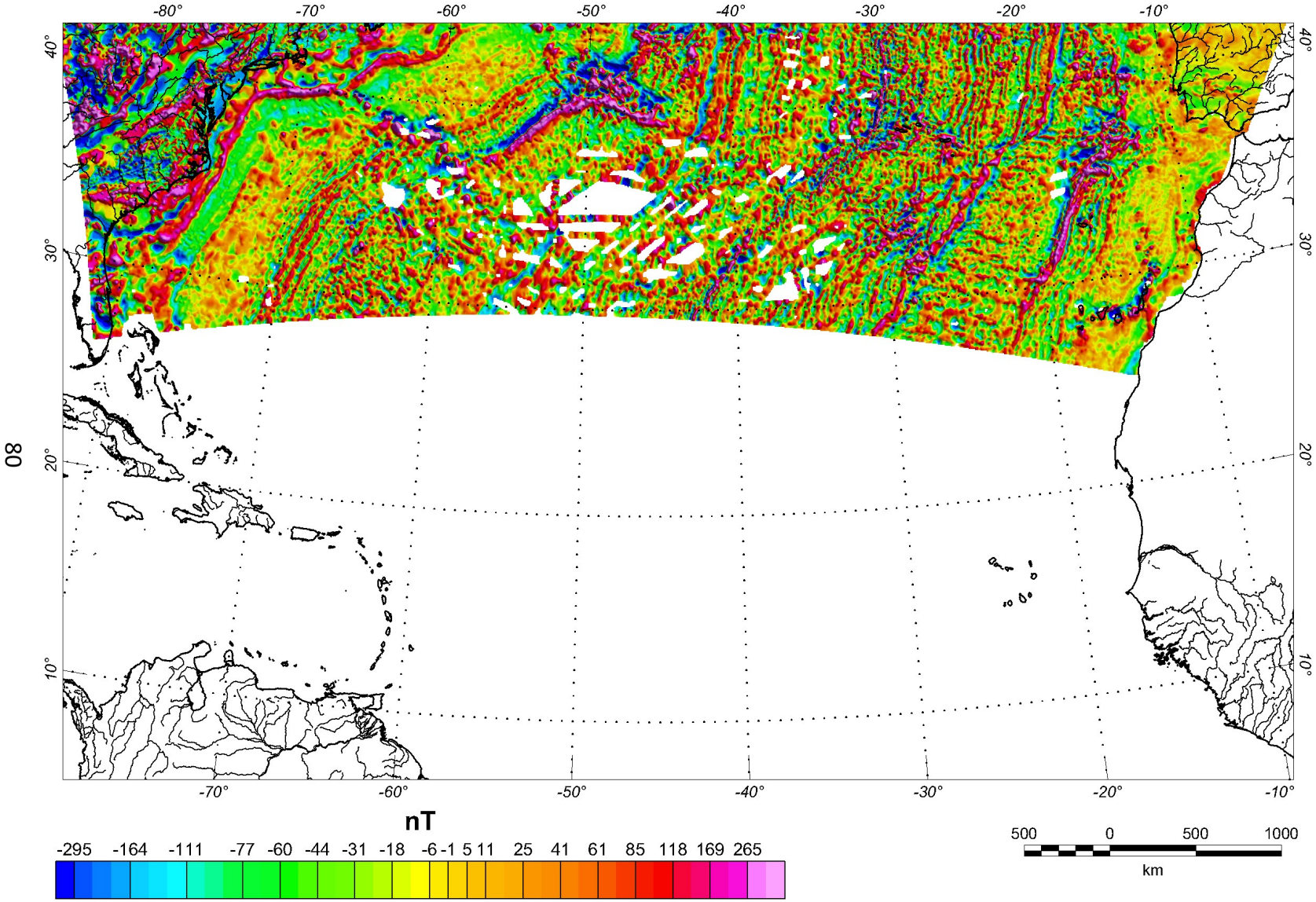
-80°
-70°
-60°
-50°
-40°
-30°
-20°
-10°
40°
30°
20°
10°
nT
-295 -164 -111 -77 -60 -44 -31 -18 -6 -1 5 11 25 41 61 85 118 169 265
500 0 500 1000
km

DNAG and GSC data are 2 km and 5 km respectively. Both data sets include millions of data points and involved the efforts of many organizations from several countries.

Magnetic anomaly profile data used in this study were acquired along shiptracks over the central Atlantic Ocean. These data, which involve hundreds of cruises, are maintained by the National Oceanic and Atmospheric Administration / National Geophysical Data Center (NOAA/NGDC), as the global GEOphysical DAta System (GEODAS) database, and by the GSC. GEODAS data were acquired from 1960 through 1993 over an irregular network of cruise locations, track headings, and data sample intervals (Figure 3.4). The Kroonvlag project, carried out from 1967 to 1980, involved continuous seismic reflection and magnetic measurements on board freighters, traveling between the English Channel and locations around the central Atlantic Ocean (Collette *et al.* 1984), that are maintained by the GSC (Figure 3.5). About 41,000 line km of magnetic data were acquired during 1967 and 1968 along 42 east-west transects in the western central Atlantic Ocean (Vogt *et al.*, 1971) (Figure 3.5). These anomaly profiles and transects were digitzed from enlarged figures.

Data over the central Atlantic Ocean have been extracted from the extensive grid and profile data sets described above with the cruise data organized into 9501 lines, totaling almost 1,644,000 line km of data.

3.3.2 Gravity Data

The satellite-derived free air gravity anomaly grid over the central Atlantic Ocean is a two arc-minute grid of fairly uniform coverage (Sandwell and Smith, 1997) (Figure 3.6). Global satellite-derived gravity data have been calculated from satellite altimetry data

Figure 3.4

GEODAS Magnetic data shiptrack locations. Magnetic anomaly profile data acquired along shiptracks over the central Atlantic Ocean used in this study consists of hundreds of cruises in databases maintained by the National Oceanic and Atmospheric Administration / National Geophysical Data Center (NOAA/NGDC), which is the global GEOphysical DAta System (GEODAS) database.

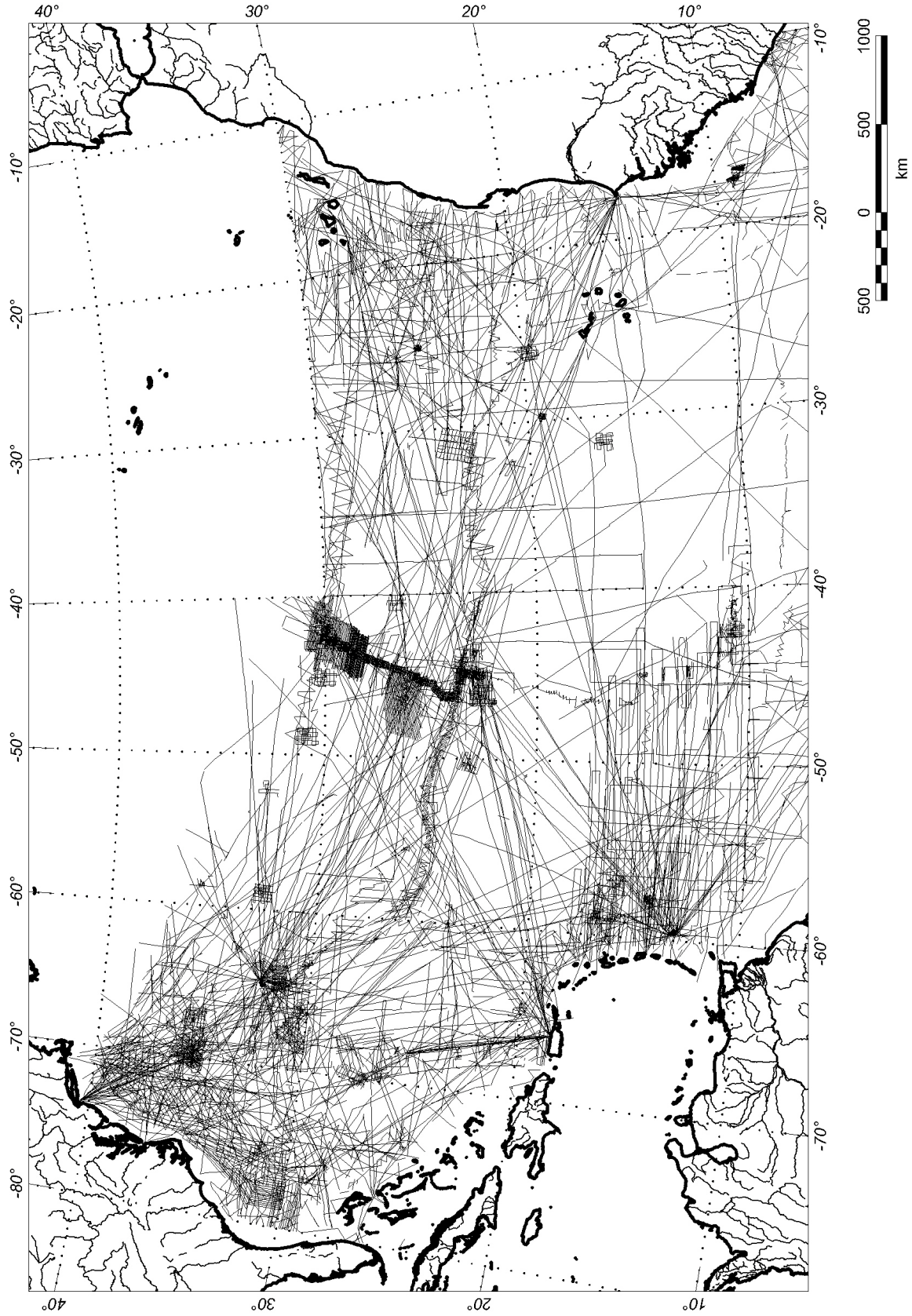
40°
30°
20°
10°
-10°
-20°
-30°
-40°
-50°
-60°
-70°
-80°
1000
500
0
500
km

Figure 3.5

GSC and Vogt et al. (1971) Magnetic data shiptrack locations. The Kroonvlag project was carried out from 1967 to 1980 and involved continuous seismic reflection and magnetic measurements on board freighters traveling between the English Channel and locations around the central Atlantic Ocean (Collette et al. 1984) and are maintained by the GSC (thin lines). About 41,000 line km of magnetic data was acquired along shiptracks during 1967 and 1968 along east-west transects in the western central Atlantic Ocean (Vogt et al., 1971) (Thick lines).

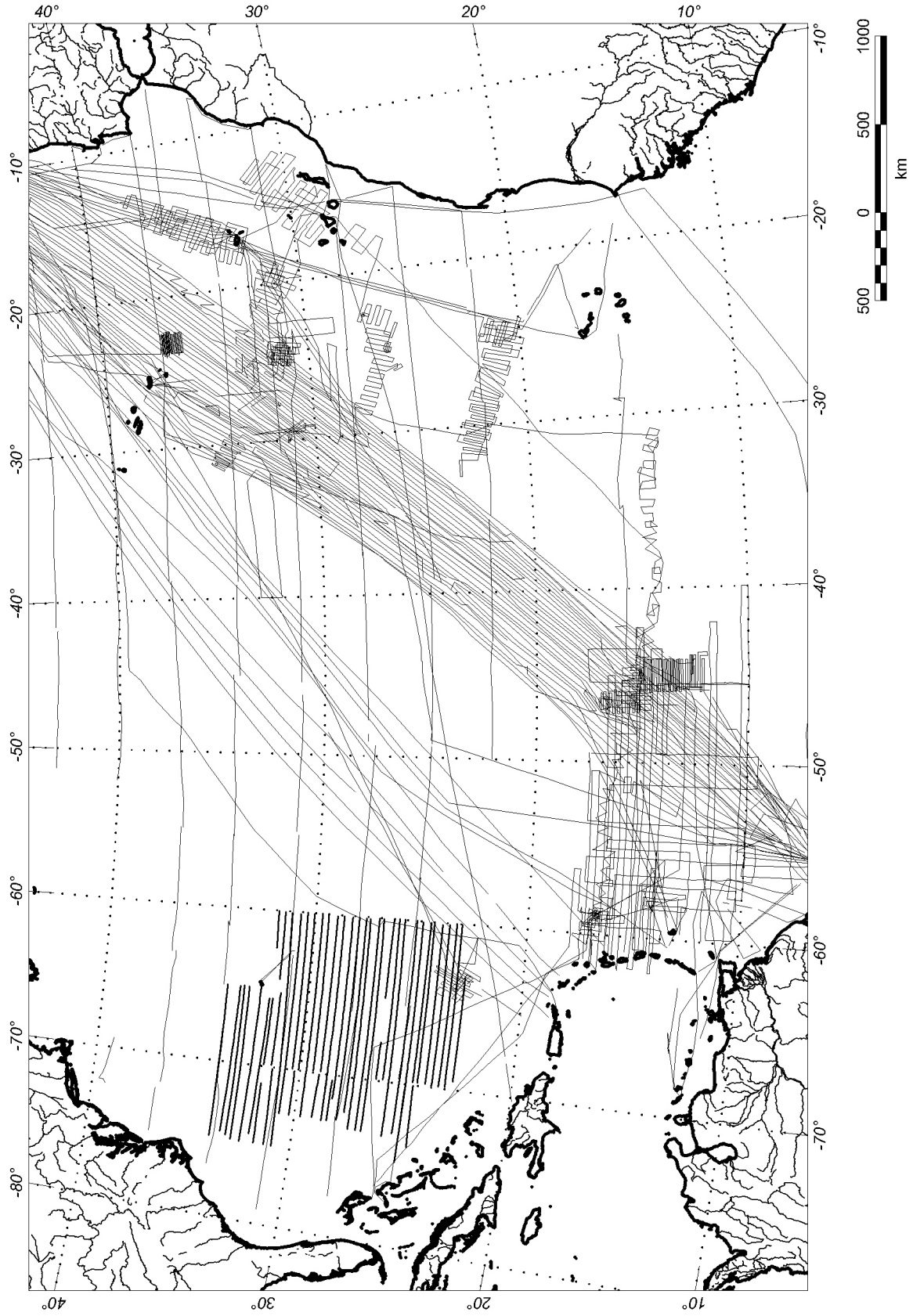
40°
30°
20°
10°
-10°
-20°
-30°
-40°
-50°
-60°
-70°
-80°
1000
500
0
500
km

Figure 3.6

Satellite-derived free air gravity anomalies (Sandwell and Smith, 1997). The grid cell interval is 2 arc-minutes.

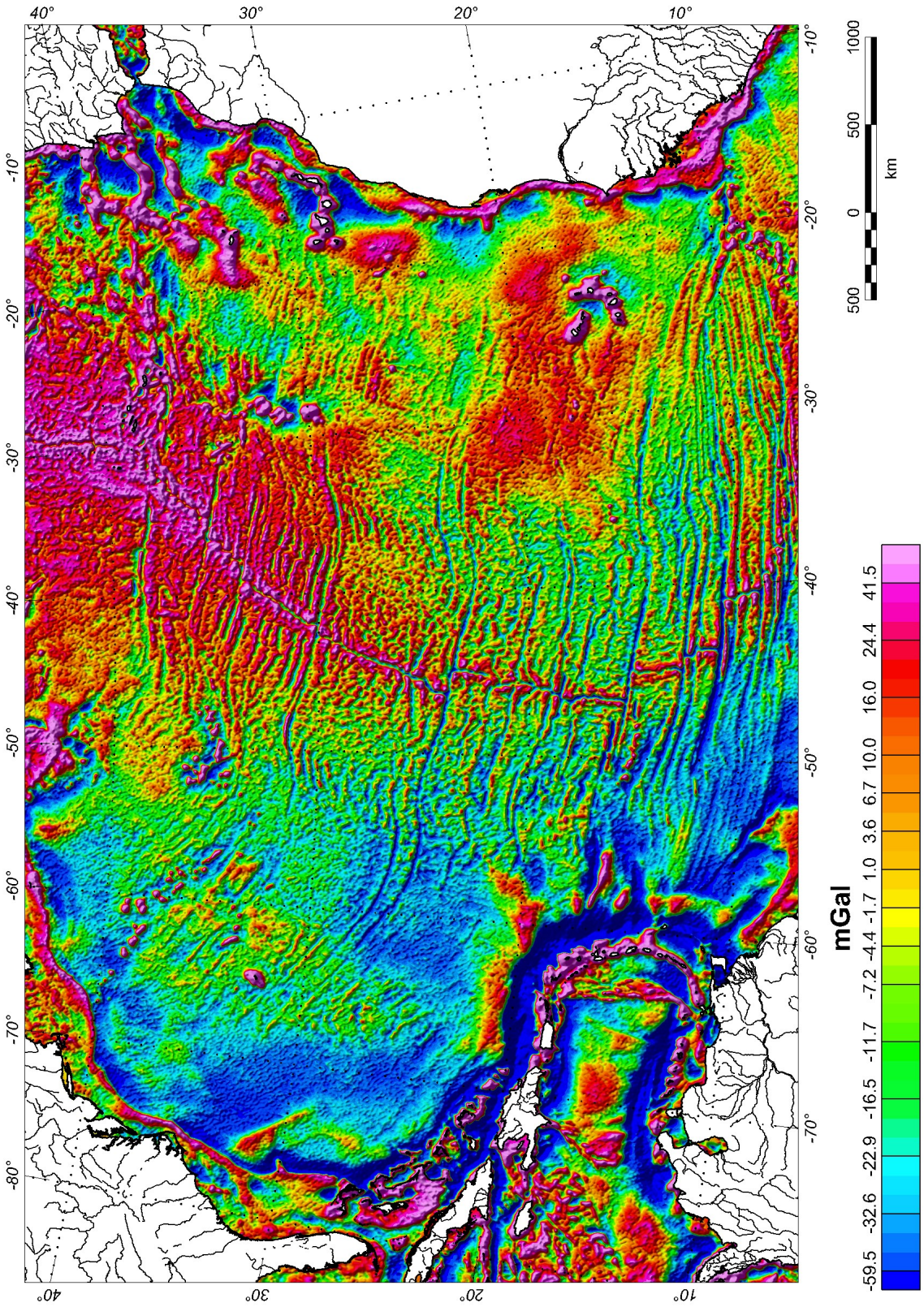
40°
30°
20°
10°
-10°
-20°
-30°
-40°
-50°
-60°
-70°
-80°
1000
500
0
500
km
mGal
41.5
24.4
16.0
10.0
6.7
3.6
1.0
-1.7
-4.4
-7.2
-11.7
-16.5
-22.9
-32.6
-59.5

acquired during the Geosat Geodetic Mission and the ERS 1 Geodetic Phase along closely spaced satellite tracks (Sandwell and Smith, 1997). They report that the data resolution is about 5 milligals in amplitude over 20 kilometer wavelengths. Shipboard gravity data from the NOAA/NGDC were not used in the present study because the satellite-derived gravity data are sufficient to map fracture zones.

3.4 Methods

Interpreting the kinematic history between two tectonic plates requires determining finite difference poles that describe the relative motion necessary to restore the plates over various time intervals. Finite difference Euler poles are calculated from points on two plates that were once coincident. In ocean basins, magnetic anomalies produced by geomagnetic polarity reversals lie along great circles that intersect at the Euler poles, assuming that ridge segments are orthogonal to the orientation of extension. Transform faults coincide with small circles about the Euler poles, and the trace of transform faults and fracture zones form flowlines that indicate the relative direction of motion between the plates over various time intervals. Finite difference Euler poles can therefore be determined by using the intersections of several great and small circles over specific, small time intervals. The extent to which these finite difference poles describe the actual relative motion is dependent upon the time scale over which they are determined.

In this analysis, all seafloor spreading rates, unless otherwise specified, are half-rates, which refers to the rate of accretion on a single plate. Magnetic anomaly amplitudes

are referred to as very low, low, high, and very high where the peak-to-trough magnitudes are less than 10 nT, tens of nT, hundreds of nT, and thousands of nT, respectively. Mesozoic isochron ages used in this study are reported by Channell *et al.*(1995) and Sager *et al.*, (1998).

3.4.1 Fracture Zones and Flowlines

Fracture zones are composed of active transform segments between seafloor spreading ridges and their fossil, off-axis traces (Fox and Gallo, 1984; Muller and Roest, 1992). They exhibit a distinct crustal structure, particularly when seafloor spreading is slow such as in the central Atlantic: the crust thins dramatically to as little as 2 km, probably due to decreased magma supply at the ridge-transform intersections (Fox and Gallo, 1984). Short transform offsets are defined to be less than 30 km and should not be used for kinematic reconstructions because they can be transient and unstable over time (Fox and Gallo, 1984). Long transform offsets are defined to be greater than 80 km, and very long offsets (300 km or greater) should not be used for kinematic reconstructions because they can be overprinted by complex structures related to changes in plate motion (Collette and Roest, 1992; Fox and Gallo, 1984). As plate motion changes over time, these very long offsets cannot easily adjust and compressional or extensional structures form along the transforms (Bonatti, 1994; Menard and Atwater, 1968).

The offsets of the Atlantis, Kane and Fifteen-Twenty fracture zones are 60 km, 130 km, and 170 km. Muller and Roest (1992) classified the Atlantis and Kane to be medium length fracture zones. Klitgord and Schouten (1986) indicate that fracture zones and flowlines in the central Atlantic are closely correlated and that fracture zone jumps,

parallel to the MAR, are rare. Therefore the Atlantis, Kane and Fifteen-Twenty fracture zones are utilized to best approximate finite difference rotations in the central Atlantic.

Paths that describe the relative motion between two accreting plates over time are flowlines, and fracture zones provide approximations of these paths by recording changes in seafloor spreading direction (Collette and Roest, 1992; Klitgord and Schouten, 1986). Therefore, specific conjugate segments of a flowline coincide with small circles about Euler poles of rotation that would reconstruct the relative motion along these segments. Fracture zones can be identified by their characteristic signatures in magnetic and gravity data. Magnetic lineations related to geomagnetic polarity reversals are often offset along fracture zones, and free air gravity anomalies over fracture zones are typically minima. Therefore we interpret fracture zones from maps of gravity and magnetic anomalies (Figures 3.2, 3.3 and 3.6).

3.4.2 Geomagnetic Isochrons

Magnetic anomalies produced by geomagnetic polarity reversals are isochrons that are associated with rocks accreted along the MAR during specific time intervals (Chrons). They are identified in a two-step process: 1) by simultaneous interpretation of gridded and profile magnetic anomalies to correlate significant features, and 2) comparing selected anomaly profiles with synthetic profiles calculated from 2D magnetic seafloor spreading models based on established geomagnetic polarity reversal scales (Channell *et al.*, 1995; Sager *et al.*, 1998).

Correlating anomalies can be complicated by several factors related to geology, the Earth's magnetic field, and the data. Data limitations are related to the quality of

instrumentation, positioning, sampling, and processing. The shape of an anomaly over a given magnetized source body depends on the shape, depth and orientation of the source body as well as the magnetic field intensity and direction. Therefore the shapes of individual anomalies as well as sequences of anomalies are important characteristics for identifying Chrons. Over distances of tens to hundreds of kilometers changes in anomaly character are usually gradual (Klitgord and Schouten, 1986; Vogt, 1986).

The magnetic data coverage over the North American flank of the central Atlantic includes extensive shiptrack coverage as well as gridded data sets; however, the data coverage over the African flank suffers from low shiptrack data density and the lack of gridded data south of 30°N. Therefore, we interpret Mesozoic Chrons from the Bahamas to just northeast of the Atlantis fracture zone for the North American flank, but only along a 200 km wide corridor between the Atlantis and Kane fracture zones for the African flank.

The best technique for correlating magnetic anomalies is to consider groups, or sequences of anomalies for line-to-line coherency. Anomalies produced by geomagnetic polarity reversals should be consistent and roughly parallel to a seafloor spreading center, and anomalies produced by basement relief are typically shorter and less organized. Initially (Step 1), prominent anomalies coinciding approximately with magnetic isochrons mapped by Muller *et al.* (1997) were identified on maps: M0, M4, M10, M16, M21, and M25. Then additional anomalies were identified between this first set of prominent anomalies by approximating distances based on time intervals defined by geomagnetic polarity reversals (Channell *et al.*, 1995; Sager *et al.*, 1998). Landward of M25, anomalies were identified by approximating distances based on time intervals and

by comparing anomaly shapes with Chrons identified by Roeser *et al.* (2002) and Sager *et al.* (1998).

Twenty-three magnetic anomaly profiles were selected between Atlantis and Kane fracture zones from the North American flank, and 13 were selected between Atlantis and Kane fracture zones from the African flank, to compare correlated anomalies with synthetic anomalies generated from a 2D seafloor spreading model based on the geomagnetic polarity reversal scale (Step 2). Anomaly profiles were projected to series of parallel straight line segments and displayed at the same horizontal scales, then correlated anomalies were identified as Chrons according to their similarity with the synthetic profiles (Table 3.1).

3.4.3 Finite-Difference Poles

The Euler poles about which the relative rotations of two tectonic plates are approximated are the two intersections of the Earth's surface with a rotation axis. The axis of a pair of Euler poles passes through the center of the earth and the motion between the plates can be described by the geographic coordinates of the pole and a rotation angle for a specified finite motion. Therefore a single rotation can be described four ways: positive or negative motion with respect to either plate, and about either pole location. We calculate stage poles over major time intervals for the North American and African plates separately, and total reconstruction poles between the plates over the same time intervals for sets of control points located on the two plates. These were located at the intersections of magnetic anomalies (C34, M0, M25) with Atlantis, Kane, and Fifteen-Twenty fracture zones (Table 3.2).

Chron	Time Interval	Chron	Time Interval
M0	**120.60 to 121.00**	M20	144.70 to 145.52
M1	123.19 to 123.55	**M21**	**146.56 to 147.06**
M3	124.05 to 125.67	M22	148.79 to 149.49
M4	**126.57 to 126.91**	M23	150.69 to 150.91 and 150.93 to 151.40
M10N	130.49 to 130.84	**M24**	**151.72 to 151.98 and 152.00 to 152.15**
M12A	133.99 to 134.08	**M25**	**154.00 to 154.31**
M14	134.81 to 135.57	M28	156.19 to 156.51
M16	**137.85 to 138.50**	M29	157.27 to 157.53
M17	138.89 to 140.51	M32	159.68 to 159.77
M18	141.22 to 141.63	M37	164.50 to 164.60
M19	143.07 to 143.36	M40	167.22 to 167.33
M20n-1	143.77 to 143.84		

Table 3.1

Interpreted geomagnetic isochrons. Isochrons M0 through M28 were classified by Channell et al. (1995) and M32 through M40 were classified by Sager et al. (1998). Isochrons mapped by Muller et al. (1997) are bold.

		Latitude	Longitude
MAR	Atlantis	30.053540	-42.319763
	Kane	23.710878	-45.625965
	Fifteen-Twenty	15.274925	-45.802580
C34 West	Atlantis	31.362394	-55.333472
	Kane	26.781704	-58.677409
	Fifteen-Twenty	**18.136984**	**-60.993819**
C34 East	Atlantis	29.098803	-29.803073
	Kane	23.853540	-32.647269
	Fifteen-Twenty	14.470362	-33.718313
M0 West	Atlantis	34.500242	-62.367465
	Kane	30.781670	-66.114727
	Fifteen-Twenty	23.390525	-68.836762
M0 East	Atlantis	27.420556	-22.815688
	Kane	20.655864	-25.125158
	Fifteen-Twenty	12.502492	-24.765997
M25 West	Atlantis	36.955983	-66.494426
	Kane	32.834469	-70.411400
	Fifteen-Twenty	25.372563	-73.394109
M25 West	Atlantis	25.993803	-19.241114
	Kane	19.426952	-20.486982
	Fifteen-Twenty	11.330468	-18.592948

Table 3.2

Control points used to calculate stage and total reconstruction poles.

A method similar to that described by Engebretson *et al.* (1984) was used to find the best fit Euler pole for pairs of control points defined by the intersections between interpreted geomagnetic isochrons and fracture zones. Each pair of control points is considered to have been coincident such that a plate rotation exists that will restore them to this single point. The errors between these restored pairs of control points along the Atlantis, Kane and Fifteen-twenty Fracture Zones are minimized for three major time intervals: 1) from the present to Chron C34 (84 Ma), 2) from Chron C34 to Chron M0 (120.6 Ma), and 3) from Chron M0 to Chron M25 (154 Ma).

A computer program was created that minimizes the sum of the squared errors between one set of control points and the rotated set of control points. It requires an input geographic seed location (latitude and longitude), for the center of a scan matrix, and a scan increment (in degrees). It builds, then searches the scan matrix for the best-fit Euler pole. Once the best-fit pole is located, its coordinates are returned and re-input into the program as the next seed location using a smaller scan increment. For each position in the scan matrix an average rotation angle is calculated using the pairs of control points. One set of control points is then rotated towards the other set of control points, which restores the plate position over the time interval represented by the pair of control points. Errors between these restored points are then minimized using a least-squares method. Convergence to a solution yielding a 90% confidence region is achieved in 3 or 4 iterations.

3.5 Results

From south to north, the Fifteen-Twenty, Kane, and Atlantis Fracture Zones span most of the central Atlantic, or about 2000 km, and they extend west and east close to the coasts of North America and Africa, or almost 6000 km. These fracture zones have been mapped by tracing gravity minima through the transform offsets. Solid lines reflect high confidence in the fracture zone trace, and dashed lines reflect less confidence (Figure 3.7).

Geomagnetic Chrons M0 to M40 have been identified and mapped on the North American flank from the Fifteen-Twenty to the Atlantis Fracture Zones (Figures 3.8). The DNAG gridded magnetic data show anomalies produced by polarity reversals, especially anomalies coinciding with Chrons M0 through M25 (Figures 3.9 and 3.10). To the west of Chron M25 and just south of 34°N, the gridded Arctic magnetic data are superior to the DNAG magnetic anomaly grid (Figures 3.2 and 3.3): the DNAG grid over this region is essentially flat, and the Arctic grid include subtle long wavelength anomalies. Refraction data indicate oceanic crust beneath the interpreted JMQZ Chrons, or M26 to M41 (Figures 3.8, 3.10 and 3.11), (Ewing and Ewing, 1959; Houtz, R. E., 1980; Katz and Ewing, 1956). Crustal boundaries mapped by Uchupi *et al.* (1984a, 1984b) indicate that oceanic crust extends inboard almost to the ECMA. Subtle, broad anomalies, similar to gridded JMQZ anomalies, between ECMA and BSMA also support this interpretation of oceanic crust.

Sparse data coverage, from Fifteen-Twenty to Atlantis Fracture zones near the African coast, make comprehensive correlation over the entire range difficult. However,

Figure 3.7

Fracture zones and geomagnetic isochrons in the central Atlantic Ocean. Fracture zones and Mid-Atlantic Ridge (MAR) axis are thick blue lines. Global Chrons are red (Muller et al., 1997). Control points used for plate reconstructions located at the intersections of fracture zones and isochrons are yellow circles (see Table 3.2). East Coast Magnetic Anomaly (ECMA) and Blake Spur Magnetic Anomaly (BSMA) over the North American flank, and S1 and S3 magnetic anomalies over the African flank, are magenta. Green boxes outline detailed maps of Figures 3.8 through 3.13.

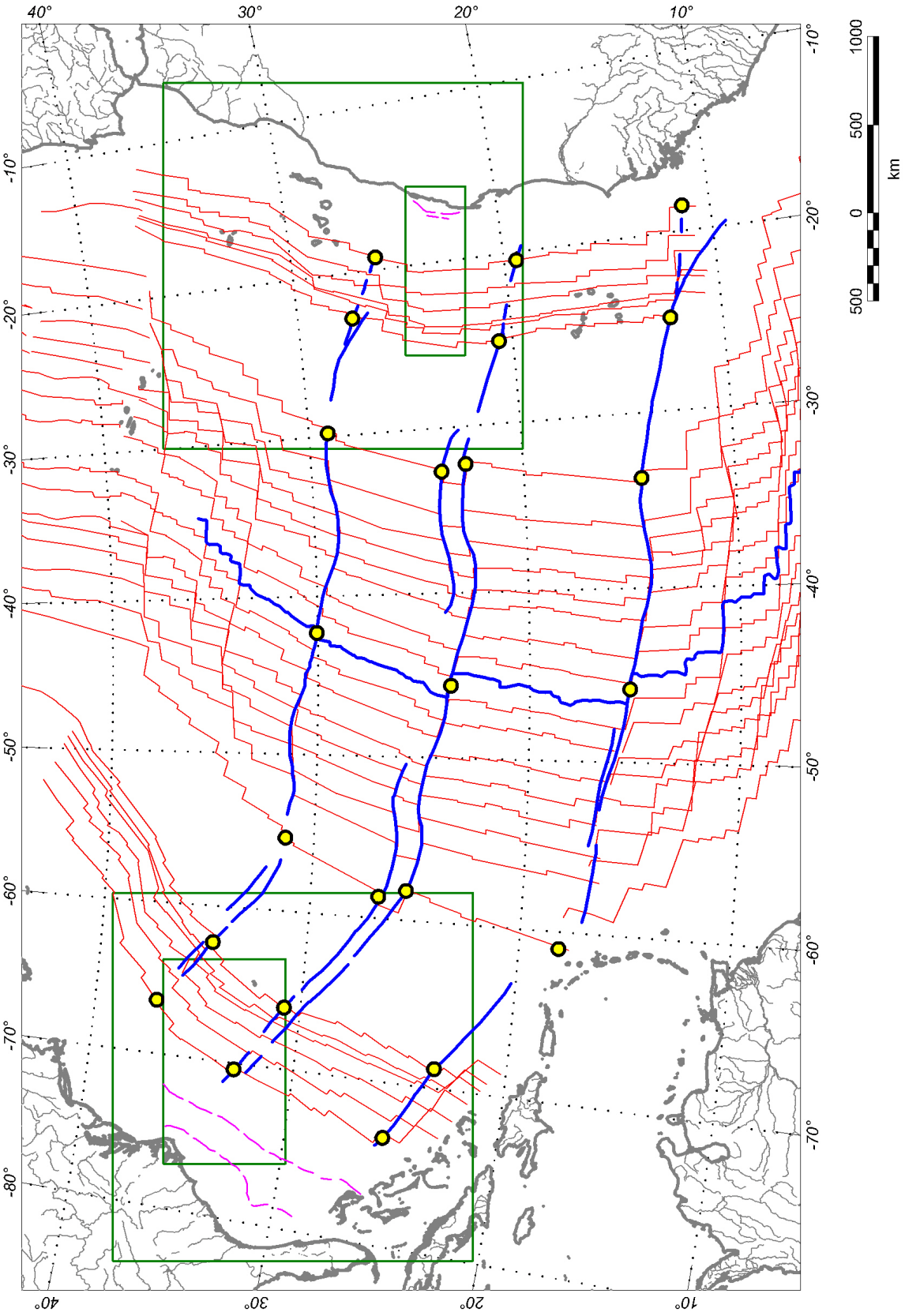
40°
30°
20°
10°
-10°
-20°
-30°
-40°
-50°
-60°
-70°
-80°
1000
500
0
500
km

Figure 3.8

Fracture zones and geomagnetic isochrons – North America. Fracture zones and the MAR are thick black lines. Identified Chrons are blue. Global Chrons are green (Muller et al., 1997). Control points used for plate reconstructions are located at the intersections of fracture zones and isochrons are yellow circles (see Table 3.2). Inverted red triangles and heavy red lines are locations of refraction data that indicate oceanic (see Table 3.6). ECMA and BSMA are magenta. Mappable limits of continental and oceanic crust (Uchupi et al., 1984a, 1984b) are violet. The Blake Spur Fracture Zone (BSFZ) is heavy dashed gray. Yellow shade corresponds to possible continental extension of the Blake Plateau (Dunbar and Sawyer, 1989). The Green box outlines detailed maps of Figures 3.9 through 3.11.

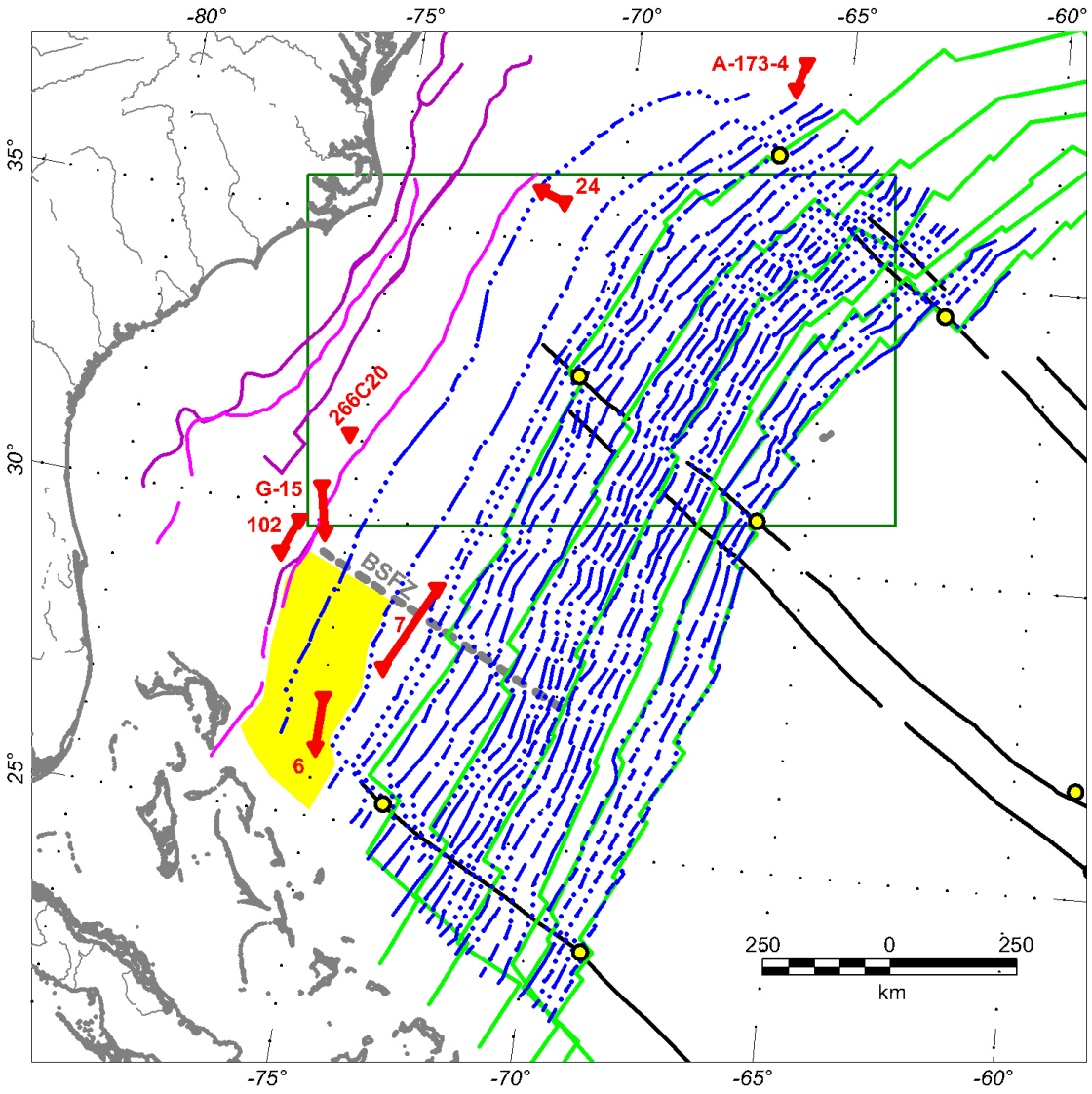
-80°
-75°
-70°
-65°
-60°
35°
30°
25°
A-173-4
24
266C20
G-15
102
BSFZ
7
6
250
0
250
km

Figure 3.9

Total intensity magnetic anomalies and magnetic data shiptracks – North America. DNAG (east) and Arctic Mag (west) total intensity grids are separated by the thick white line. GEODAS, GSC and track digitized from Vogt et al. (1971) are black lines.

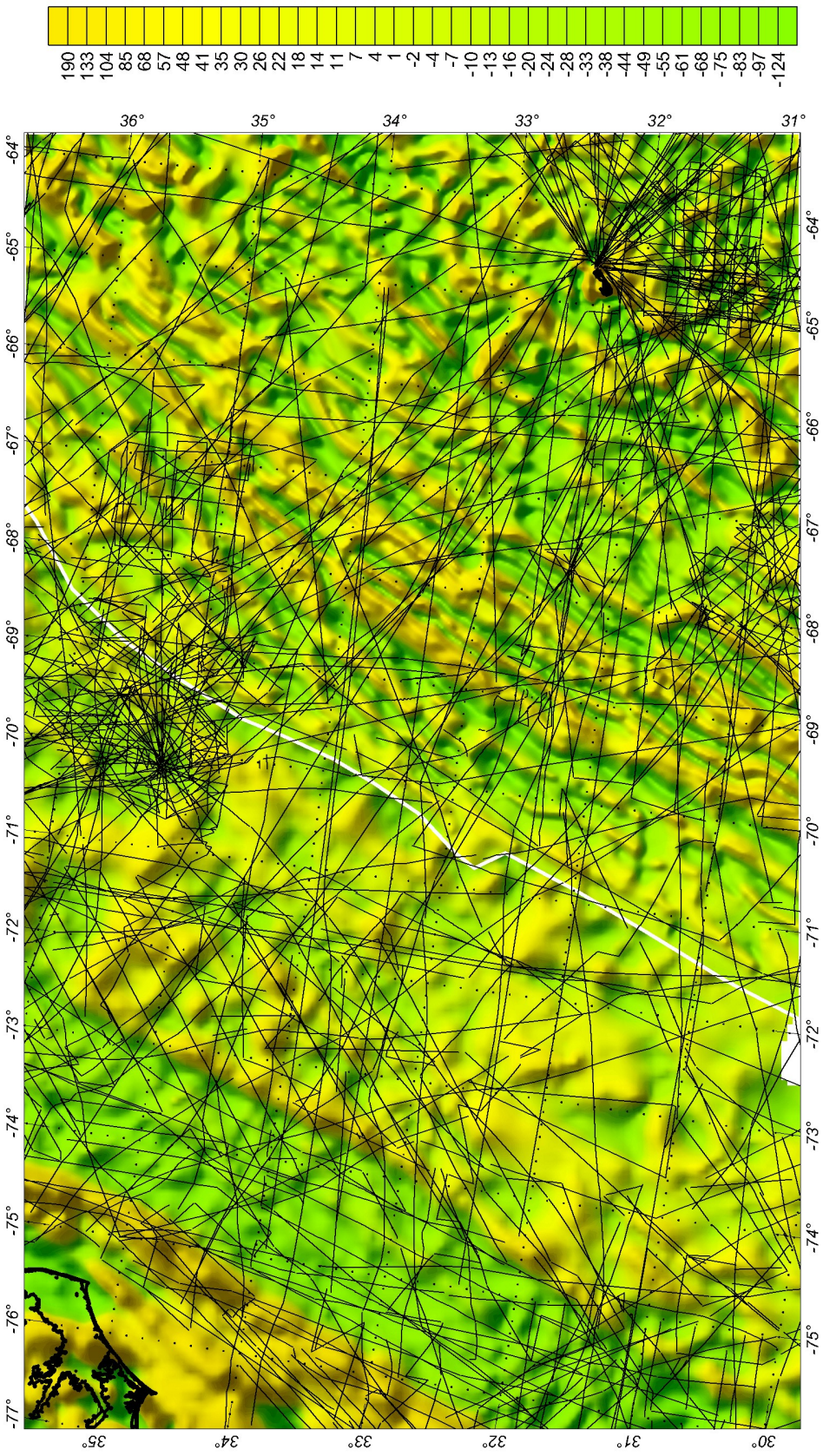
190
133
104
85
68
57
48
41
35
30
26
22
18
14
11
7
4
1
-2
-4
-7
-10
-13
-16
-20
-24
-28
-33
-38
-44
-49
-55
-61
-68
-75
-83
-97
-124
36°
35°
34°
33°
32°
31°
-64°
-65°
-66°
-67°
-68°
-69°
-70°
-71°
-72°
-73°
-74°
-75°
-76°
-77°
35°
34°
33°
32°
31°
30°

Figure 3.10

Total intensity magnetic anomalies and interpretation – North America. DNAG (east) and Arctic Mag (west) total intensity grids are separated by the thick white line. Identified Chrons are blue (see Table 3.1). Global Chrons (Muller et al., 1997) are red. Fracture zones are heavy black lines and control points are yellow circles (see Table 3.2). Inverted red triangles and heavy red lines are locations of refraction data that indicate oceanic (Table 3.6). Between the ECMA and BSMA two linear anomaly trends indicate the possibility of oceanic crust.

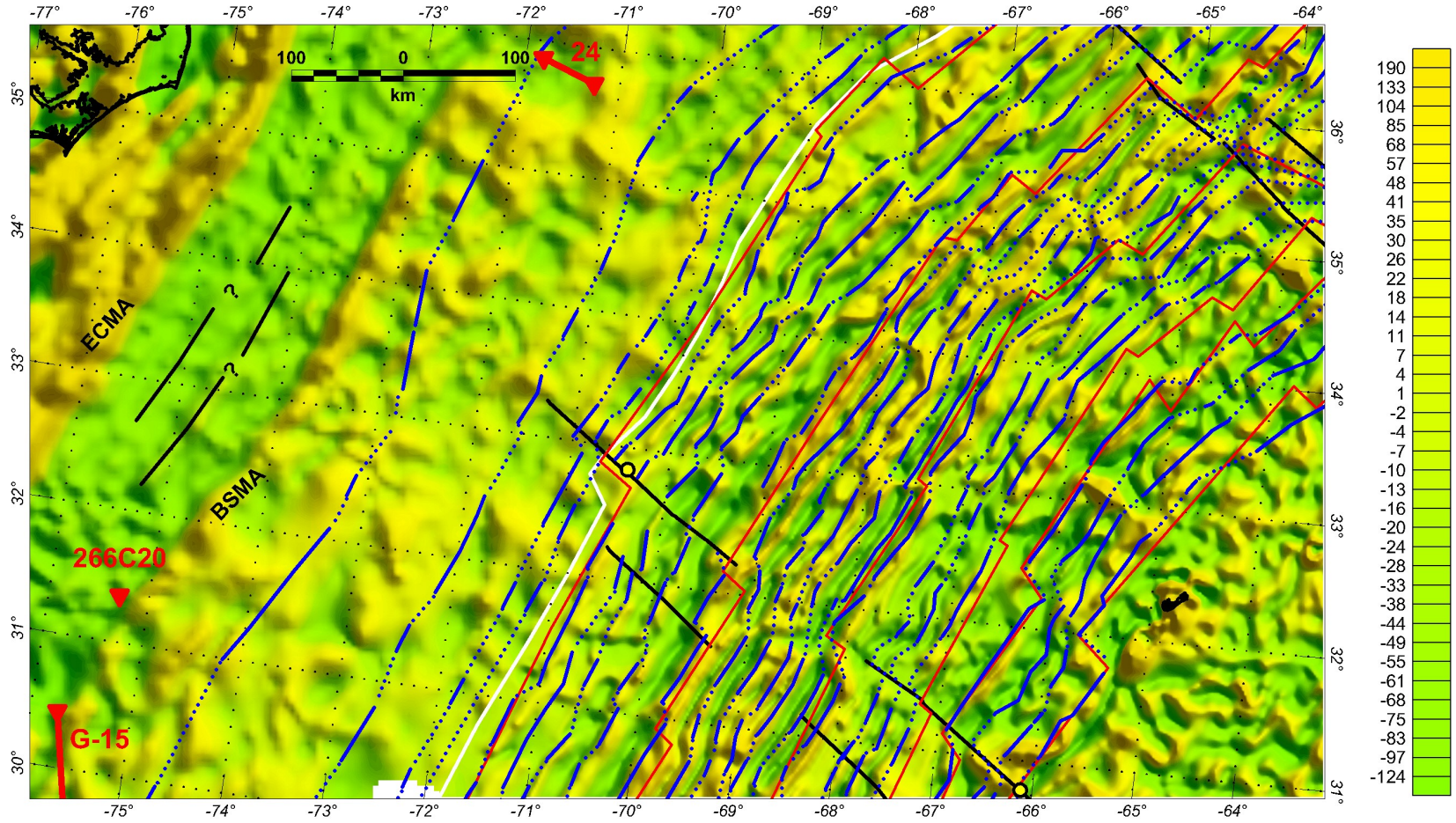
-77° -76° -75° -74° -73° -72° -71° -70° -69° -68° -67° -66° -65° -64°
35° 34° 33° 32° 31° 30°
36° 35° 34° 33° 32° 31°
100 0 100
km
24
ECMA
?
?
BSMA
266C20
G-15
190
133
104
85
68
57
48
41
35
30
26
22
18
14
11
7
4
1
-2
-4
-7
-10
-13
-16
-20
-24
-28
-33
-38
-44
-49
-55
-61
-68
-75
-83
-97
-124

Figure 3.11

Interpretation and profile correlation shiptracks – North America. Interpreted Chrons are blue (see Table 3.1). Global Chrons (Muller et al., 1997) are red. Profiles selected for Chron identification are heavy black. Inverted red triangles and heavy red lines are locations of refraction data that indicate oceanic (Table 3.6). The ECMA and BSMA are magenta.

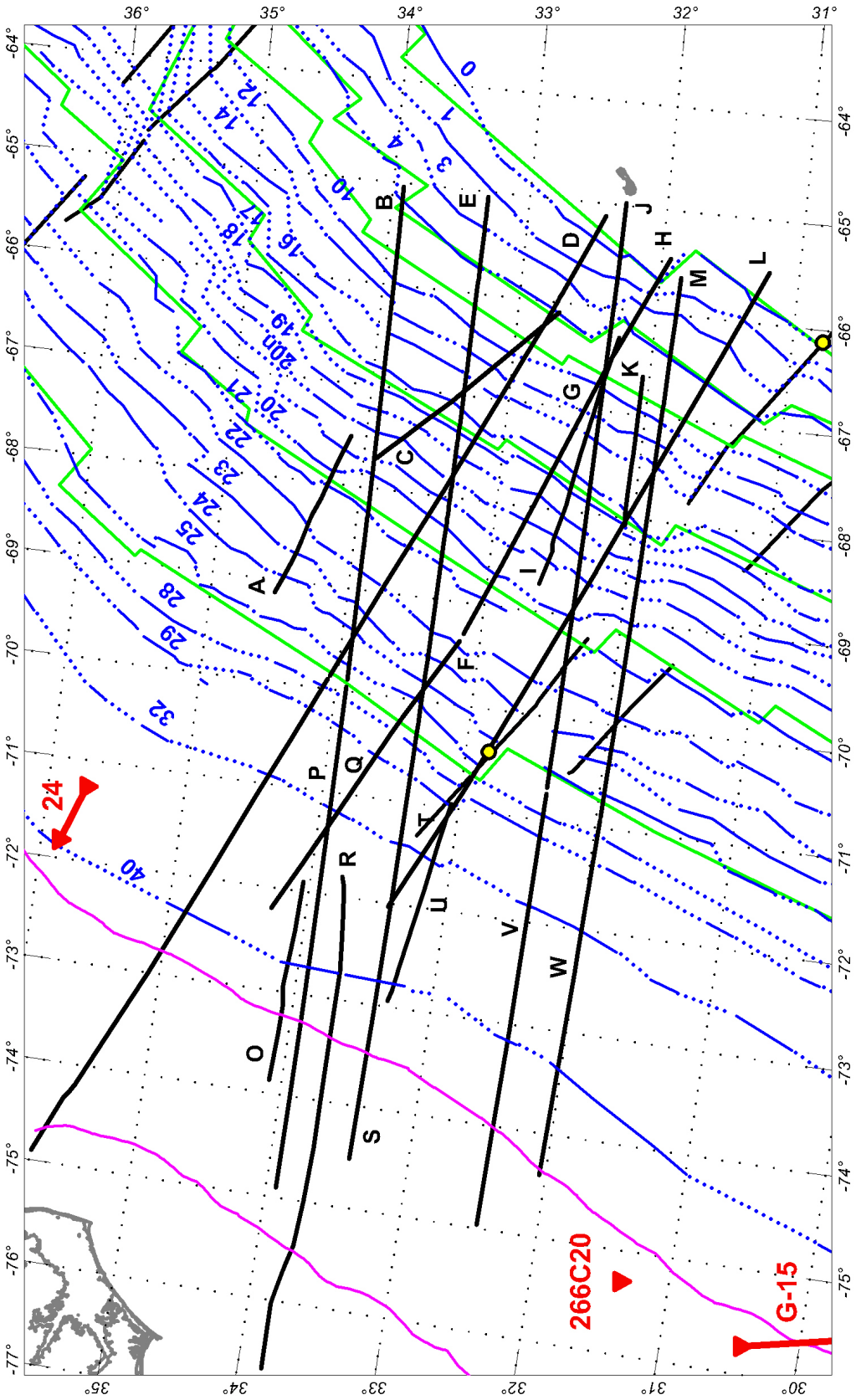
36°
35°
34°
33°
32°
31°
-64°
-65°
-66°
-67°
-68°
-69°
-70°
-71°
-72°
-73°
-74°
-75°
-76°
-77°
0
1
3
4
10
12
14
16
18
17
19
20
21
22
23
24
25
28
29
32
40
A
B
C
D
E
F
G
H
I
J
K
L
M
O
P
Q
R
S
T
U
V
W
24
266C20
G-15

thirteen lines were used to identify anomaly correlations from M0 to M40 on the African flank (Figures 3.12 and 3.13). The spreading rate for the high amplitude M0 through M25 Chrons is 12.9 mm/a (430 km over 33.4 My), which is 10.5% less than the conjugate spreading rate for the North American flank (14.4 mm/a over 480 km). However, the spreading rate for the low amplitude M25 through M40 (JMQZ) on the African flank appears to be 24.6 mm/a (320 km over 13 My), which is 22% greater than the spreading rate for the North American side (19.2 mm/a over 250 km). Therefore, an average half-spreading rate of 21.9 mm/a was computed by combining JMQZ widths from both flanks of the central Atlantic. Then synthetic profiles were calculated from models using this accretion rate. The group of anomalies over M37 appears to repeat on the profiles analyzed on the African flank (Figure 3.15).

Rotation angles about calculated stage poles for the western and eastern sides of the central Atlantic indicate significant asymmetry (Table 3.3). Confidence in the method used to calculate total reconstruction poles is supported by close correlations with poles calculated by Muller and Roest (1992) (Table 3.4). Error ellipsoids define areas where a given pole can be located with 90% confidence (Figure 3.16). Table 3.5 shows measured distances between the MAR and/or identified Chrons.

Twenty three profiles were selected between Atlantis and Kane fracture zones from the shiptrack database of the North American flank, and thirteen profiles were selected for the African flank (Figures 3.14 and 3.15). Figure 3.14 displays modeled M0-25 anomalies for both flanks and interpreted profile to profile correlations. The relatively high amplitude M0 to M25 Chrons are readily identified. However, correlation of JMQZ Chrons M28 to M41 is only fair, because of low anomaly amplitudes (Figure 3.15). The

Figure 3.12

Fracture zones and geomagnetic isochrons – Africa. Fracture zones are thick black lines. Global Chrons are green (Muller et al., 1997). Identified Chrons are blue. S1, S3 and S4 are magenta (Verhoef et al., 1991). Control points used for plate reconstructions are located at the intersections of fracture zones and isochrons are yellow circles (see Table 3.2). The Green box outlines the detailed map of Figures 3.13.

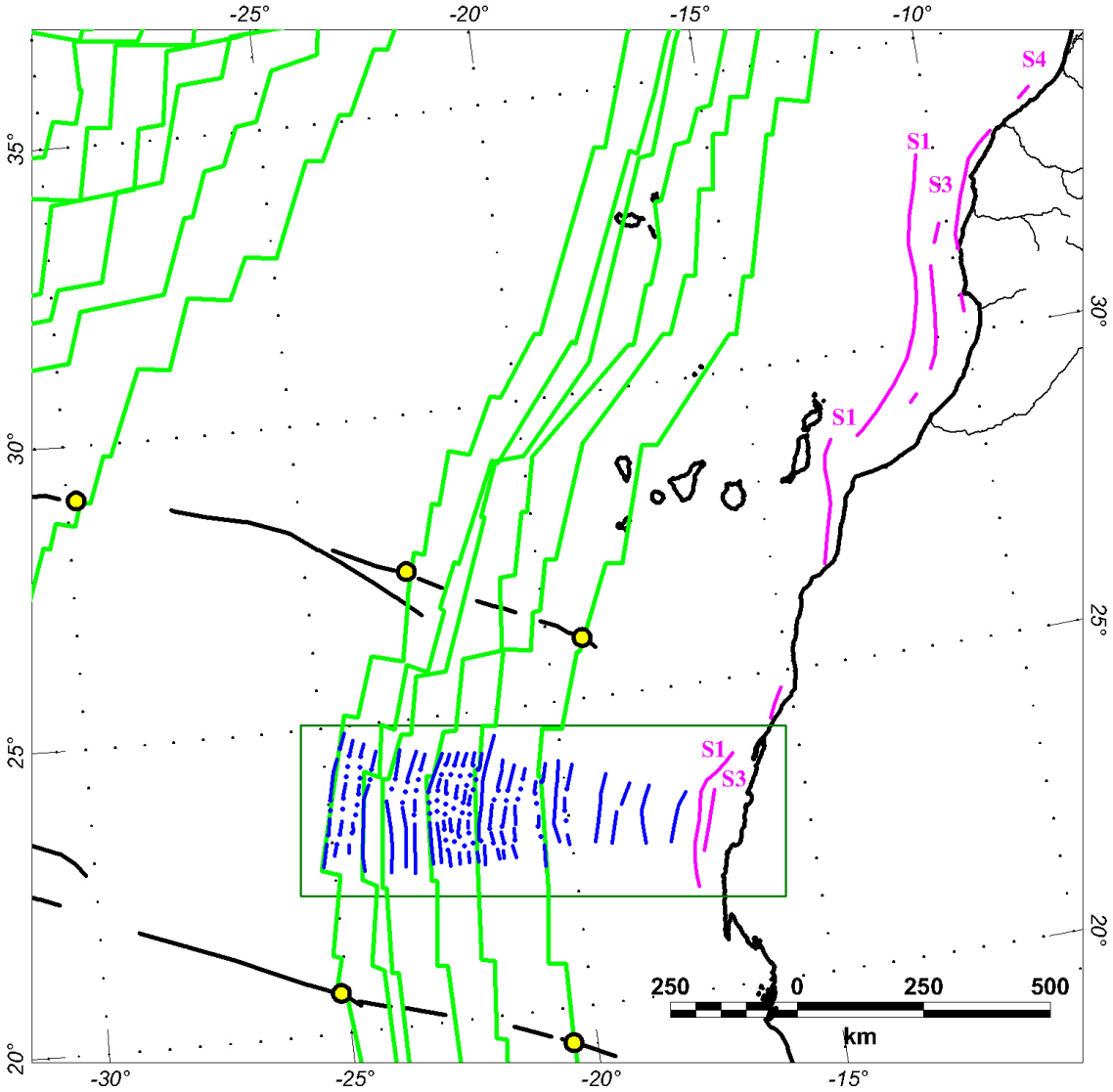
-25°
-20°
-15°
-10°
35°
30°
25°
20°
S4
S1
S3
S1
S1
S3
250
0
250
500
km
-30°
-25°
-20°
-15°

Figure 3.13

Interpretation and profile correlation shiptracks – Africa. Identified Chrons are blue (see Table 3.1). Global Chrons (Muller et al., 1997) are green. Profiles selected for Chron identification are heavy black. Anomalies S1 and S3 are magenta. The bathymetry contour interval is 200 m.

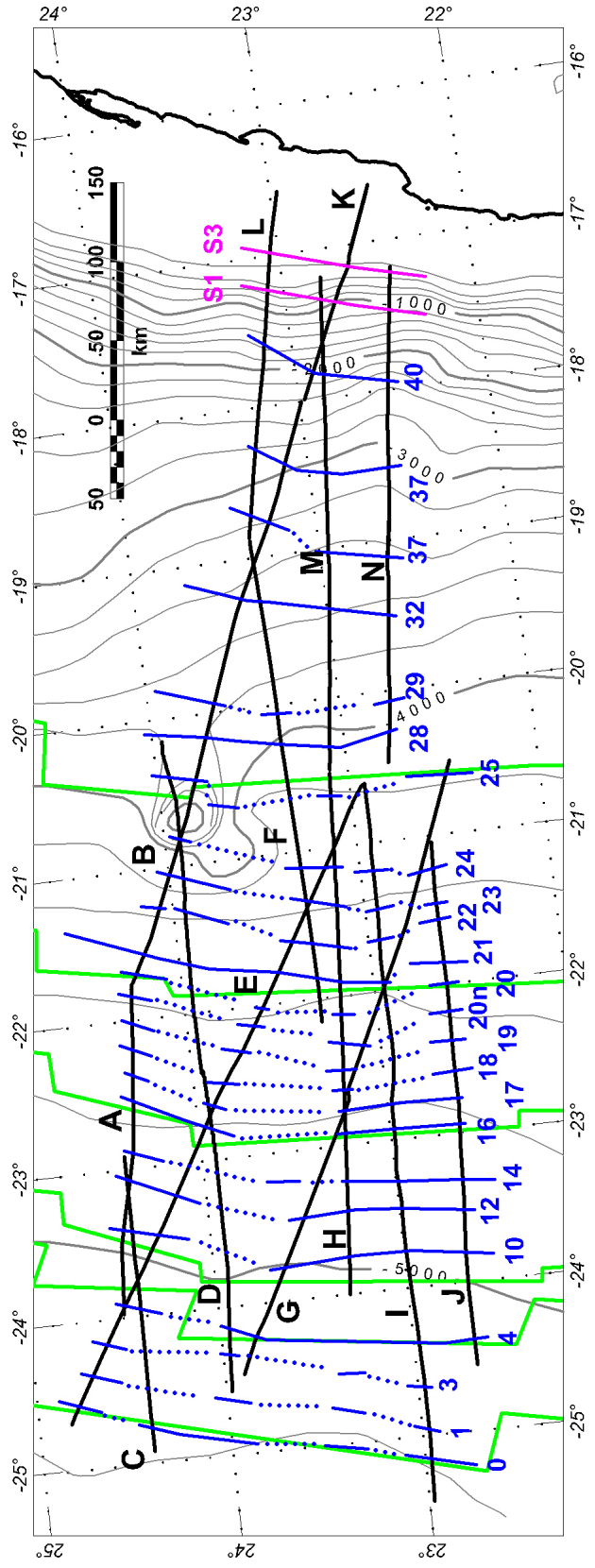
24°
23°
22°
-16°
-17°
-18°
-19°
-20°
-21°
-22°
-23°
-24°
-25°
0
50
100
150
km
S1
S3
A
B
C
D
E
F
G
H
I
J
K
L
M
N
1000
2000
3000
4000
5000
0
1
3
4
10
12
14
16
17
18
19
20n
20
21
22
23
24
25
28
29
32
37
37
40

Figure 3.14

Chron identification – M0 to M25. Chrons M0, M1, M3, M4, M10N, M12A, M14, M16, M17, M18, M19, M20n-1, M20, M21, M22, M23, M24 and M25 are identified by comparisons with synthetic profiles (bottom) created by 2D models for North America and Africa using spreading rates of 14.4 mm/a and 12.9 mm/a respectively.

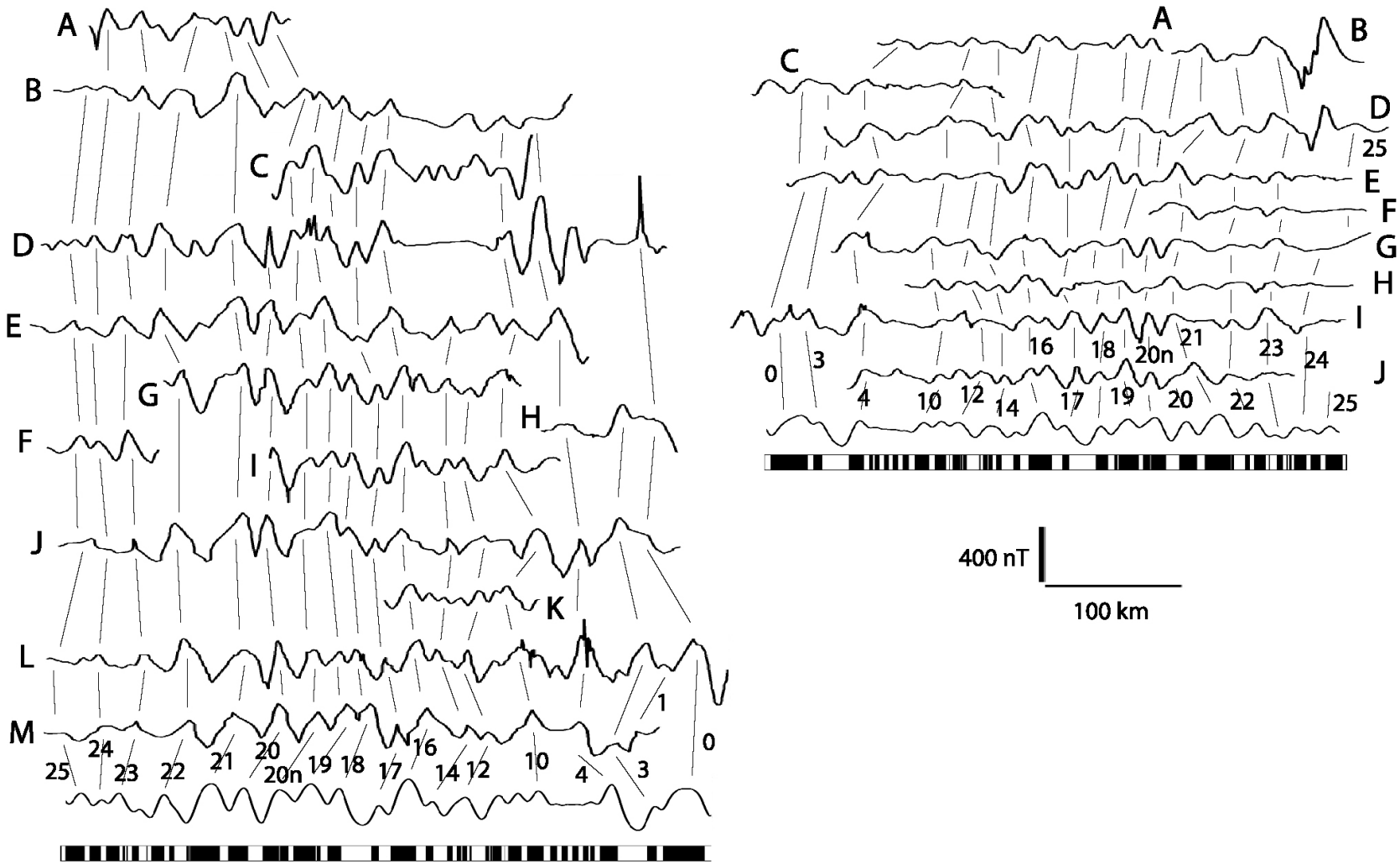
A
B
C
D
E
F
G
H
I
J
K
L
M
25
24
23
22
21
20
20n
19
18
17
16
14
12
10
4
3
1
0
400 nT
100 km

Figure 3.15

Chron identification – M28 to M40. Chrons M28, M29, M32, M37 and M40 are identified by comparisons with synthetic profiles (bottom) created by 2D models for North America and Africa. Two sets of synthetic models were generated: 1) assuming asymmetric spreading rates of 19.2 mm/a and 24.6 mm/a for North America and Africa, and 2) assuming a ridge jump that left about 35 km of the North American plate on the African side at 164 Ma: the constant spreading rate of 21.9 mm/a is used for both sides and Chrons M35 through M38n.1 are reversed and repeated on Africa.

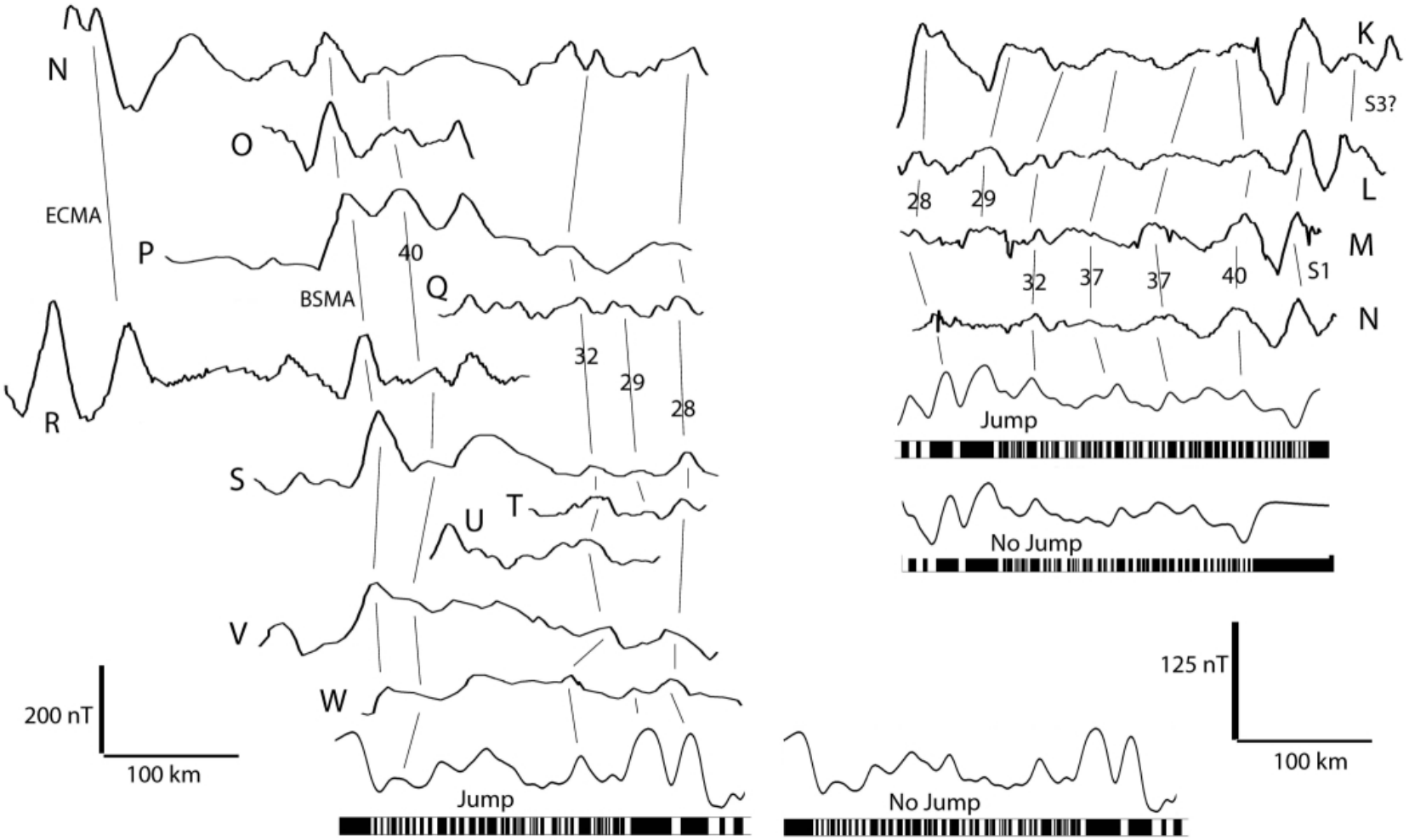
N
O
ECMA
P
BSMA
40
Q
32
29
28
R
S
T
U
V
W
200 nT
100 km
Jump
No Jump
K
S3?
L
28
29
M
32
37
37
40
S1
N
Jump
No Jump
125 nT
100 km

Figure 3.16

Finite-difference pole confidence regions. Error ellipse grids show 90% confidence regions for all calculated stage and total reconstruction poles. Total reconstruction poles reported by Muller and Roest (1992) are yellow circles. Stage poles were calculated for the Mid-Atlantic Ridge (MAR) to Chron 34 (84 Ma), Chron 34 to Chron M0 (120.6 Ma), and Chron M0 to Chron M25 (154 Ma) for North American and African flanks of the central Atlantic: SPE = Stage Pole East (African plate), SPW = Stage Pole West (North American Plate), TRP = Total Reconstruction Pole.

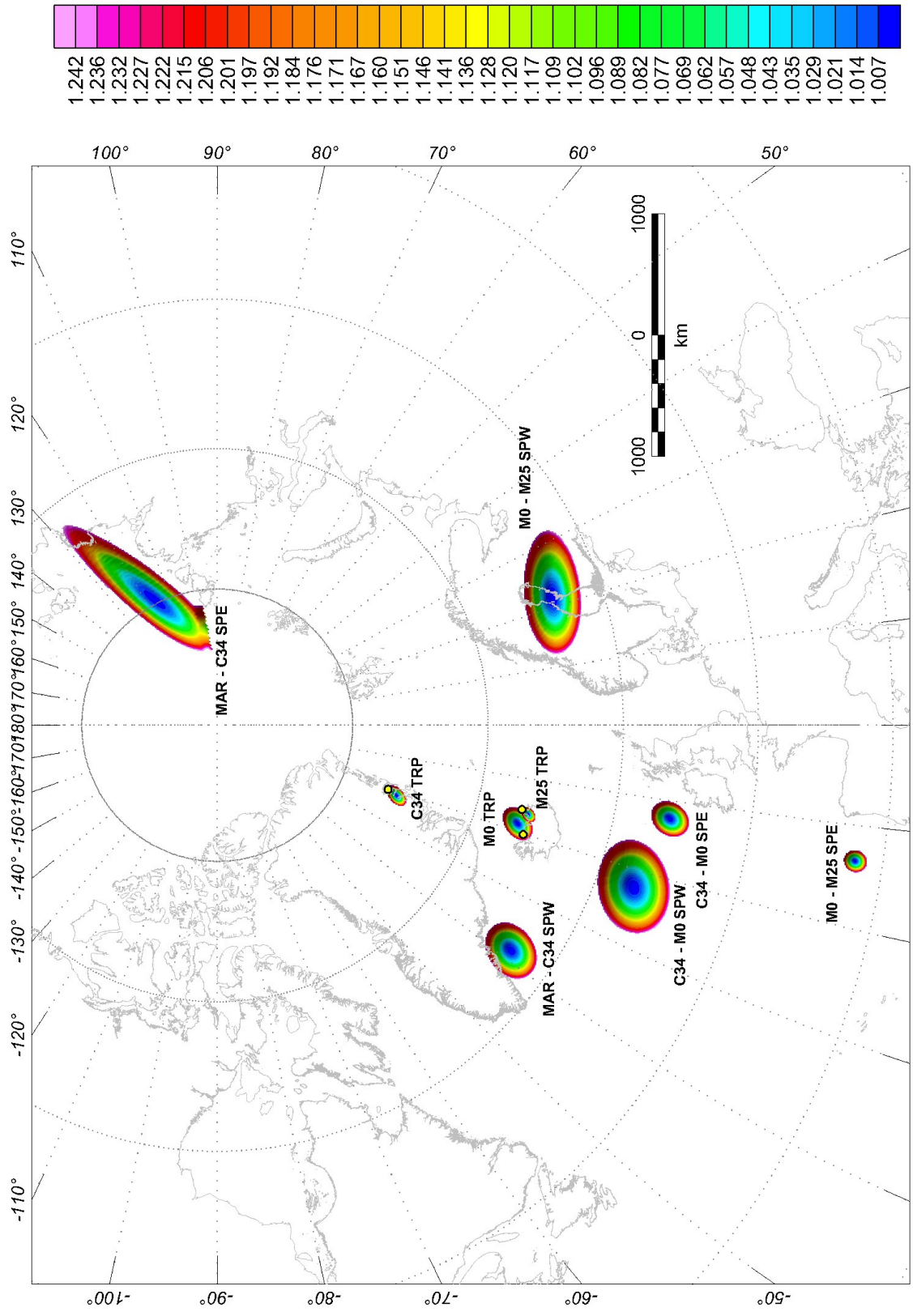
1.242
1.236
1.232
1.227
1.222
1.215
1.206
1.201
1.197
1.192
1.184
1.176
1.171
1.167
1.160
1.151
1.146
1.141
1.136
1.128
1.120
1.117
1.109
1.102
1.096
1.089
1.082
1.077
1.069
1.062
1.057
1.048
1.043
1.035
1.029
1.021
1.014
1.007
1000
0
1000
km
MAR - C34 SPE
M0 - M25 SPW
C34 TRP
M0 TRP
M25 TRP
MAR - C34 SPW
C34 - M0 SPW
C34 - M0 SPE
M0 - M25 SPE

		Latitude	Longitude	Rotation	Error
West:	**MAR to C34**	**62.65°N**	**36.2°W**	**20.00°**	**0.80°**
East:	C34 to MAR	78.85°N	127.95°E	11.81°	0.66°
West:	C34 to M0	57.10°N	22.65°W	11.94°	0.88°
East:	**M0 to C34**	**55.25°N**	**10.00°W**	**12.88°**	**0.74°**
West:	**M0 to M25**	**63.55°N**	**21.55°E**	**4.87°**	**0.29°**
East:	M25 to M0	42.10°N	13.45°W	11.82°	0.26°

Table 3.3

Stage poles calculated from North American and African sides of the central Atlantic Ocean.

	Latitude	Longitude	Rotation	Error
C34, SWEAT	**75.75°N**	**21.55°W**	**30.21°**	**0.456°**
C34, Muller and Roest	76.55°N	20.73°W	29.60°	
M0, SWEAT	66.70°N	18.55°W	54.23°	1.40°
M0, Muller and Roest	66.09°N	20.17°W	54.45°	
M25, SWEAT	66.10°N	16.45°W	65.84°	0.76°
M25, Muller and Roest	66.70°N	15.85°W	64.90°	

Table 3.4

Total reconstruction poles calculated from North American and African sides of the central Atlantic Ocean.

	Distance	Rate	Percentage
Asymmetric spreading			
West: MAR to C34	1420 km	16.9 mm/a	+ 10.0%
East: MAR to C34	1280 km	15.2 mm/a	
West: C34 to M0	810 km	22.1 mm/a	- 3.5%
East: C34 to M0	837 km	22.9 mm/a	
West: M0 to M25	480 km	14.4 mm/a	+ 10.5%
East: M0 to M25	430 km	12.9 mm/a	
Ridge jumps			
West: M25 to M40	250 km	19.2 mm/a	- 22.0%
East: M25 to M40	320 km	24.6 mm/a	
West: BSMA to ECMA	180 km	12.0 mm/a	+ 600.0%
East: S1 to S2	30 km	2.0 mm/a	

Table 3.5

Mean spreading half-rates calculated from the east-west distances between the Atlantic and Kane fracture zones between the MAR and interpreted Chrons. All rates assume constant spreading over the time intervals. Asymmetric spreading greater than 10.5% has not yet been documented therefore two ridge-jumps occurred: 1) eastward at about 170 Ma leaving African lithosphere between ECMA and BSMA, and 2) westward between 164 Ma and 159 Ma leaving North American lithosphere between S2 and S1. Seafloor spreading models for this later jump assumed constant spreading of 21.9 mm/a (Figure 3.15).

distance spanned by the JMQZ province on the African flank is about 70 km greater than the JMQZ province on the North American flank, and inspection of the profile data over these provinces reveals that more correlatable anomalies exist on the African flank indicating that the discrepancy in the width of the JMQZ is not from asymmetrical spreading. To make this point, we show two sets of modeled seafloor spreading anomalies, one assumes asymmetric spreading and the other assumes a ridge jump that occurred between Chrons M38 (164 Ma) and M32 (159 Ma).

3.6 Interpretation

The primary difficulty associated with mapping fracture zones using satellite-derived free air gravity data over long distances, such as from the MAR to the continental shelves of North America and Africa, is that the expression of transform faults in bathymetry and gravity data is variable. This variability can be related to transform migration or sediment deposition but results in fracture zones that can be difficult to map. Muller and Roest (1992) estimated the average error for identifying fracture zone locations from satellite-derived gravity data to be 5 km. To facilitate identification of fracture zones, the satellite-derived gravity data were enhanced to emphasize the shorter wavelength anomalies produced by fracture zones. Fracture zones are typically 20 to 50 km wide and they produce gravity anomalies that are generally less than 200 km in wavelength. Therefore the residual data were generated by subtracting a 100 km upward continued gravity grid from the original free air gravity grid.

The landward projections of Atlantis, Kane and Fifteen-Twenty fracture zones, using satellite-derived gravity data alone, extend to Chron 21, 75 km inboard of Chron 25, and Chron 25 respectively for the North American flank. The Atlantis fracture zone trace was extended landward to over 100 km inboard of Chron M40 by combining DNAG magnetic data with satellite-derived gravity data. M-Series Chrons are offset left-laterally (with respect to motion) approximately 80 km along parts of this fracture zone on this flank. The landward projections of Kane and Fifteen-Twenty fracture zones on the African flank, mapped west to east, extend to Chron M16, and are shown dashed to Chron M25 indicating less confidence in their locations. The volcanic Great Meteor Seamount and Saharian Seamounts complexes mask parts of the Atlantis fracture zone on the African plate. For that reason its trace is dashed between Chrons C34 and M25 indicating less confidence in its location.

3.6.1 Geomagnetic isochrons

Based on the overall character of the magnetic field, the central Atlantic can be divided into five magnetic provinces (Rona *et al.*, 1970; Vogt *et al.*, 1971, 1986). These distinct provinces coincide with: 1) MAR to Chron C34; 2) the Cretaceous Magnetic Quiet Zone (CMQZ); 3) high-amplitude M-Series anomalies M0 through M25 (M0-25); 4) low-amplitude M-Series or JMQZ; 5) the zone between the BSMA and ECMA, or, following Vogt (1986), the Inner Magnetic Quiet Zone (IMQZ). Except for the IMQZ, the magnetic provinces form bands of magnetic anomalies on the eastern and western flanks of the central Atlantic. Magnetic province widths of IMQZ, JMQZ, and M0-25 are approximately 180 km, 250 km, and 480 km on the North American flank between the

Atlantis and Kane fracture zones. The magnetic boundary at the CMQZ, also called the Bermuda Discontinuity (Vogt *et al.*, 1971), separates the high amplitude, linear magnetic anomalies of the M0-25 province from the somewhat chaotic, uncorrelatable anomalies of the CMQZ. On the African flank, magnetic province widths of JMQZ and M0-25 are approximately 320 km and 430 km (Table 3.5). The conjugate anomaly pair to ECMA and BSMA on the North American flank are S3 and S1 on the African flank, and the distance between S3 and S1 is about 30 km.

High amplitude M0-25 anomalies allow identification and mapping of several Chrons, but identification of anomalies in the JMQZ is complicated by their low amplitudes and great depths to the basement (Layer 2 of oceanic crust) off North America and Africa. Further complexity is introduced by the Tropic Seamount off Africa, which is located between the northern ends of interpreted Chrons M24 and M25 (Figure 3.14) and it produces a high amplitude (> 400 nT) anomaly along profiles B and D (Figure 3.15). Anomaly M25, which is typically a lower amplitude anomaly, cannot be identified on profile B and only tentatively on profile D.

In the Pacific Ocean, anomalies in the JMQZ over the Pigafetta Basin, just east of the Northern Mariana Basin, are produced at basement depths of 6 to 6.5 km. For that reason, two deep-tow profiles were acquired over an approximately 11 My sequence (156 to 167.5 Ma) and 88 Chrons between M29 and M41 were identified (Sager *et al.*, 1998). After upward continuation of profiles to sea level, only 44% of the Chrons were retained (Sager *et al.*, 1998). Basement depths in the JMQZ off North America are about 7 to 9 km (Uchupi *et al.*, 1984a, 1984b), therefore we have chosen a basement depth for our 2D

seafloor spreading model of 8 km for the North American flank. We use the same basement depth for our models on the Africa flank for consistency.

The M0-25 province, considered from the youngest to the oldest parts, offshore North America is a region characterized by distinctive packages of anomalies (Figure 3.14). M0 has a prominent positive peak just landward of a sharp anomaly minimum. M0 is followed by a sequence of two or three peaks associated with the M1, M3 and M4 Chrons. M1 is sometimes undetectable. M4 typically has the greatest amplitude of these three anomalies, similar in amplitude to M0. Landward of M4, following an interval lacking coherent anomaly trends, are Chrons M10N, M12A and M14. M10N coincides with the outboard anomaly of a broad high package of anomalies. M12A and M14 are slightly lower in amplitude than M10, but coincide with distinctive peaks that, together with M10N, can be mapped with consistency from the Atlantis to the Fifteen-Twenty fracture zones. The package of anomalies bounded by M16 to M21 includes seven Chrons: M16, M17, M18, M19, M20n-1, M20 and M21. Chrons M16, M20 and M21 are the highest amplitude anomalies overall in the package, but are not consistently mappable over the interval from the Atlantis to the Fifteen-Twenty fracture zones. Where they are mappable, these Chrons are consistent with respect to their relative spatial position. Between M16 and M20, Chrons M17, M18, M19 and M20n-1 are just as consistent with respect to their position, although Anomaly M17, just east of Anomaly M16, is often lower in amplitude. Between the Atlantis and the Kane fracture zones, the next three prominent anomalies are Chrons M22, M23 and M24. However as Kane is approached from the north, a small westward offset results in another anomaly being inserted between M21 and M22. South of Kane, the sliver of crust producing this intervening

anomaly is truncated and the earlier pattern is resumed. Again, as Fifteen-twenty is approached from the north, an intervening anomaly between M23 and M24 must be inserted. Conjugate wedges on the African flank, just north of the Kane and Fifteen-Twenty fracture zones, cannot be confirmed in this analysis. M25 is more difficult to identify. It is generally a broad anomaly, with the Chron coinciding with the highest amplitude at the crest of its eastern flank. In many places the western flank of this anomaly is much lower in amplitude and even undetectable.

M0-25 anomalies on the African side of the central Atlantic do not identically mirror those on the North American side (Figure 3.14), but distinctive anomalies can be correlated and interpreted so that the same Chrons are identified on both sides of the Atlantic. M0 anomalies over Africa are similar to M0 anomalies over North America. They are characterized by a sharp outboard minimum followed by a relatively continuous high amplitude peak landward. Chrons M1 to M4 are also similar to Chrons on the North American flank. Chrons M10N, M12A and M14 are evenly spaced peaks, but M12A is often identified as the eastern peak of a pair of low amplitude anomalies superimposed on a broader anomaly between M10N and M14. M16 is identified as the western peak of a pair of anomalies. Chrons M17 through M21 over the African flank are similar to the same package of anomalies over the North American flank by an evenly spaced sequence of anomaly maxima. As for the North American flank, Chron M17 is commonly a low amplitude peak near the landwark flank of Chron M16. In contrast to the North American flank, however, Chron M21 over Africa is consistently higher in amplitude and more prominent than M20. This might be the result of our comparatively limited area of investigation on the African side. Chrons M22, M23 and M24 are the next landward set

of peaks on the African side and are easily mapped. Chron M25 is difficult to map because of its relatively lower amplitude. It is transitional to JMQZ and it is mapped by correlating a broad, subtle anomaly high.

Interpreting JMQZ anomalies is challenging, not only because of low amplitudes, but also because a large discrepancy in width exists between the conjugate sides (Figure 3.15). The African JMQZ is about 70 km wider than the North American JMQZ, which would require over 20% asymmetric spreading (Table 3.5). The combined width of the conjugate JMQZs is 570 km and the total spreading rate is 43.8 mm/a. Therefore the time required to generate 35 km of repeated lithosphere at a 21.9 mm/a half-spreading rate is 1.6 Ma. Synthetic JMQZ seafloor spreading anomalies were generated from west-to-east and east-to-west (reversed) models assuming 21.9 mm/a half-spreading rates. Comparing these synthetic profiles indicates that a sequence of small reversals in the region of M35 and M37 appears to be repeated on the African flank, and that this sequence is absent on the North American flank. Therefore the repeated lithosphere, from these models, coincides with oceanic crust created between M35 and M38n.1 or about 1.6 My (Sager *et al.*, 1998). We conclude that the lithosphere that was abandoned over a 1.6 My interval occurred within the 5 My period between Chron M32 and Chron M38, or 159.5 Ma to 164.5 Ma. The increased distance between the correlated Chrons M37 (the easternmost set) and M40 on the African flank suggests that spreading rates may have varied. Therefore, determining the precise extent and timing of the ridge jump is not possible at this time because of the lack of detail in the magnetic data, and the possibility that both spreading centers were active at the same time.

Correlated JMQZ anomalies over the North American flank include M28, M29, M32 and M40. The distinctive M28 and M29 anomaly pair are similar in amplitude to M25 and can be mapped with confidence in several locations. Chron M32 is sometimes difficult to identify, but like M28 and M29, a distinct peak that is slightly higher in amplitude than the surrounding anomalies occurs in several locations. M40 is a persistent anomaly high that is mapped approximately 50 to 75 km outboard of the BSMA.

Correlated JMQZ anomalies over the African flank include M28, M29, M32, M37 (repeated) and M40. Mirroring North America, M28 and M29 are mapped as a pair of peaks similar to, and just landward of, M25. M32 over the African flank also mirrors M32 over North America. It is a distinct peak that is slightly higher in amplitude than the surrounding anomalies. The characteristic package of anomalies between Chrons M35 and M37 are superimposed on a broad high with a 20 nT peak over M37. M40 is a prominent relatively high amplitude anomaly that is mapped about 65 km outboard of S1.

The ECMA and BSMA over the North American flank (Klitgord and Schouten, 1986; Vogt, 1986), and the S1 and S3 anomalies over the African flank (Roeser *et al.*, 2002; Verhoef *et al.*, 1991) appear to be conjugate pairs of anomalies. These prominent magnetic anomalies, inboard of the JMQZ, extend hundreds of km parallel to the coasts of North America and Africa. Vogt (1973; 1986) suggested that the BSMA is related to an eastward jump of the spreading center prior to 170 Ma, indicating the presence of oceanic crust between ECMA and BSMA. Supporting this conclusion, Uchupi *et al.* (1984a, 1984b) have mapped the landward limit of oceanic crust to be about 25 km outboard of the ECMA. A single refraction data point (Figure 3.8) also indicates that the crust of the IMQZ is oceanic (Houtz, 1980).

On the African side, prominent high amplitude anomalies, inboard of the M-Series, include S1, S3 and S4 with S1 being the farthest outboard anomaly (Roeser *et al.*, 2002). Roest *et al.* (1992) interpreted S1 and BSMA to be conjugate oceanic anomalies. Inboard of these anomalies, the S3 and ECMA anomalies are similar in character and form prominent linear trends. We interpret S3 and ECMA to be conjugate anomalies that approximate the ocean – continent crustal boundaries of North America and Africa.

Our identification of M40 on the flanks of the Atlantic is consistent with the interpretation that the high-amplitude western and eastern basin bounding anomalies, ECMA, BSMA, S1 and S3, are conjugate pairs and that they constrain a ridge jump that occured before the BSMA formed. Roeser *et al.* (2002) identified Chrons M25 to M41 off the coast of Morocco and reported that poorly defined Seaward Dipping Reflectors coincide with S1. They assigned an age of 170 Ma for that anomaly. Anomaly S3 coincides with a large gravity anomaly (over 80 mGal), however, the basement rocks beneath these anomalies are overlain by extensive salt deposits (Roest *et al.*, 1992). Because of the presence of several volcanic complexes associated with the Canary Islands, Roeser *et al.* (2002) modeled seafloor topography to ensure that interpreted anomalies were produced by geomagnetic polarity reversals. The width of the IMQZ is about 180 km and the width of S1 to S3 is about 30 km, which is consistent with Vogt's (1971, 1973, 1986) suggestion of a ridge jump. This early jump probably occurred before 167 Ma (M40). To estimate the age of the BSMA, applying a constant spreading rate of 21.9 mm/a over the time between Chron 40 and the BSMA, and between Chron 40 and S1, which are separated by distances of about 65 km, results in 2.97 My. Adding this

result to the age of M40 indicates that this early ridge jump occurred about 170 Ma, as postulated by Vogt (1986).

Correlated M0-25 and JMQZ anomalies from the North American and African sides of the central Atlantic are compared in Figures 3.14 and 3.15. In addition to comparing conjugate sets of anomalies, the anomalies are also correlated with synthetic anomalies generated from 2D models. Six 2D magnetic models were generated using 4 km thick blocks representing sections of the geomagnetic polarity time series. Four kilometers is large for the magnetized part of oceanic crust, but typical models using thinner layers produce sharp anomalies that are often smoothed afterwards by applying Gaussian polarity transitions to facilitate anomaly correlations. Using thicker blocks is an alternative method to accomplish the similar results. Each M0-25 sequence of anomalies is compared to anomalies calculated from a 2D seafloor spreading model. The spreading rates used to generate the models for North American and African sides were 14.4 mm/a and 12.9 mm/a. Each JMQZ sequence of anomalies was compared to two sets of anomalies calculated from 2D seafloor spreading models. In one set, asymmetric seafloor spreading was assumed for the North American (19.2 mm/a) and the African (24.6 mm/a) flanks. In the second set a ridge jump with about 35 km of abandoned lithosphere on the African side, and 35 km of missing lithosphere on the North American side, is assumed with a symmetrical spreading rate of 21.9 mm/a for both seafloor spreading models.

3.6.2 Ridge jumps and asymmetric spreading

The kinematic history of the central Atlantic was described by Klitgord and Schouten (1986) as consisting of fairly stable periods of constant spreading that are

interrupted by times of major plate reorganizations. They suggested that these major plate reorganizations occurred during initial basin opening and at times corresponding with BSMA, M21, M10N, M4, and M0. Their analysis involved calculating stage poles between many chrons on both sides of the Atlantic. We restrict our analysis to the M0-25 and JMQZ sequences, which include three of the major episodes identified by Klitgord and Schouten (1986): initial opening, BSMA and M21. The narrow swath of anomalies interpreted over the African side in this study do not allow for an analysis similar to that of Klitgord and Schouten (1986), but measured distances between identified Chrons do allow for calculations with respect to asymmetric spreading and ridge jumps.

Asymmetric spreading is characterized by excess accretion of seafloor on one side of a seafloor spreading center and is typically less than 5% but can be as much as 10.5% (Muller *et al.*, 1998). In their analysis, which focused on spreading rates since 84 Ma, Muller *et al.* (1998) determined spreading rates from a grid derived from the global geomagnetic isochron data set (Muller *et al.*, 1997).

The spreading rate for the JMQZ reported by Klitgord and Schouten (1986) was 19 mm/a, which is close to the JMQZ rate calculated for the North American flank in this analysis (19.2 mm/a), but differs significantly from the JMQZ rate calculated for the African flank of 24.6 mm/a in this analysis. M0-25 spreading rates offshore Morocco are 10 mm/a for M0 to M21, 16 mm/a for M21 to M25, and 10 mm/a for JMQZ (Roeser *et al.*, 2002). This slow rate for the JMQZ is explained by its close proximity to the stage pole, which describes the plate motion over this time (Figure 3.16).

Between the Atlantis and the Kane fracture zones we calculate: 1) mean distances from MAR to Chron C34, Chron C34 to M0, Chron M0 to M25, and Chron M25 to

Chron M40; 2) the half spreading rates; and 3) the percentage difference for both North American and African sides of the central Atlantic Ocean (Table 3.5). The mean distance between BSMA and ECMA (the IMQZ) is 180 km and is believed to develop over an 18 My time interval, yielding the total spreading rate for this interval to be 10 mm/a.

Mammerickx and Sandwell (1986) describe four stages in the evolution of a seafloor spreading ridge jump: 1) The lithosphere is weakened by thinning at the site of the future spreading center, 2) Normal faults form above the weakness, and mantle material upwells from below, 3) Slow spreading starts at the weakness, and the spreading rate decreases at the old spreading center, and 4) The seafloor rises at the new location as the spreading rate increases, and the seafloor subsides as spreading decreases at the abandoned location. Mammerickx *et al.* (1988) identified nine fossil micro-plates that formed as the result of plate reorganization in the Pacific Ocean as well as two present-day micro-plates that have formed along the East Pacific Rise as a result of plate reorganization. Goff and Cochran (1996) reported that evidence required to document a ridge jump is the presence of a fossil ridge segment, or magnetic anomalies related to the transferred lithosphere.

The asymmetric spreading required to create ocean crust in the North American and African JMQZs is about 22% (Table 3.5), which is a two-fold increase over the maximum asymmetry reported by Muller *et al.* (1998). We therefore conclude that a ridge jump occurred within the IMQZ at about 170 Ma. We inspected African JMQZ anomalies for evidence of repetition. The sequence of anomalies around M38 appear to show repetition and account for an additional ~70 km of oceanic crust. The proximity of the African JMQZ stage pole, and the fanning of North American M0-25 and JMQZ

anomalies to the south, indicate that this distance increases southward to the Guinea Nose. Furthermore, Roeser *et al.* (2002) reported that interpreted anomalies over the Seine Abyssal Plain, offshore Morocco, approached S1 northward at a 10° angle, which reflects close proximity to the rotation pole for this interval.

3.6.3 Plate reconstructions

Klitgord and Schouten (1986) reported that fits for plate tectonic reconstructions may be based on several factors including the geometrical fits of conjugate coastlines, geologic fits, seafloor spreading anomalies, and paleomagnetic data. We have used rotation poles calculated from control points identified at the intersections of fracture zones with Chrons C34, M0 and M25 (Table 3.2). Reconstructions are achieved by using poles calculated between the MAR and C34, M0, and M25 for each side of the central Atlantic.

Figures 3.17 though 3.22 show North American and African plate reconstructions for 84 Ma, 120.6 Ma and 154 Ma, coinciding with Chrons C34, M0 and M25. Plates have been rotated with respect to the trace of the MAR because errors associated with pole position are minimized since smaller angles are involved. Rotated data sets include satellite-derived free air gravity anomaly grids, coastlines, global Chrons (Muller *et al.*, 1997), interpreted fracture zones and Chrons from this study, and digitized BSMA, ECMA, S1 to S4 magnetic anomalies as well as mapped oceanic and continental crustal boundaries along North America (Uchupi *et al.*, 1984a, 1984b).

Our reconstruction of fracture zone gravity anomalies for C34 and M0 (Figures 3.17 and 3.19) match across the MAR adding confidence to our method of plate reconstruction.

Figure 3.17

North America – Africa plate reconstruction by closing the central Atlantic on both sides to Chron C34 (83 Ma). The angles of rotation are 20.0° for North America and 11.8° for Africa. Satellite-derived free air gravity anomaly grid cell is 3.7 km.

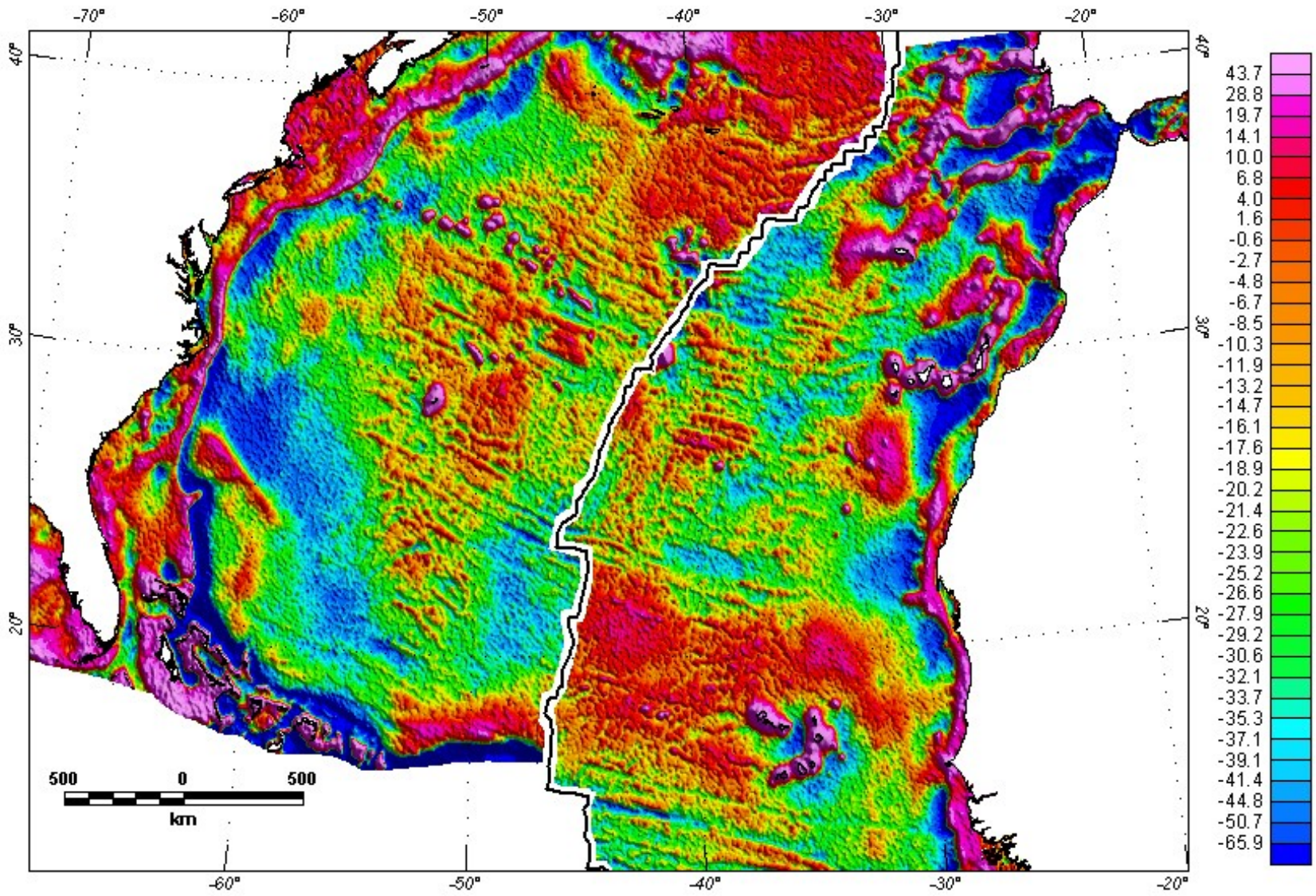
-70°
-60°
-50°
-40°
-30°
-20°
40°
30°
20°
500
0
500
km
43.7
28.8
19.7
14.1
10.0
6.8
4.0
1.6
-0.6
-2.7
-4.8
-6.7
-8.5
-10.3
-11.9
-13.2
-14.7
-16.1
-17.6
-18.9
-20.2
-21.4
-22.6
-23.9
-25.2
-26.6
-27.9
-29.2
-30.6
-32.1
-33.7
-35.3
-37.1
-39.1
-41.4
-44.8
-50.7
-65.9

Figure 3.18

North America – Africa plate reconstruction by closing the central Atlantic on both sides to Chron C34 (83 Ma). The angles of rotation are 20.0° for North America and 11.8° for Africa. Rotated magnetic and basement elements: interpreted Chrons are thin dotted and solid blue lines; global Chrons (Muller et al., 1997) are green; BSMA and ECMA anomalies over North America, and S1, S3 and S4 anomalies over Africa are magenta; mappable limits of continental and oceanic crust in North America (Uchupi et al., 1984a, 1984b) are violet. The MAR and fracture zones are heavy solid lines.

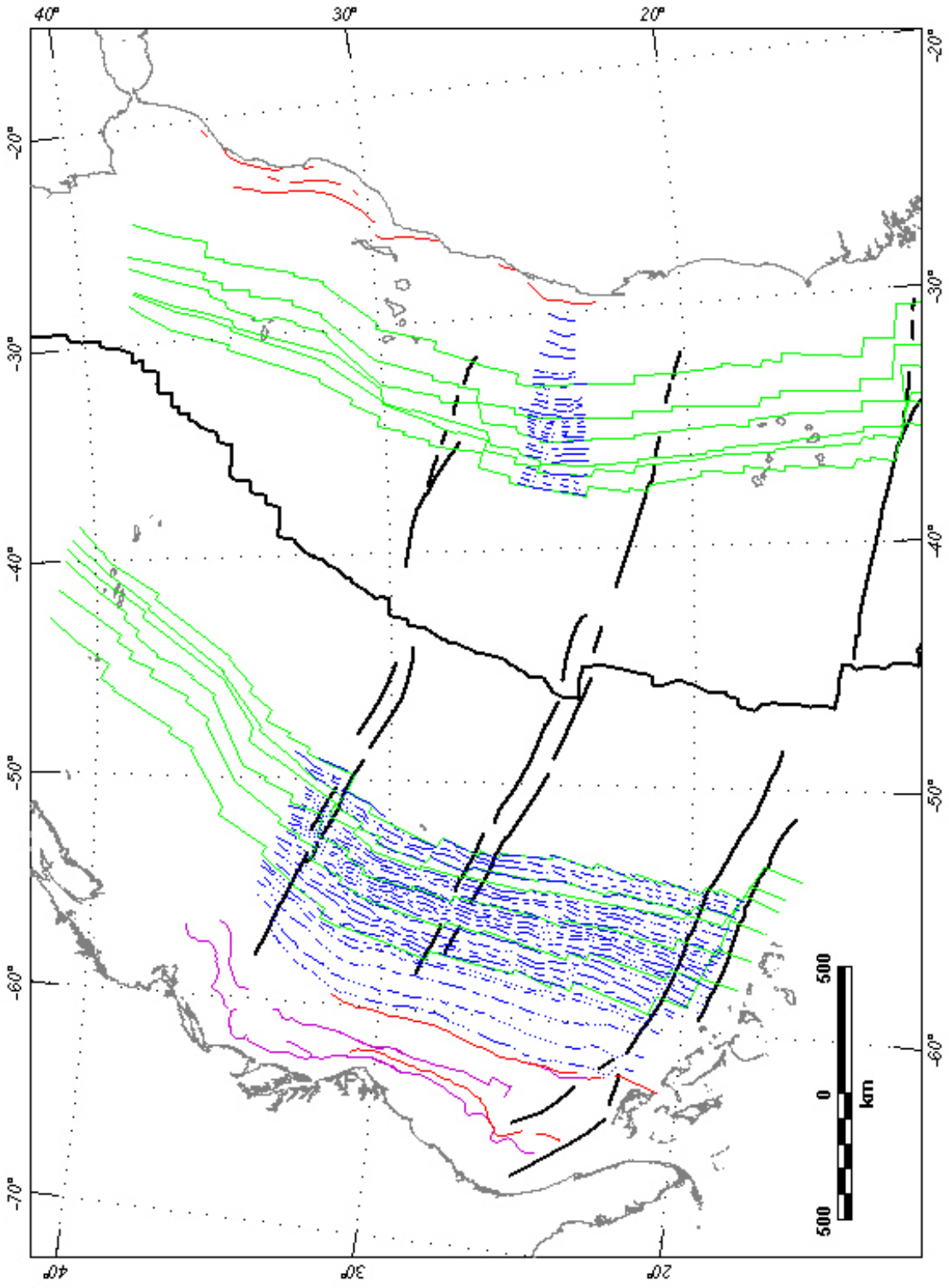
40°
30°
20°
-20°
-30°
-40°
-50°
-60°
-70°
500
0
km
500

Figure 3.19

North America – Africa plate reconstruction by closing the central Atlantic on both sides to Chron M0 (120.6 Ma). The angles of rotation are 31.90° for North America and 22.98° for Africa. Satellite-derived free air gravity anomaly grid cell is 3.7 km.

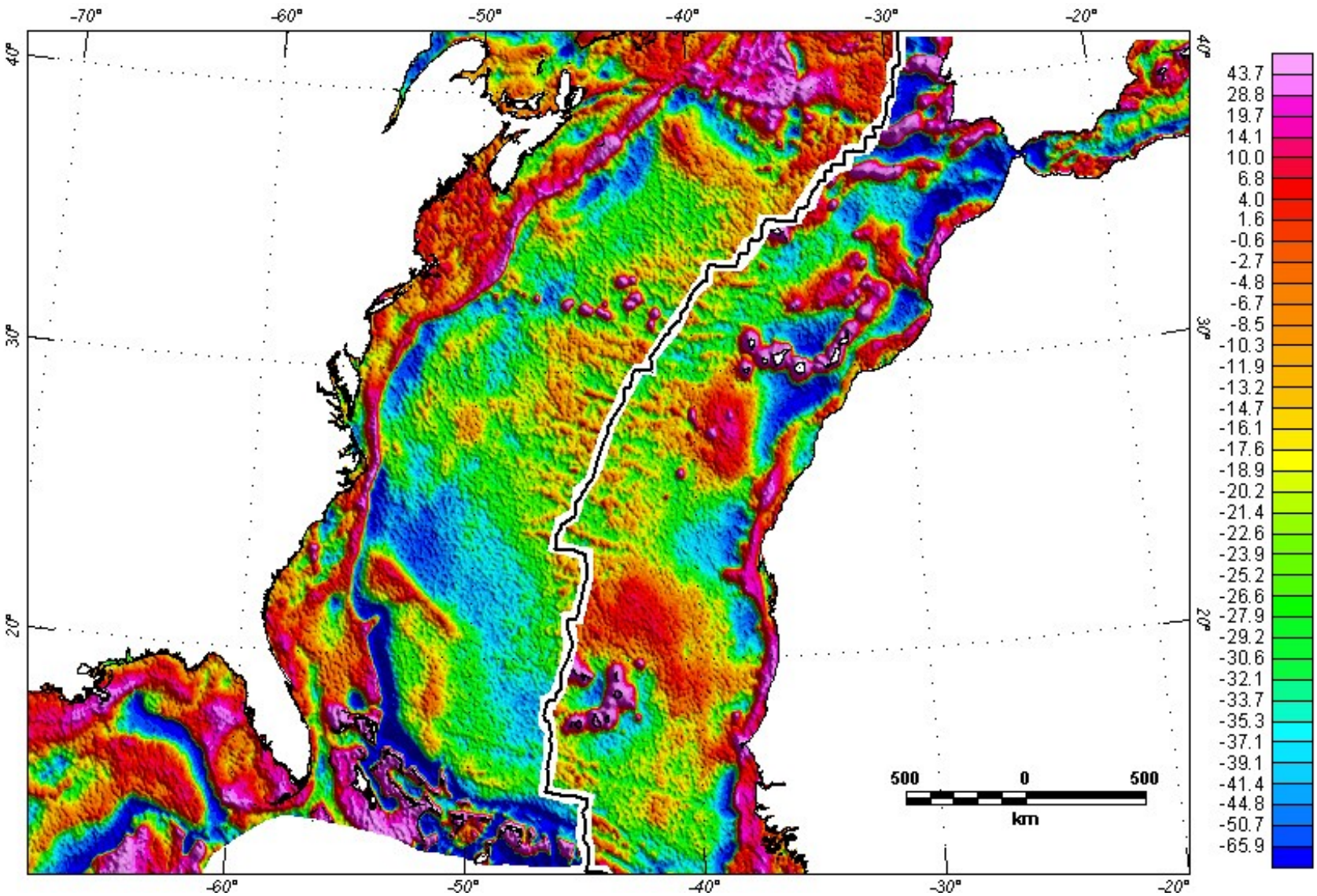
-70°
-60°
-50°
-40°
-30°
-20°
40°
30°
20°
43.7
28.8
19.7
14.1
10.0
6.8
4.0
1.6
-0.6
-2.7
-4.8
-6.7
-8.5
-10.3
-11.9
-13.2
-14.7
-16.1
-17.6
-18.9
-20.2
-21.4
-22.6
-23.9
-25.2
-26.6
-27.9
-29.2
-30.6
-32.1
-33.7
-35.3
-37.1
-39.1
-41.4
-44.8
-50.7
-65.9
500
0
500
km

Figure 3.20

North America – Africa plate reconstruction by closing the central Atlantic on both sides to Chron M0 (120.6 Ma). The angles of rotation are 31.90° for North America and 22.98° for Africa. Rotated magnetic and basement elements: interpreted Chrons are thin dotted and solid blue lines; global Chrons (Muller et al., 1997) are green; BSMA and ECMA anomalies over North America, and S1, S3 and S4 anomalies over Africa are magenta; mappable limits of continental and oceanic crust in North America (Uchupi et al., 1984a, 1984b) are violet. The MAR and fracture zones are heavy solid lines.

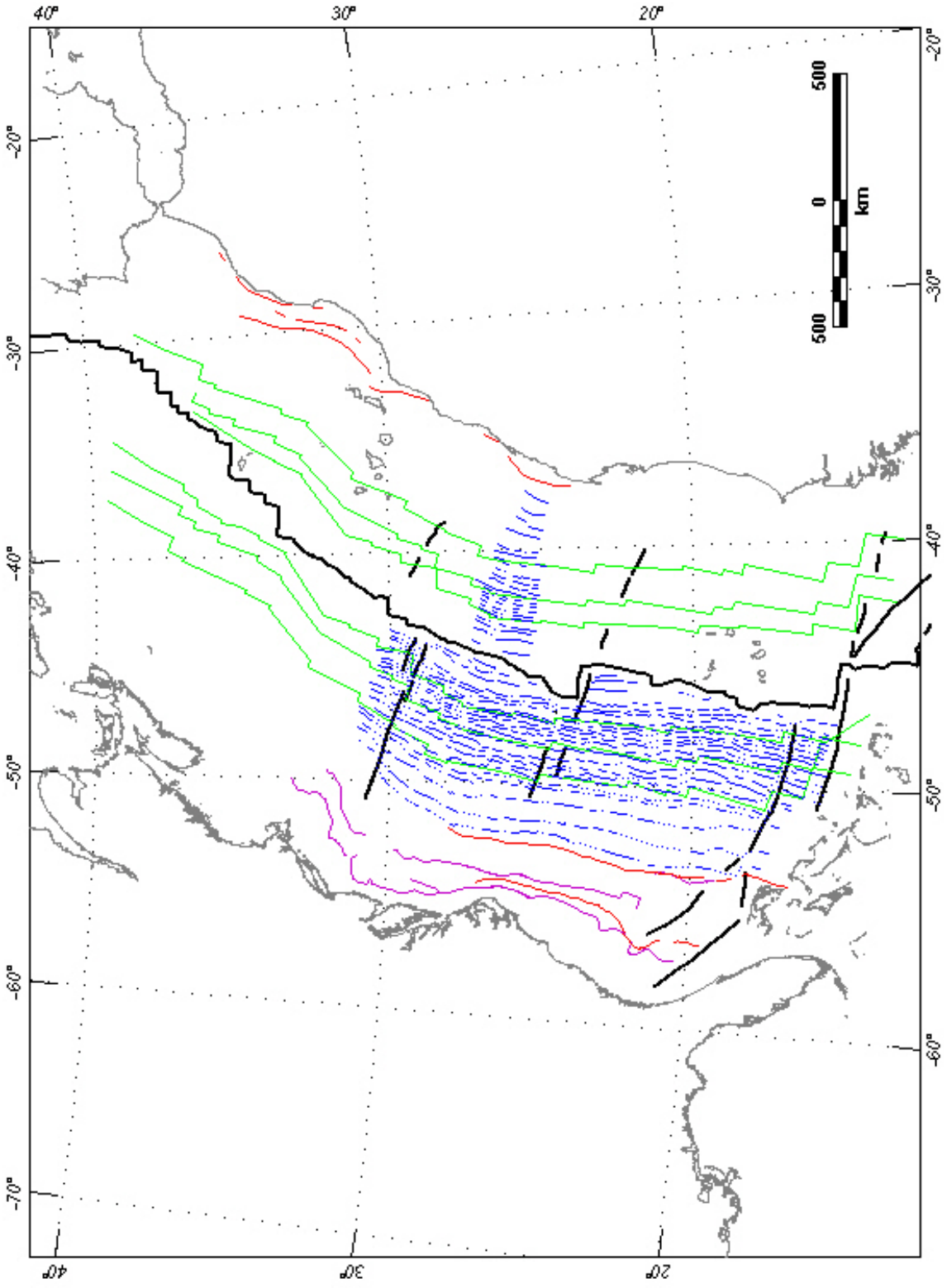
40°
30°
20°
-20°
-30°
-40°
-50°
-60°
-70°
500
0
500
km

Figure 3.21

North America – Africa plate reconstruction by closing the central Atlantic on both sides to Chron M25 (154 Ma). The angles of rotation are 36.34° for North America and 29.86° for Africa. Satellite-derived free air gravity anomaly grid cell is 3.7 km.

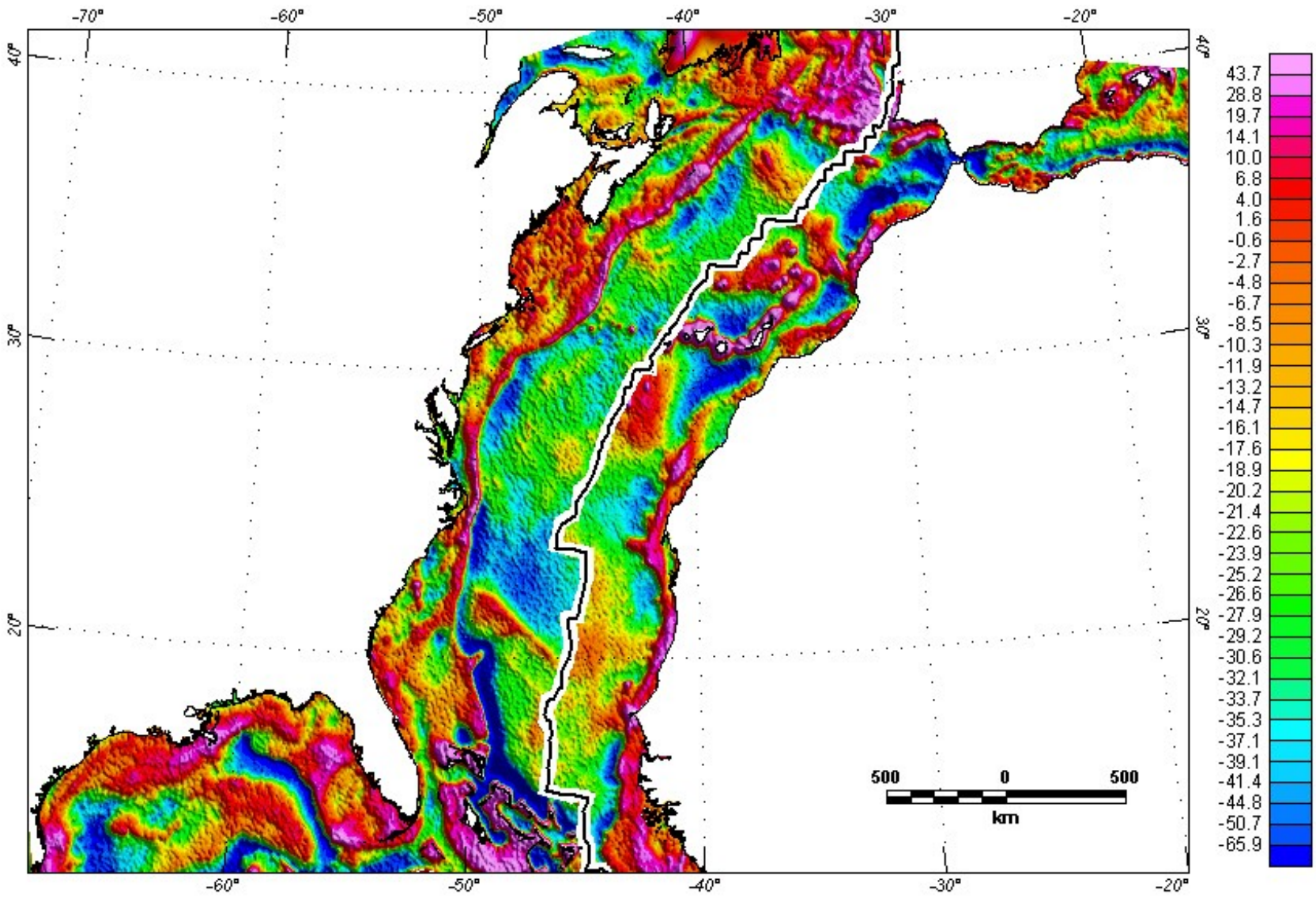
-70°
-60°
-50°
-40°
-30°
-20°
40°
30°
20°
500
0
500
km
43.7
28.8
19.7
14.1
10.0
6.8
4.0
1.6
-0.6
-2.7
-4.8
-6.7
-8.5
-10.3
-11.9
-13.2
-14.7
-16.1
-17.6
-18.9
-20.2
-21.4
-22.6
-23.9
-25.2
-26.6
-27.9
-29.2
-30.6
-32.1
-33.7
-35.3
-37.1
-39.1
-41.4
-44.8
-50.7
-65.9

Figure 3.22

North America – Africa plate reconstruction by closing the central Atlantic on both sides to Chron M25 (154 Ma). The angles of rotation are 36.34° for North America and 29.86° for Africa. Rotated magnetic and basement elements: interpreted Chrons are thin dotted and solid blue lines; global Chrons (Muller et al., 1997) are green; BSMA and ECMA anomalies over North America, and S1, S3 and S4 anomalies over Africa are magenta; mappable limits of continental and oceanic crust in North America (Uchupi et al., 1984a, 1984b) are violet. The MAR and fracture zones are heavy solid lines.

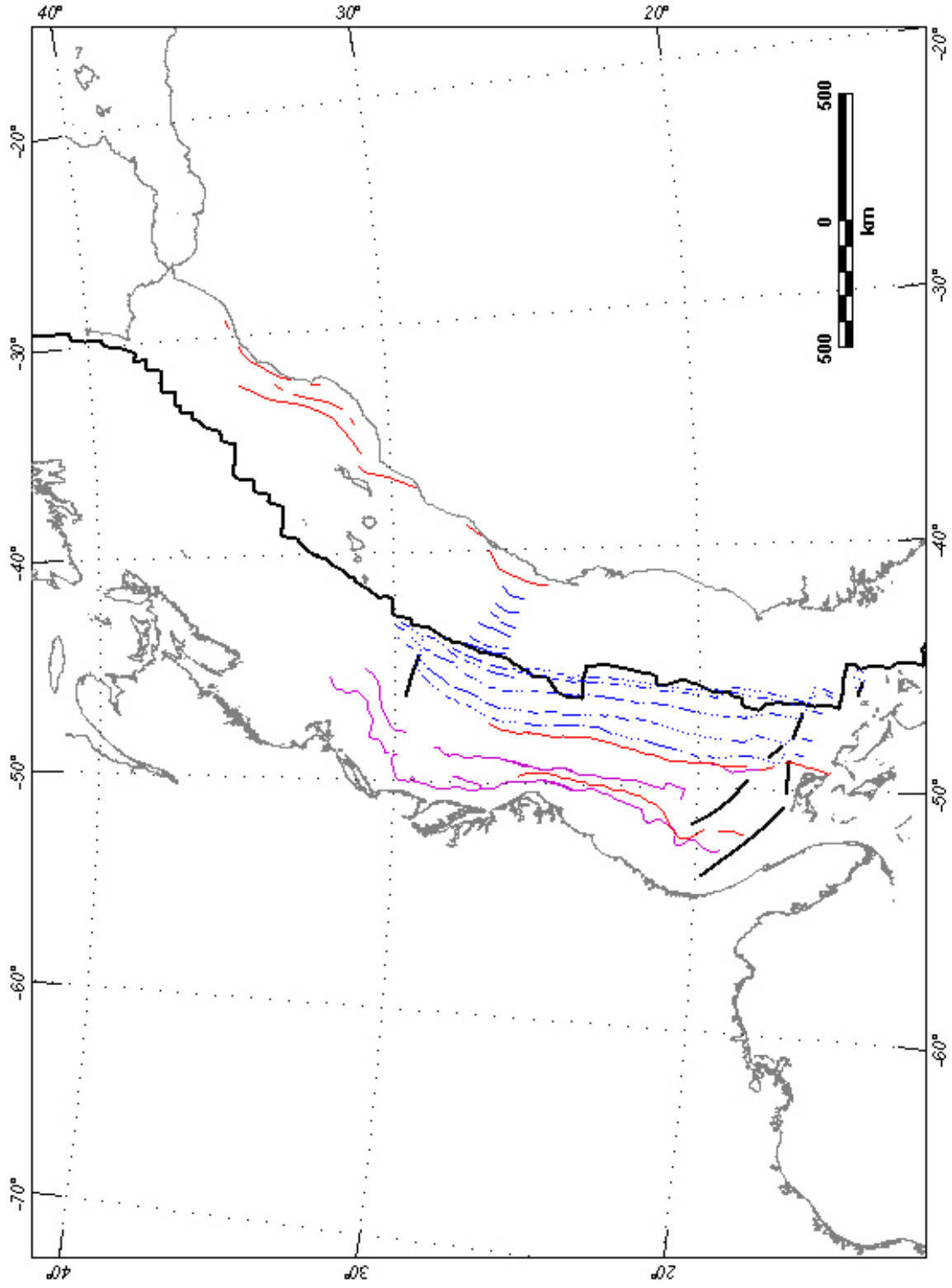
40°
30°
20°
-20°
-30°
-40°
-50°
-60°
-70°
500
0
500
km

Inspection of M25 reconstruction (Figure 3.22) illustrates: 1) the difference in width between the conjugate JMQZ provinces; and 2) the difference in width between the conjugate ECMA-BSMA and S1-S3 anomaly pairs.

3.7 Discussion

3.7.1 Blake Plateau

Seafloor spreading in the central Atlantic is marked by the onset of postrift deposition in early Middle Jurassic time, or at about 185 Ma (Withjack *et al.*, 1998). Dunbar and Sawyer (1989) suggest that the preexisting structural grain of the continental crust controlled the amount of continental extension prior to breakup. They concluded that seafloor spreading begins first along segments that follow the structural grain, that extension prior to breakup is symmetrical, and that extension parallel to the structural grain is two to three times less than the extension that crosses preexisting structural grains. They further concluded that the total range of continental extension in the central Atlantic ranges from 200 km to over 600 km, and that this variability is largely controlled by the preexisting weaknesses within the structural grain and the ultimate orientation of the continental break. The largest extension of the North American flank in the central Atlantic is over 600 km in the Blake Plateau, south of the Blake Spur Fracture zone (BSFZ) (Dunbar and Sawyer, 1989). Chrons M20 to M25 are offset 30 to 50 km, right-laterally, by the BSFZ (Figure 8).

The Blake Plateau continental boundary, as mapped by Dunbar and Sawyer (1989), extends southeastward to Chron M32 as mapped in this study (Figure 8). Inboard

of this margin, we have mapped a southern 280 km dashed length of Chron M40. Although JMQZ anomalies are difficult to correlate, our interpretation is consistent with an oceanic BSMA and the mapped limit of oceanic crust (Uchupi *et al.*, 1984b), which are located about 200 km landward of Dunbar and Sawyer's (1989) proposed southeastward extent of the Blake Plateau.

Seismic refraction data in this part of the Blake Plateau include lines interpreted by Ewing and Ewing (1959), Katz and Ewing (1956), and Sheridan *et al.* (1966). Table 3.6 summarizes basement and Moho depths and crustal thicknesses determined from seismic refraction data in the North American flank. Line 102 lies over the northwest projection of the BSFZ and the crustal thickness of the fracture zone, 2.8 km to 4.4 km, is consistent with the crustal thickness of other fracture zones in the Atlantic Ocean (Fox and Gallo, 1984). The range of basement and Moho velocities of seismic refraction data are 4.8 to 6.8 km/s and 7.5 to 8.1 km/s. Basement velocities of 4.8 km/s at Station 266C20 and 5.5 km/s at Line 24 are within the range of Layer 2 velocities (White *et al.*, 1992). The remaining basement velocities range between 6.7 km/s and 6.8 km/s indicate lower crust (Christensen and Mooney, 1995; White *et al.*, 1992). The slow 7.5 km/s Moho velocity of Line 102 is interpreted to represent an anomalous velocity associated with the BSFZ. Similarly, the 7.7 km/s Moho velocity of Line A-173-4, which lies along mapped Chron 25 offset northeast of the Atlantis fracture zone (Muller *et al.*, 1997), may represent an anomalous velocity associated with a fracture zone. If this anomalous data point is discarded, then the range of Moho velocities is 7.9 km/s to 8.1 km/s.

White *et al.* (1992) reported the results of three world-wide compilations of oceanic crustal thickness and layer velocities. Mean velocities for Layer 2, Layer 3, and

Line/Station Number	Basement Depth (km)	Moho Depth(km)	Crustal Thickness	Source
A-173-4	6.6	11.0	4.4	Ewing and Ewing, 1959
24	6.7	12.1	5.4	Katz and Ewing, 1956
266C20	8.2	16.1	7.9	Houtz, 1980
G-15	8.1	14.8	6.7	Ewing and Ewing, 1959
102	8.4	12.0	3.6	Sheridan et al., 1966
7	7.0	13.4	6.4	Katz and Ewing, 1956
6	6.6	12.5	5.9	Katz and Ewing, 1956

Table 3.6

Seismic refraction depths in the North Atlantic flank of the central Atlantic (see Figure 3.8). Basement refers to the top of Layer 2 or Layer 3 and depths are below sea level.

upper mantle are 5.09 ± 0.74 km/s, 6.69 ± 0.26 km/s, and 8.15 ± 0.31 km/s respectively. The mean thickness of oceanic crust is 6.33 ± 1.85 km. Christensen and Mooney (1995) reported the average thickness of extended continental crust as 30.5 km. They subdivided continental crustal velocities into three groups: upper (5.7 to 6.4 km/s), middle (6.4 to 6.8 km/s), and lower (6.8 to 7.8 km/s). Tanimoto (1995) reported average continental crustal thickness as 39 km. Difficulties associated with interpreting seismic refraction data in deep basins are related to the lack of velocity contrasts, source energy, and the length of the survey line. Often Layer 2 of oceanic crust cannot be interpreted because it is thin (generally 2 km or less), or at great depths where the seismic velocities of overlying sediments, such as salt or carbonates, approach the relatively low crustal velocity of Layer 2. Therefore, in deep ocean basins, only a single crustal layer is often identified.

The Blake Plateau overlies a broad basin that is characterized by 5 to 6 km basement depths, but exceeds 8 km just north of 30°N, 78°W (Crosby *et al.*, 1984). Sheridan *et al.* (1966) interpreted an 800 km long east-west cross section, constructed through several smaller refraction profiles, from the west coast of Florida at 30°N eastward to about 76°W at 29°N. Sheridan *et al.* (1966) interpreted a 2 km thick, 5.3 to 5.5 km/s, layer overlying basement to be volcanic rocks and a 2.5 km basement structure (5.7 to 6.1 km/s), located inboard of seismic refraction Line 102, to be a basement ridge along the outer edge of the Blake Plateau. The deepest horizon detected between the volcanic rocks and the basement, at 3 to 4 km depths of the plateau, is defined by velocities ranging between 5.5 and 6.0 km/s. Sheridan *et al.* (1966) suggested that these velocities might be equivalent to those of the Paleozoic basement rocks of Florida.

Although a comprehensive understanding of the history and makeup of the Blake Plateau is beyond the scope of this study, we suggest that the thick (about 2 km), high velocity (5.5 km/s to 6.0 km/s) layer interpreted by Sheridian *et al.* (1966) could be volcanic rocks on the oceanic basement of the Blake Plateau. Therefore, based on similarities of anomalies along nine profiles over the plateau southwest of the BSFZ, we have tentatively extended Chon M40 over the plateau with dashed lines.

Extending from the northeast edge of the Blake Plateau to the Atlantis fracture zone, near the BSMA and Chrons 40 and 32, basement and Moho depths at four locations indicate oceanic crust (Ewing and Ewing, 1959; Houtz, 1980; Katz and Ewing, 1956) (Table 3.6). Extrapolation along the coast to the southwest further suggests that the crust of the southeasternmost part of the Blake Plateau is oceanic.

Refraction data confirm the existence of oceanic crust extending landward at least to the BSMA. Moho depths have not been determined beneath the deep Carolina Trough and Blake Plateau. However interpretations of reflection data summarized by Withjack *et al.* (1998) indicate that a zone of Seaward-Dipping Reflectors coincides with the ECMA from its southern end at about 30°N along the North American continental shelf to about 43°N just south of Nova Scotia. The amplitudes, trends, and lengths of ECMA, BSMA, and S1 to S3 are similar to M0-M25 Series anomalies. We interpret subtle linear magnetic trends between ECMA and BSMA, which are suggestive of geomagnetic polarity reversals, to further support the presence of oceanic crust between these two anomalies.

3.7.2 Chron Identification

Anomaly profiles were interpreted in their acquisition position, superimposed on gridded magnetic data, to identify trends defined by similar anomaly character. Anomaly correlation is variable from line to line and along lines. A strong correlation might exist along part of a line, but might be non-existent along another part of a line. Strong line to line correlations are connected with solid lines connected by dotted lines on maps (Figures 8, 9, 11, 12, and 13). Geomagnetic isochrons are identified by comparing selected anomaly profiles along shiptracks with synthetic profiles generated from 2D seafloor spreading models, incorporating parts of the polarity reversal scale at appropriate spreading rates (Figures 14 and 15).

Because of their higher amplitudes, M0-25 Series anomalies are readily identified and mapped, but JMQZ anomalies are more difficult to identify because anomaly amplitudes are lower, the anomalies are typically located over the deepest parts of the basin near the continental margins, and because of the rapid frequency of polarity reversals during this time. For both M0-25 and JMQZ sequences of anomalies, the anomaly amplitudes over the eastern side of the central Atlantic are about 25-33% less than the corresponding anomaly amplitudes over the western side.

Vogt *et al.* (1970) indicated that magnetic anomaly amplitudes over the JMQZ, or smooth zone, could be the result of a period of rapid polar wander or that they formed at the magnetic equator. Sager *et al.* (1998) reported that Chrons M27 to M30 have been verified by magnetic stratigraphy, and that while magnetostratigraphic data corresponding to M38 and older Chrons are lacking, short wavelength anomalies are

similar to other paleointensity variations corresponding to periods of 150 to 300 Ky. They noted that magnetization strength data are poorly constrained, and concluded that Jurassic geomagnetic field behavior was unusual. If the modeled polarity reversals exist, then the geomagnetic polarity reversal rate is extraordinarily high: about 12 per My or 20% higher than for the period between M25 and M26, which would then be the second highest reversal rate (Sager *et al.*, 1998). They also suggested that instead of geomagnetic polarity reversals, the anomalies could be produced by paleointensity fluctuations.

3.7.3 Ridge Jumps

The relocation of seafloor spreading centers, or ridge jumps, has been documented along the MAR near Ascension Fracture Zone (Brozena, 1986), seven locations west of the East Pacific Rise including two ridge jumps underway on the East Pacific Rise (Luhr *et al.*, 1986; Morton and Ballard, 1986; Mammerickx *et al.*, 1988; Mammerickx and Sandwell, 1986), south of the Chilean Ridge (Mammerickx *et al.*, 1988), and three locations in the north Pacific (Mammerickx *et al.*, 1988). The evidence cited for a ridge jump now taking place along the East Pacific Rise, near 19°S, are two parallel ridges separated by a 200 m deep valley (Morton and Ballard, 1986). They suggest that spreading shifted 3 km to the west within the past 40,000 y. Between Mexico and the Galapagos Ridge, Luhr *et al.* (1986) documented several ridge jumps over the past 12 Ma with jumps ranging up to 550 km.

In the central Atlantic the large difference in width between the conjugate BSMA-ECMA and S1-S3 anomalies (Figure 3.22) indicates that a ridge jump must have occurred before Chron 40 (167.5 Ma). The large difference in width and the number of

correlatable anomalies, between the North American and African JMQZ provinces indicates that a ridge jump occurred, probably between 164 Ma and 159 Ma. Although the present spreading rate between North America and Africa is slow (about 22 mm/a, DeMets *et al.*, 1990), its kinematic history includes periods of sustained asymmetric spreading and total spreading rates ranging as high as 45 mm/a.

We identify ridge jumps at 170 Ma and 164 Ma, early in the history of the formation of the central Atlantic Ocean. These ridge jumps are probably related to changes in plate motions as North America separated from Gondwana. It has not escaped our attention that these ridge jumps, especially the latter, could correspond with the opening of the Gulf of Mexico.

3.8 Conclusions

Simultaneous interpretation of gridded magnetic anomaly data sets, and hundreds of magnetic anomaly profiles, in the central Atlantic Ocean has enabled us to perform detailed mapping of several M-Series Chrons within the range between M0 to M25, as well as the Jurassic Magnetic Quiet Zone (JMQZ or M25 to M40) magnetic anomaly provinces. We have identified periods of asymmetric spreading and evidence that supports the existence of a ridge jump at about 170 Ma, which was first suggested by Vogt (1986). We have found new evidence that indicates a later ridge jump between 164 Ma and 159 Ma.

We have identified and mapped: M0, M1, M3, M4, M10N, M12A, M14, M16, M17, M18, M19, M20n-1, M20, M21, M22, M23, M24 and M25. The low amplitude JMQZ Chrons include M28, M29, M32, M38 and M40.

Distances measured separately from the MAR to Chron C34, Chron C34 to Chron M0, and Chron M0 to Chron M25 for the North American and African sides of the central Atlantic indicate that asymmetric spreading occurred over nearly the entire history of the ocean (Table 3.5). For the past 84 Ma accretion has been faster on the North American side by an average of 10%, between 84 Ma and 120.6 Ma accretion averaged 3.5% faster on the African side, and between 120.6 Ma and 154 Ma accretion on the North American side was faster by an average of10.5%.

We have identified Chron 40 (167.5 Ma), which is 65 km outboard of the Blake Spur Magnetic Anomaly (BSMA) off the continental shelf of North America, as well as 65 km outboard of anomaly S1 off the continental shelf of Africa. The large distance remaining over ocean floor on the respective coasts indicate that a ridge jump occurred at approximately 170 Ma. This ridge jump was an eastward shift of the spreading center, but the lack of correlatable magnetic anomalies between the BSMA and the East Coast Magnetic Anomaly (ECMA) does not allow an estimate of the distance spanned by the jump. The width of the JMQZ off Africa is about 70 km greater than the width of the JMQZ off North America (or about 22% greater). Magnetic data indicate the presence of additional correlatable anomalies over the African JMQZ, indicating the presence of a westward ridge jump between 164 Ma and 159 Ma.

4. REFERENCES

Angeles-Aquino, F. J., Reyes-Nunez, J., Quezada-Muneton, J. M., Meneses-Rocha, J. J., 1994, Tectonic evolution, structural styles, and oil habitat in Campeche Sound, Mexico: Trans., Gulf Coast Assoc. Geol. Soc., 44, 53-62.

Antoine, J., Ewing, J., 1963, Seismic refraction measurements on the margins of the Gulf of Mexico: J. Geophys. Res., 68, 1975-1996.

Antoine, J. W., Harding, J. L., 1963, Structure of the continental shelf, northeastern Gulf of Mexico: College Station, Texas A & M Research Foundation, A & M Proj. 286 – Ref. 63-13T.

Antoine, J. W., Harding, J. L., 1965, Structure beneath continental shelf, northeastern Gulf of Mexico: Am. Assoc. Petr. Geol. Bull., 49, 157-171.

Basile, C., Mascle, J., Popoff, M., Bouillin, J. P., Mascle, G., 1993, The Ivory Coast – Ghana transform margin: a marginal ridge structure deduced from seismic data: Tectonophysics, 222, 1-19.

Ben-Avraham, Z., Hartnady, C. J. H., Kitchin, K. A., 1997, Structure and tectonics of the Agulhas – Falkland fracrure zone: Tectonophysics, 282, 83-98.

Bird, D. E., 2001, Shear margins: continent – ocean transform and fracture zone boundaries: The Leading Edge, 20, 150-159.

Bird, D. E., Hall, S. A., Casey, J. F., Burke, K., 2001, Geophysical evidence for a possible late Jurassic mantle plume in the Gulf of Mexico (abs.): Eos, Trans., Am. Geophys. Union, 82 (47), Fall Meeting Supp., F1185.

Blakely, R. J., 1995, Potential theory in gravity & magnetic applications: New York, Cambridge University Press, 435 p.

Bonatti, E., Ligi, M., Gasperini, L., Peyve, A., Raznitsin, Y., Chen, Y. J., 1994, Transform migration and vertical tectonics at the Romanche Fracture Zone, equatorial Atlantic: J. Geophys. Res., 99 (B11), 21779-21802.

Brozena, J. M., 1986, Temporal and spatial variability of seafloor spreading processes in the northern South Atlantic: J. Geophys. Res., 91 (B1), 497-510.

Buffler, R. T., 1989, Distribution of crust, distribution of salt, and the early evolution of the Gulf of Mexico basin: *in*, Gulf of Mexico salt tectonics, associated processes and exploration potential: SEPM 10th Ann. Res. Conf., Gulf Coast Sec., 25-27.

Buffler, R. T., Sawyer, D. S., 1985, Distribution of crust and early history, Gulf of Mexico Basin: Trans., Gulf Coast Assoc. Geol. Soc., 35, 333-334.

Buffler, R. T., Thomas, W. A., 1994, Crustal structure and evolution of the southeastern margin of North America and the Gulf of Mexico basin: *in*, Speed, R. C., Phanerozoic Evolution of North American Continent – Ocean Transitions: Boulder, CO, Geol. Soc. Am., DNAG Continent – Ocean Transect Vol., 219-264.

Buffler, R. T., Watkins, J. S., Shaub, F. J., Worzel, J. L., 1980, Structure and early geologic history of the deep central Gulf of Mexico basin: *in*, Pilger, R. H. Jr., ed., The origin of the Gulf of Mexico and the early opening of the central North Atlantic Ocean: Baton Rouge, Louisiana State Univ., Proceed. Symposium, 3-16.

Bunch, A. W. H., 1979, A detailed seismic structure of Rockall Bank (55°N, 15°W) – a synthetic seismogram analysis: Earth Planet. Sci. Lett., 45, 453-463.

Burke, K., 1988, Tectonic evolution of the Caribbean: Ann. Rev. Earth Planet. Sci., 16, 201-230.
Caress, D. W., McNutt, M. K., Detrick, R. S., Mutter, J. C., 1995, Seismic imaging of hotspot-related crustal underplating beneath the Marquesas Islands: Nature, 373, 600-603.
Channell, J. E. T., Erba, E., Nakanishi, M., Tamaki, K., 1995, Late Jurassic – Early Cretaceous time scales and oceanic magnetic anomaly block models: *in*, Geochronology, time scales and global stratigraphic correlation: SEPM Spec. Pub. 54, 51-63.
Christensen, N. I., Mooney, W. E., 1995, Seismic velocity structure and composition of the continental crust: a global view: J. Geophys. Res., 100 (B7), 9761-9788.
Christenson, G., 1990, The Florida lineament: Trans., Gulf Coast Assoc. Geol. Soc., 40, 99-115.
Clift, P. D., Lorenzo, J., Carter, A., Hurford, A. J., ODP Leg 159 Scientific Party, 1997, Transform tectonics and thermal rejuvenation on the Côte d'Ivoire – Ghana margin, west Africa: J. Geol. Soc. Lond., 154, 483-489.
Collette, B. J., Roest, W. R., 1992, Further investigations of the North Atlantic between 10° and 40°N and an analysis of spreading from 118 Ma ago to Present: in, Proc. Kon. Ned. Akad. V. Wetensch., Ser. B, 95 (2), 159-206.
Collette, B. J., Slootweg, A. P., Verhoef, J., Roest, W. R., 1984, Geophysical investigations of the floor of the Atlantic Ocean between 10° and 38°N (Kroonvlag-project): *in*, Proceed. Kon. Ned. Akad. V. Wetensch., Ser. B, 87 (1), 1-80.
Committee for the Magnetic Anomaly Map of North America, 1985, Magnetic Map of North America: Boulder, Geol. Soc. Am., 5 sheets, scale 1:5,000,000.
Cordell, L., 1973, Gravity analysis using an exponential density-depth function – San Jacinto Graben, California: Geophysics, 38, 684-690.
Cram, I. H. Jr., 1961, A crustal structure refraction survey in south Texas: Geophysics, 26, 560-573.
Crosby, J. T., Uchupi, E., Manley, P. L., Bolmer, S. T. Jr., Eudsen, J. D. Jr., Gleason, R. J., Ewing, J. I., 1984, Depth to basement: *in*, Bryan, G. M., Heirtzler, J. R., eds., Eastern North American continental margin and adjacent ocean floor, 28° to 36°N and 70° to 82°W: Woods Hole, Mar. Sci. Int., Atlas 5, p. 9.
Davies, D., Francis, T. G. H., 1964, The crustal structure of the Seychelles Bank: Deep-Sea Res., 11, 921-927.
Dehlinger, P., Jones, B. R., 1965, Free-air gravity anomaly map of the Gulf of Mexico and its tectonic implications, 1963 edition: Geophysics, 30, 102-110.
Del Castillo, L., 1974, Marine geophysics along the Gulf of Mexico and the Yucatan Peninsula coastal area in Mexico: Phys. Earth Planet. Int., 9, 227-247.
DeMets, C., Gordon, R. G., Argus, D. F., Stein, S., 1990, Current plate motions: Geophys. J. Int., 101, 425-478.
Dewey, J. F., 1975, Finite plate implications: some implications for the evolution of rock masses at plate margins: Am. J. Sci., 275-A, 260-284.
Diegel, F. A., Karlo, J. F., Schuster, D. C., Shoup, R. C., Tauvers, P. R., 1995, Cenozoic structural evolution and tectono-stratigraphic framework of the northern Gulf Coast

continental margin: *in*, Jackson, M. P. A., Roberts, D. A., Snelson, S., eds., Salt tectonics: a global perspective: Am. Assoc. Petr. Geol. Mem. 65, 109-151.
Droz, L., Mougenot, D., 1987, Mozambique Upper Fan: origin of depositional units: Am. Assoc. Petr. Geol. Bull., 71 (11), 1355-1365.
Dunbar, J. A., Sawyer, D. S., 1989, Patterns of continental extension along the conjugate margins of the central and North Atlantic Oceans and Labrador Sea: Tectonics, 8, 1059-1077.
Dunbar, J. A., Sawyer, D. S., 1987, Implications of continental crust extension for plate reconstruction: an example from the Gulf of Mexico: Tectonics, 6, 739-755.
Ebeniro, J. O., O'Brien, W. P. Jr., Shaub, F. J., 1986, Crustal structure of the south Florida Platform, eastern Gulf of Mexico: an ocean-bottom seismograph refraction study: Mar. Geophys. Res., 8, 363-382.
Ebeniro, J. O., Y. Nakamura, Y., Sawyer, D. S., O'Brien, W. P. Jr., 1988, Sedimentary and crustal structure of the northwestern Gulf of Mexico: J. Geophys. Res., 93, 9075-9092.
Edwards, R. A., Whitmarsh, R. B., Scrutton, R. A., 1997, Synthesis of the crustal structure of the transform continental margin off Ghana, northern Gulf of Guinea: Geo-Marine Lett., 17, 12-20.
Engebretson, D. C., Cox, A., Gordon, R. G., 1984, Relative motions between oceanic plates of the Pacific basin: J. Geophys. Res., 89 (B12), 10291-10310.
Ewing, J., Antoine, J., Ewing, M., 1960, Geophysical measurements in the western Caribbean Sea and in the Gulf of Mexico: J. Geophys. Res., 65, 4087-4126.
Ewing, J., Ewing, M., 1959, Seismic-refraction measurements in the Atlantic Ocean basins, in the Mediterranean Sea, on the Mid-Atlantic Ridge, and in the Norwegian Sea: Bull. Geol. Soc. Am., 70, 291-318.
Ewing, J. I., Worzel, J. L., Ewing, M., 1962, Sediments and oceanic structural history of the Gulf of Mexico: J. Geophys. Res., 67, 2509-2527.
Fox, P. J., Gallo, D. G., 1984, A tectonic model for ridge-transform-ridge plate boundaries: Implications for the structure of oceanic lithosphere: Tectonophysics, 104, 205-242.
Francis, T. J. G., Raitt, R. W., 1967, Seismic refraction measurements in the southern Indian Ocean: J. Geophys. Res., 72, 3015-3041.
Furumoto, A. S., Thompson, N. J., Woollard, G. P., 1965, The structure of Koolau Volcano from seismic refraction studies: Pacific Sci., 19, 306-314.
Furumoto, A. S., Woollard, G. P., 1965, Seismic refraction studies of the crustal structure of the Hawaiian Archipelago: Pacific Sci., 19, 315-319.
Gadd, S. A., Scrutton, R. A., 1997, An integrated thermomechanical model for transform continental margin evolution: Geo-Marine Lett., 17, 21-30.
Goff, J. A., Cochran, J. R., 1996, The Bauer scarp ridge jump: a complex tectonic sequence revealed in satellite altimetry: Earth Planet. Sci. Lett., 141, 21-33.
Gordon, R. G., DeMets, C., 1989, Present-day motion along the Owen Fracture Zone and Dalrymple Trough in the Arabian Sea: J. Geophys. Res., 94 (B5), 5560-5570.
Gose, W. A., Belcher, R. C., Scott, G. R., 1982, Paleomagnetic results from northeastern Mexico: evidence for large Mesozoic rotations: Geology, 10, 50-54.

Grant, F. S., West, G. W., 1965, Interpretation Theory in Applied Geophysics: New York, McGraw-Hill, 583 p.

Grevemeyer, I., Flueh, E. R., Teichert, C., Bialas, J., Klaschen, D., Kopp, C., 2001, Crustal architecture and deep structure of the Ninetyeast Ridge hotspot trail from active – source ocean bottom seismology: Geophys. J. Int., 144, 414-431.

Hales, A. L., 1973, The crust of the Gulf of Mexico: a discussion: Tectonophysics, 20, 217-225.

Hales, A. L., Helsley, C. E., Nation, J. B., 1970a, Crustal structure study on Gulf coast of Texas: Am. Assoc. Petr. Geol. Bull., 54, 2040-2057.

Hales, A. L., Helsley, C. E., Nation, J. B., 1970b, P travel times for an oceanic path: J. Geophys. Res., 75, 7362-7381.

Hall, D. J., Cavanaugh, T. D., Watkins, J. S., McMillen, K. J., 1982, The rotational origin of the Gulf of Mexico based on regional gravity data: *in*, Watkins, J. S., Drake, C. L., Studies in continental margin geology: Tulsa, Am. Assoc. Petr. Geol. Mem. 34, 115-126.

Hall, S., 2001, The development of large structures in the deepwater northern Gulf of Mexico: Houston Geol. Soc. Bull., 43 (8), 20-23.

Hall, S. A., Najmuddin, I. J., 1994, Constraints on the tectonic development of the eastern Gulf of Mexico provided by magnetic anomaly data: J. Geophys. Res., 99 (B4), 7161-7175.

Hayes, D. E., Houtz, R. E., Jarrard, R. D., Mrozowski, C. L., Watanabe, T., 1978, Crustal structure: Boulder, Geol. Soc. Am., Map and Chart Ser. MC-25, 4-5.

Houtz, R. E., 1980, Crustal structure of the North Atlantic on the basis of large – airgun – sonobuoy data: Geol. Soc. Am. Bull., Part I, 91, 406-413.

Humphris, C. C. Jr., 1979, Salt movement on continental slope, northern Gulf of Mexico: Am. Assoc. Petr. Geol. Bull, 63, 782-798.

Ibrahim, A. K., Carye, J., Latham, G., Buffler, R. T., 1981, Crustal structure in Gulf of Mexico from OBS refraction and multichannel reflection data: Am. Assoc. Petr. Geol. Bull., 65, 1207-1229.

Ibrahim, A. K., Uchupi, E., 1982, Continental oceanic crustal transition in the Gulf coast geosyncline: *in*, Watkins, J. S., Drake, C. L., eds., Studies in continental margin geology: Am. Assoc. Petr. Geol. Mem. 34, 155-165.

Katz, S., Ewing, M., 1956, Seismic-refraction measurements in the Atlantic Ocean, part VII: Atlantic Ocean basin, west of Bermuda: Bull. Geol. Soc. Am., 67, 475-510.

Keller, G. R., Shurbet, D. H., 1975, Crustal structure of the Texas Gulf coastal plain: Geol. Soc. Am. Bull., 86, 807-810.

Kim, S. D., Nagihara, S., Nakamura, Y., 2000, P- and S-wave velocity structures of the Sigsbee abyssal plain of the Gulf of Mexico from ocean bottom seismometer data: Transactions, Gulf Coast Assoc. Geol. Soc., 50, 475-483.

Klitgord, K. D., Popenoe, P., Schouten, H., 1984, Florida, a Jurassic transform plate boundary: J. Geophys. Res., 89, 7753-7772.

Klitgord, K. D., Schouten, H., 1986, Plate kinematics of the central Atlantic: *in*, Vogt, P. R., Tucholke, B. E., eds., The geology of North America, The western North Atlantic region: Boulder, Geol. Soc. Am., M, 351-378.

Lorenzo, J. M., 1997, Sheared continent – ocean margins: an overview: Geo-Marine Lett., 17, 1-3.
Lorenzo, J. M., Mutter, J. C., Larson, R. L., Northwest Australia Study Group, 1991, Development of the continent – ocean transform boundary of the southern Exmouth Plateau: Geology, 19, 843-846.
Lorenzo, J. M., Vera, E. E., 1992, Thermal uplift and erosion across the continent – ocean transform boundary of the southern Exmouth Plateau: Earth Planet. Sci. Lett., 108, 70-92.
Lorenzo, J. M., Wessel, P., 1997, Flexure across a continent – ocean fracture zone: the northern Falkland / Malvinas Plateau, South Atlantic: Geo-Marine Lett., 17, 110-118.
Luhr, J. F., Nelson, S. A., Allan, J. F., Carmichael, S. E., 1986, Active rifting in southwestern Mexico: manifestations of an incipient eastward spreading-ridge jump: Geology, 13, 54-57.
Mackie, D. J., Clowes, R. M., Dehler, S. A., Ellis, R. M., Morel-À-L'Huissier, P., 1989, The Queen Charlotte Islands refraction project. Part II. Structural model for transition from Pacific plate to North American plate: Can. J. Earth Sci., 26, 1713-1725.
Mammerickx, J., Naar, D. F., Tyce, R. L., 1988, The Mathematician paleoplate: J. Geophys. Res., 93, 3025-3040.
Mammerickx, J., Sandwell, D., 1986, rifting of old oceanic lithosphere: J. Geophys. Res., 91 (B2), 1975-1988.
Martin, R. G., 1980, Distribution of salt structures in the Gulf of Mexico: U. S. Geol. Surv., Map MF-1213.
Martin, R. G., Case, J. E., 1975, Geophysical studies in the Gulf of Mexico: *in*, Nairn, A. E. M., Stehli, F. G., eds., The ocean basins and margins: New York, Plenum Press, The Gulf of Mexico and the Caribbean, 3, 65-106.
Marton, G., Buffler, R. T., 1994, Jurassic reconstruction of the Gulf of Mexico Basin: Int. Geol. Rev., 36, 545-586.
Mascle, J., Mougenot, D., Blarez, E., Marinho, M., Virlogeux, P., 1987, African transform continental margins: examples from Guinea, the Ivory Coast and Mozambique: Geol. J. Thematic Issue, 22, 537-561.
Matthews, D. H., Davies, D., 1966, Geophysical studies of the Seychelles Bank: Philosophical Transactions of the Royal Society of London, Ser. A., 259, 227-239.
McKenzie, D., 1978, Some remarks on the development of sedimentary basins: Earth Planet. Sci. Lett., 40, 25-32.
Menard, H. W., Atwater, T. M., 1968, Changes in direction of sea floor spreading: Nature, 219, 463-467.
Metcalfe, I., 1996, Pre-Cretaceous evolution of SE Asian terranes: in, R. Hall, D. Blundell, eds., Tectonic evolution of Southeast Asia, Geol. Soc. Spec. Pub., 106, 97-122.
Minshull, T. A., White, R. S., Barton, P. J., Collier, J. S., 1992, Deformation at plate boundaries around the Gulf of Oman: Mar. Geol., 104, 265-277.
Molina-Garza, R. S., Van der Voo, R., Urrutia-Fucugauchi, J., 1992, Paleomagnetism of the Chiapas Massif, southern Mexico: evidence for rotation of the Maya Block and implications for the opening of the Gulf of Mexico: Geol. Soc. Am. Bull., 104, 1156-1168.

Mooney, W. D., Andrews, M. C., Ginzburg, A., Peters, D. A., Hamilton, R. M., 1983, Crustal structure of the northern Mississippi Embayment and a comparison with other continental rift zones: Tectonophysics, 94, 327-348.
Mooney, W. D., Laske, G., Masters, G., 1998, CRUST 5.1: A global crustal model at 5°x5°: J. Geophys. Res., 103, 727-747.
Moore, G. W., Del Castillo, L., 1974, Tectonic evolution of the southern Gulf of Mexico: Geol. Soc. Am. Bull., 85, 607-618.
Morgan, W. J., 1983, Hotspot tracks and the early rifting of the Atlantic: Tectonophysics, 94, 123-139.
Morton, J. L., Ballard, R. D., 1986, East Pacific Rise at lat 19°S: evidence for a recent ridge jump: Geology, 14, 111-114.
Muller, R. D., Roest, W. R., 1992, Fracture zones in the North Atlantic from combined Geosat and Seasat data: J. Geophys. Res., 97 (B3), 3337-3350.
Muller, R. D., Roest, W. R., Royer, J. –Y., 1998, Asymmetric sea-floor spreading caused by ridge-plume interactions: Nature, 396, 455-459.
Muller, R. D., Roest, W. R., Royer, J. –Y., Gahagan, L. M., Sclater, J. G., 1997, Digital isochrons of the world's ocean floor: J. Geophys. Res., 102 (B2), 3211-3214.
Muller, R. D., Smith, W. H. F., 1993, Deformation of the oceanic crust between the North American and South American plates: J. Geophys. Res., 98 (B5), 8275-8291.
Nakamura, Y., Sawyer, D. S., Shaub, F. J., MacKenzie, K., Oberst, J., 1988, Deep crustal structure of the northwestern Gulf of Mexico: Trans., Gulf Coast Assoc. Geol. Soc., 38, 207-215.
Olsen, P. E., McCune, A. R., Thomson, K. S., 1982, Correlation of the early Mesozoic Newark Super Group by vertebrates, principally fishes: Am. J. Sci., 282, 1-44.
Peel, E. J., Hossack, J. R., Travis, C. J., 1995, Genetic structural provinces and salt tectonics of the Cenozoic offshore U.S. Gulf of Mexico: a preliminary analysis: *in*, Jackson, M. P. A., Roberts, D. G., Snelson, S., eds., Salt tectonics: a global perspective: Am. Assoc. Petr. Geol. Mem. 65, 153-175.
Pindell, J. L., 1985, Alleghenian reconstruction and subsequent evolution of the Gulf of Mexico, Bahamas, and Proto-Caribbean: Tectonics, 4 (1), 1-39.
Pindell, J. L., 1994, Evolution of the Gulf of Mexico and the Caribbean: *in*, Donovan, S. K., Jackson, T. A., eds., Caribbean geology: an introduction: Kingston, Univ. West Indies Pub. Assoc., 13-39.
Pindell, J., Dewey, J. F., 1982, Permo-Triassic reconstruction of western Pangea and the evolution of the Gulf of Mexico / Caribbean region: Tectonics, 1, 179-211.
Prims, J., Furlong, K. P., Rohr, K. M. M., Govers, R., 1997, Lithospheric structure along the Queen Charlotte margin in western Canada: constraints from flexural modeling: Geo-Marine Lett., 17, 94-99.
Pszczolkowski, A., 1999, The exposed passive margin of North America in Western Cuba: *in*, Mann, P., ed., Caribbean basins, Hsu, K. J., series ed., Sedimentary basins of the world, vol. 4: Amsterdam, Elsevier Science B. V., 93-121.
Reid, I. D., Jackson, H. R., 1997, A review of three transform margins off eastern Canada: Geo-Marine Lett., 17, 87-93.
Roeser, H. A., Steiner, C., Schreckenberger, B., Block, M., 2002, Structural development of the Jurassic Magnetic Quiet Zone off Morocco and identification of Middle

Jurassic magnetic lineations: J. Geophys. Res., 107 (B10), 2207, doi:10.1029/2000JB000094.
Roest, W. R., Danobeitia, J. J., Verhoef, J., Collette, B. J., 1992, Magnetic anomalies in the Canary Basin and the Mosozoic evolution of the central North Atlantic: Mar. Geophys. Res., 14, 1-24.
Rona, P. A., Brakl, J., Heirtzler, J. R., 1970, Magnetic anomalies in the northeast Atlantic between the Canary and Cape Verde Islands: J. Geophys. Res., 75 (35), 7412-7420.
Ross, M. I., Scotese, C. R., 1988, A hierarchical tectonic model of the Gulf of Mexico and Caribbean region: Tectonophysics, 155, 139-168.
Sager, W. W., Weiss, C. J., Tivey, M. A., Johnson, H. P., 1998, Geomagnetic polarity reversal model of deep-tow profiles from the Pacific Jurassic Quiet Zone: J. Geophys. Res., 103, 5269-5286.
Salvador, A., 1987, Late Triassic – Jurassic paleogeography and origin of Gulf of Mexico Basin: Am. Assoc. Petr. Geol. Bull., 71, 419-451.
Salvador, A., 1991, Origin and development of the Gulf of Mexico basin: *in*, Salvador, A., ed., The Gulf of Mexico basin: Boulder, Geological Society of America, The geology of North America, J, 389-444.
Sandwell, D. T., Smith, W. H. F., 1997, Marine gravity anomaly from Geosat and ERS 1 satellite altimetry: J. Geophys. Res., 102 (B5), 10039-10054.
Schouten, H., Klitgord, K. D., 1994, Mechanistic solutions to the opening of the Gulf of Mexico: Geology, 22, 507-510.
Scrutton, R. A., 1970, Results of a seismic refraction experiment on Rockall Bank: Nature, 227, 826-827.
Shepherd, A. V., 1983, A study of the magnetic anomalies in the eastern Gulf of Mexico: Master's thesis, University of Houston, Houston, TX, 197 p.
Sheridan, R. E., Drake, C. L., Nafe, J. E., Hennion, J., 1966, Seismic-refraction study of continental margin east of Florida: Bull. Am. Assoc. Petr. Geol., 50 (9), 1972-1991.
Sinha, M. C., Louden, K. E., Parsons, B.,1981, The crustal structure of the Madagascar Ridge: Geophys. J. Int., 66, 351-377.
Steiner, M. in press, The Yucatan (Maya) block: Permian and Triassic geologic history and the Pangean to present palte tectonic record (abs.): *in*, Geol. Soc. Am. Spec. Pap.
Sundaralingam, K., Denham, D., 1987, Structure of the upper mantle beneath the Coral and Tasman Seas, as obtained from group and phase velocities of Rayleigh waves: New Zealand J. Geol. Geophys., 30, 329-341.
Sykes, T. J. S., 1996, A correction for sediment load upon the ocean floor: Uniform versus varying sediment density estimations – implications for isostatic correction: Mar. Geol., 133, 35-49.
Tanimoto, T., 1995, Crustal structure of the earth: in, Ahrens, T. J., ed., Global earth physics, a handbook of physical constants: Am. Geophys. Un. Ref. Shelf, 1, 214-224.
Taylor, B., Hayes, D. E., 1980, The tectonic evolution of the South China Basin: *in*, Hayes, D. E., ed., The tectonic and geologic evolution of Southeast Asian seas and islands, Washington D.C., Am. Geophys. Un., Geophys. Mono., 23, 89-104.
Todd, B. J., Keen, C. E., 1989, Temperature effects and their geological consequences at transform margins: Can. J. Earth Sci., 26, 2591-2603.

Uchupi, E., Bolmer, S. T. Jr., Eusden, J. D. Jr., Ewing, J. I., Costain, J. K., Gleason, R. J., Glover, L. III, 1984a, Tectonic features: *in*, Ewing, J. I., Rabinowitz, P. D., eds., Eastern North American continental margin and adjzcent ocean floor, 34° to 41°N and 68° to 78°W: Woods Hole, Mar. Sci. Int., Atlas 4, p. 28.

Uchupi, E., Crosby, J. T., Bolmer, S. T. Jr., Eusden, J. D. Jr., Ewing, J. I., Costain, J. K., Gleason, R. J., Glover, L. III, 1984b, Tectonic features: *in*, Bryan, G. M., Heirtzler, J. R., eds., Eastern North American continental margin and adjacent ocean floor, 28° to 36°N and 70° to 82°W: Woods Hole, Mar. Sci. Int., Atlas 5, p. 36.

Vågnes, E., 1997, Uplift at thermo-mechanically coupled ocean – continent transforms: modeled at the Senja Fracture Zone, southwestern Barents Sea: Geo-Marine Lett., 17, 100-109.

Verheof, J., Roest, W. R., Macnab, R., Arkani-Hamed, J., Members of the Project Team, 1996, Magnetic anomalies of the Arctic and North Atlantic Oceans and adjacent Land areas: Dartmouth, Geol. Surv. Canada (Atlantic), 2 sheets, scales 1:10,000,000 and 1:6,000,000.

Verhoef, J., Collette, B. J., Danobeitia, J. J., Roeser, H. A., Roest, W. R., 1991, Magnetic anomalies off west-Africa (20°-38°N): Mar. Geophys. Res., 13, 81-103.

Vogt, P. R., 1973, Early events in the opening of the North Atlantic: *in*, Tarling, D. H., Runcorn, S. K., eds., Implications of continental drift to the earth sciences: London, Academic Press Inc., 693-712.

Vogt, P. R., 1986, Magnetic anomalies and crustal magnetization: *in*, Vogt, P. R., Tucholke, B. E., eds., The geology of North America, The western Atlantic region: Boulder, Geol. Soc. Am., M, 229-256.

Vogt, P. R., Anderson, C. N., Bracey, D. R., 1971, Mesozoic magnetic anomalies, sea-floor spreading, and geomagnetic reversals in the southwestern North Atlantic: J. Geophys. Res., 76 (20), 4796-4823.

Vogt, P. R., Anderson, C. N., Bracey, D. R., Schneider, E. D., 1970, North Atlantic magnetic smooth zones: J. Geophys. Res., 75 (20), 3955-3968.

Warren, D. H., Healy, J. H., Jackson, W. H., 1966, Crustal seismic measurements in southern Mississippi: J. Geophys. Res., 71, 3437-3458.

Watts, A. B., Brink, U. S. T., 1989, Crustal structure, flexure, and subsidence history of the Hawaiian Islands: J. Geophys. Res., 94, 10473-10500.

White, G. W., 1980, Permian – Triassic continental reconstruction of the Gulf of Mexico – Caribbean area: Nature, 283, 823-826.

White, G. W., Burke, K. C., 1980, Outline of the tectonic evolution of the Gulf of Mexico and Caribbean region: Houston Geological Society Bulletin, 22 (10), 8-13.

White, R. S., McKenzie, D., O'Noins, R. K., 1992, Oceanic crustal thickness from seismic measurements and rare earth element inversions: J. Geophys. Res., 97 (B13), 19683-19715.

Winker, C. D., Buffler, R. T., 1988, Paleogeographic evolution of early deep-water Gulf of Mexico and margins, Jurassic to Middle Cretaceous (Comanchean): AAPG Bulletin, 72, 318-346.

Withjack, M. O., Schlische, R. W., Olsen, P. E., 1998, Diachronous rifting, drifting, and inversion on the passive margin of central eastern North America: An analog for other passive margins: Am. Assoc. Petr. Geol. Bull., 82 (5A), 817-835.